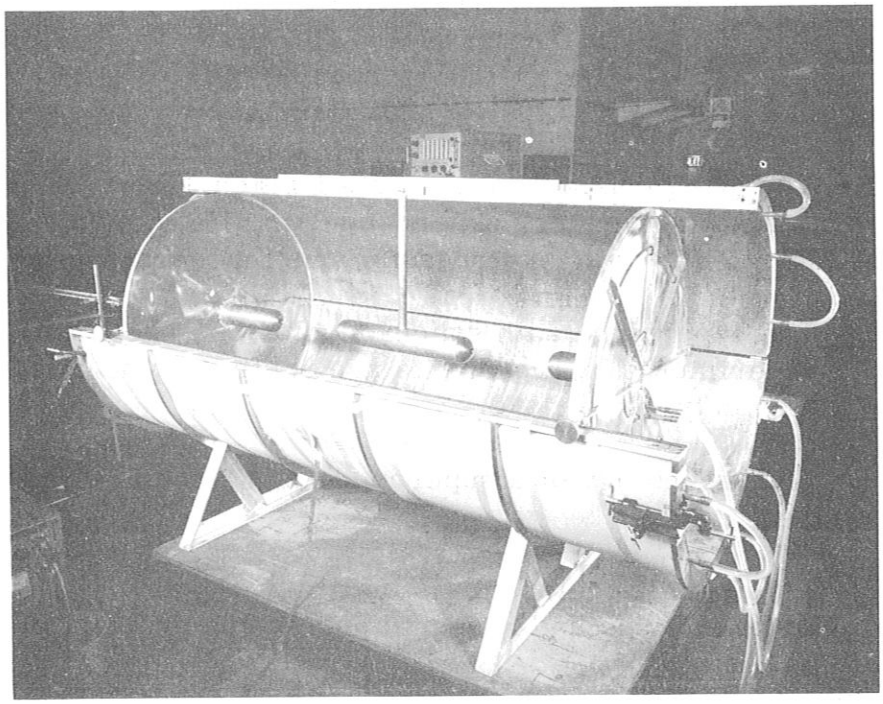

Fig. 10 ALVAREZ SECTION EXPERIMENTAL MODEL

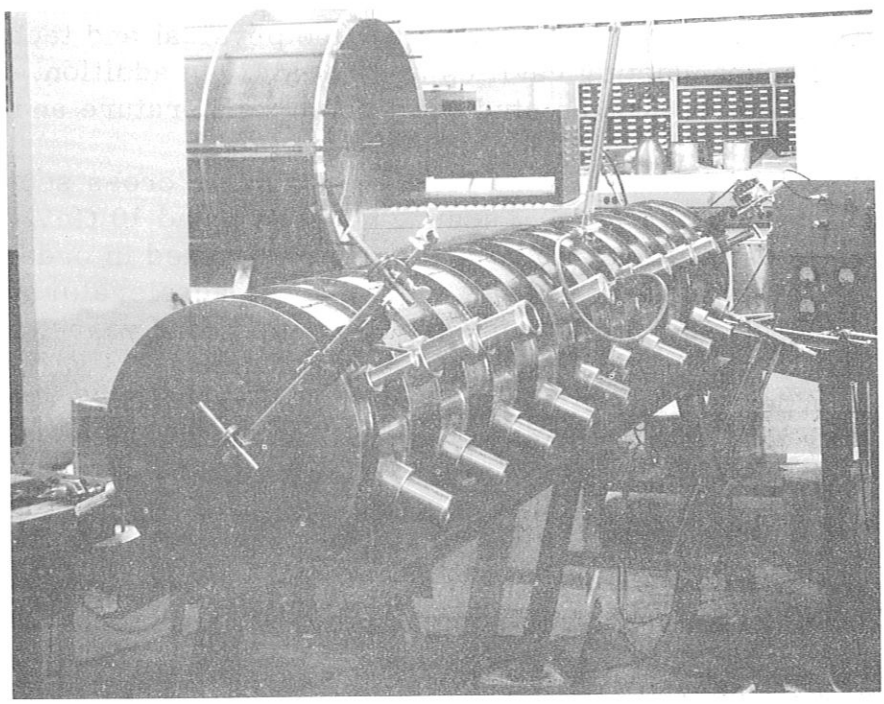

Fig. 11 CLOVERLEAF EXPERIMENTAL MODEL

STUDY FOR A SUPERCONDUCTING MULTI-GEV PROTON LINAC

H. Schopper
Karlsruhe, Germany

A study group has been established which will investigate the problems connected with a high energy superconducting linac. This type of accelerator has been selected for various reasons, the three most important of which are:

1. The experience with synchrocyclotrons has shown that for many experiments high currents are useful only if combined with a high duty cycle.

2. The technology of a superconducting accelerator is interesting in itself.

3. If a proton accelerator is built in Germany, it should be of an advanced type and it should permit the production of strange particles.

The advantages offered by a superconducting linac seem to be so attractive that we think it worthwhile to make an effort to overcome the great difficulties and to take into account the unavoidable delay in the construction.

The study group will investigate the physical and technological problems of superconducting cavities at 1200 Mc. In addition, various accelerating structures will be studied at room temperature and 400 Mc.

Since experimental data for the production cross sections of secondary particle beams are very scarce between 1 and 10 GeV, calculations based on the statistical model are being performed in order to provide a basis for the final choice of the energy of the accelerator. It is hoped that a definite proposal can be worked out within 1 or 2 years.

In order to give an impression of the implications of such a project, a few very tentative figures may be quoted. A major advantage of a superconducting linac lies in the fact that,because of the small rf losses and the good vacuum high gradients can be used,resulting in a large energy gain/m. Values of about 5 MeV/m seem possible. For a disc-loaded structure this implies maximum magnetic fields of about 200 gauss compared to the critical field of 500 gauss for Pb and 1400 gauss for Nb.

Adopting an energy of 3 GeV, the accelerator length would then be only about 600 m. For a frequency of 400 Mc, and scaling the improvement factors q obtained at Stanford for Pb at 2800 Mc to this frequency, one expects $q \simeq 40{,}000$ or perhaps even more if other superconductors are used. With an average shunt impedance of 20 M Ω/m (which seems conservative, considering the new structures discussed at this conference), one calculates a power loss for lead of P = 40 kW which has to be cooled away at liquid He-temperature.

The refrigeration system able to achieve this will require an input power of about 20 MW and is estimated to cost approximately 6 M$. Since the saving on the rf system is much higher, it is to be expected that a superconducting linac will not be more expensive than an ordinary linac with the same energy but a much lower duty cycle.

NAGLE: What current do you expect to get?

SCHOPPER: The current will be limited mainly by the shielding and the power the target can stand. Most of the rf power will go into the beam, of course. Assuming a current of 100 μA, the beam power would be 300 kW compared to the power loss of 40 kW.

MARTIN, J. H.: Do these figures push you uncomfortably high in rf magnetic field strengths?

SCHOPPER: No, it depends on the structure of course. If we assume the ordinary iris-loaded structure, then the maximum field that you get is 260 G compared to the critical field for lead of 500 G, and 1400 G for Miobium. I forgot to mention that in calculating the power, I assumed an average shunt impedance of 20 MΩ/m, which I think is on the safe side.

WORSHAM: Have you looked at the problem of how you would build the cryostat?

SCHOPPER: We haven't made any detailed studies. This will be one of the tasks of the study group.

DICKSON: Have you done any rf measurements yet on superconducting surfaces?

SCHOPPER: Not yet, but we hope to start in about two months.

GUILBAUD: The rf magnetic field you mentioned is related to the 40 kW energy loss?

SCHOPPER: Yes, the field is proportional to the energy gain per meter which in turn is related to the energy loss.

THE NEW ZGS INJECTOR PROPOSAL

Rolland Perry
Argonne National Laboratory

The history of accelerators shows that as each one becomes operational and as new experiments are designed, there is an ever increasing demand for higher beam intensity or higher energy, or both. The ZGS is no exception to this rule. Consequently, we are presently considering an improvement program for the ZGS which includes (a) a new 200 MeV, high intensity injector system, (b) remodeling of the ZGS rf system to accommodate larger beams, (c) rebuilding of the ZGS inner vacuum chambers to withstand full atmospheric pressure and to eliminate the likelihood of radiation damage, and (d) provisions for remote handling of targetry and other highly radioactive components in the ZGS.

I shall discuss only the proposed injector system.

In the early planning of the Zero Gradient Synchrotron (ZGS), it was conservatively estimated that a 50 MeV linac could be expected to inject into the ZGS a proton beam of about 5 mA with pulse lengths of about 200μsec. This would give about 6×10^{12} protons per pulse; and assuming a capture efficiency of 50% for the ZGS, the latter should then be able to accelerate about 3×10^{12} protons per pulse to full energy. As this was nearly two orders of magnitude higher than the achievements of any then existing proton synchrotron, it was expected that the ZGS would be in a very favorable position with respect to beam intensity for some time after its completion.

When the parameters for the ZGS were finalized, the space-charge limit was determined to be about 2.6×10^{13} protons per pulse after bunching for a 50 MeV injected beam.[1] To reach this level would require an injected beam of 50 mA from the linac. Up to the present time the 50 MeV linac has injected 17 mA into the ZGS. Presumably, with careful adjustment of all parameters, 50 mA might be achieved with the rf power available. This will bring the injected beam approximately to the space-charge limit of the ZGS.

Consideration of how it might be possible to increase the output of the ZGS beyond the inherent existing space-charge limit led to the realization that increase of the injection energy would push the space-charge limit to a higher level and thus permit acceleration of a larger number of particles per pulse. Furthermore, increasing the energy of the injected beam will reduce its angular divergence and thus permit injecting through a

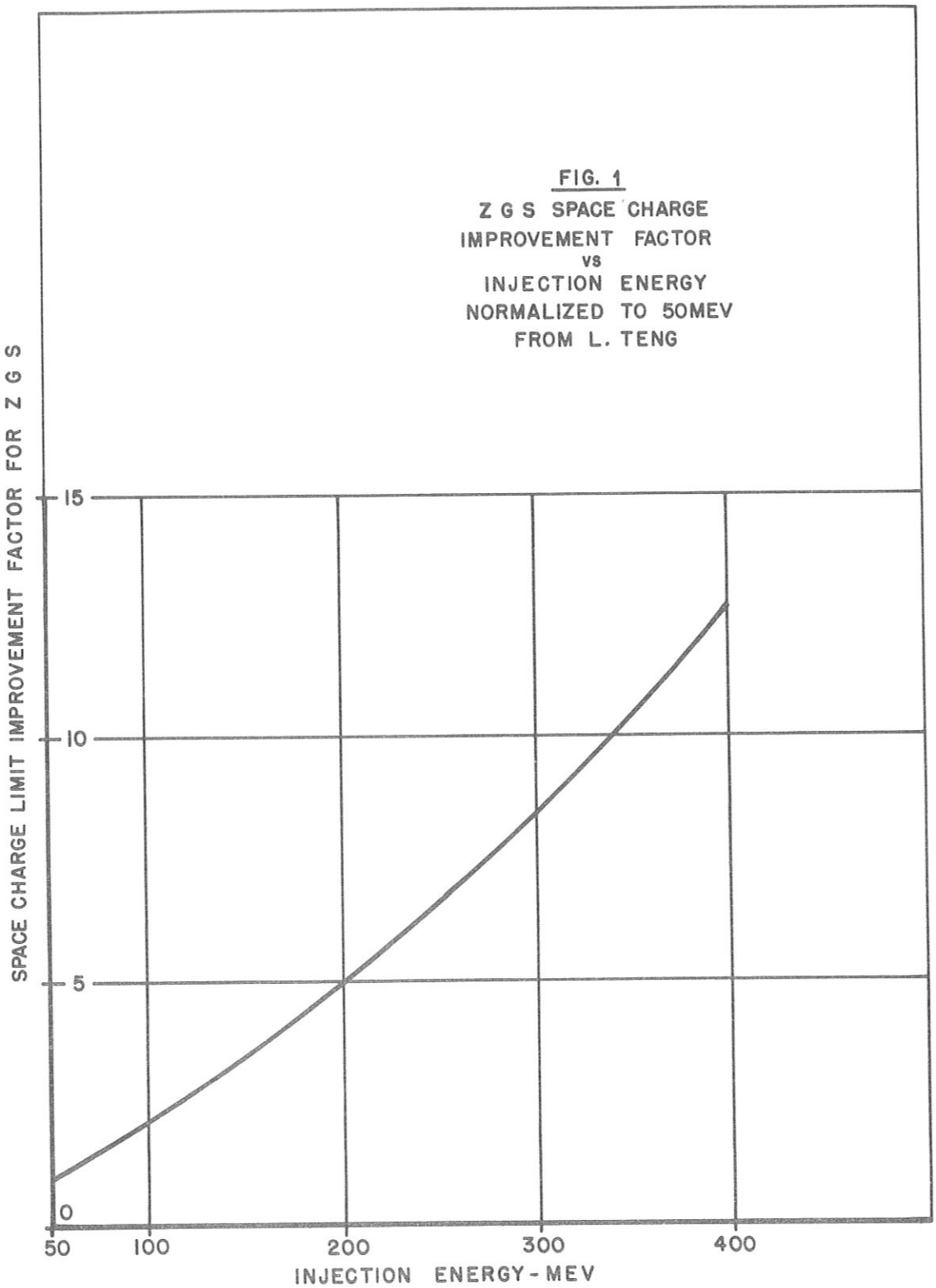
FIG. 1
Z G S SPACE CHARGE
IMPROVEMENT FACTOR
vs
INJECTION ENERGY
NORMALIZED TO 50MEV
FROM L. TENG
SPACE CHARGE LIMIT IMPROVEMENT FACTOR FOR Z G S
15
10
5
0
50
100
200
300
400
INJECTION ENERGY - MEV

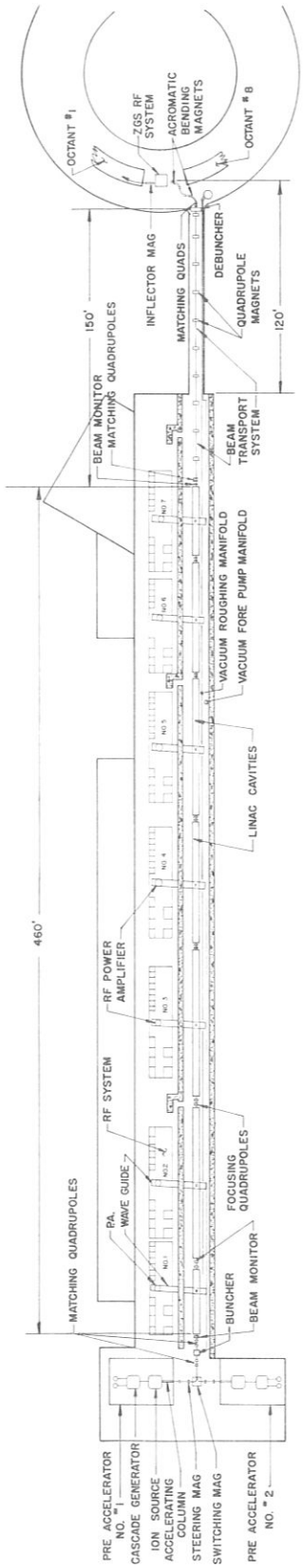

FIG. 2
200 MeV INJECTOR SYSTEM FOR THE
ZERO GRADIENT SYNCHROTRON

smaller aperture into the ZGS, with the consequence that, by decreasing the rate of rise of the ZGS guide field, the injection time can be increased to about 400 μ sec.

The space-charge limit of the ZGS at injection increases with injection energy somewhat more rapidly than linearly, as shown in Fig. 1 up to 400 MeV.

However, as the intensity of an accelerator rises, shielding requirements also increase. The safe limit of intensity for the ZGS basic shielding is believed to be about 10^{14} particles per pulse, which imposes a practical upper limit on injection energy.

Choosing an injection energy of 200 MeV provides an increase in the ZGS space-charge limit by a factor of five above the limit at 50 MeV, which would just about match the limit of the basic shielding.

The proposed injector system is comprised of the following major components shown in Fig. 2.

A 750 keV preaccelerator, including an ion source and ion focusing and accelerating elements.

A beam transport system and beam analysis system for the 750 keV ion beam.

An ion buncher for phase bunching of the ion beam.

A 200 MeV linear accelerator, comprised of seven or eight separate cavities, each driven by a high-powered rf amplifier and all properly phased together and locked to a common rf oscillator.

A beam analyzing and beam transport system for the 200 MeV proton beam.

A set of achromatic deflecting magnets to conduct the proton beam into the Zero Gradient Synchrotron and place it on its proper orbit.

It is planned to inject the 200 MeV beam into the ZGS at the No. 1 straight section but along a beam line which will permit building and testing the new system completely, except for the beam transport and debuncher portion, before disturbing the existing system. It is expected that a period of three years will be required for construction and testing and about six months for installation of the connecting equipment and modifications to the ZGS equipment.

Two complete preaccelerators are planned in order to reduce the probability of down time of the ZGS facility due to ion source or other preaccelerator problems. The beam switching magnet will permit use of either preaccelerator beam for injection. At the same time the beam from the other preaccelerator could be deflected in the opposite direction for beam analysis, etc.

The parameters selected for the preaccelerator are as follows:

Beam energy	750 keV $\pm$ 0.1%
Peak proton beam current	200 mA
Beam pulse duration	400 - 800 μsec.
Pulse repetition rate	5 - 10 per sec.
Beam emittance	10 π - 17 π cm-mr.

An ion source development program is presently under way, including investigation of the Russian plasma expansion cup idea. Also, in cooperation with MURA personnel, plans are being made for testing short accelerating column designs, with the hope of attaining improved beam quality by use of rapid acceleration in a controlled field configuration.

The beam from the preaccelerator will be focused through the apertures of a multiple-harmonic buncher by a set of quadrupole magnets and will be matched into the first cavity of the linac by another set of quadrupole lenses. Beam pulse transformers, Faraday cups, and beam-defining slits will be placed appropriately along the beam path to permit amplitude and beam quality measurements ahead of the linac. An electrostatic deflection type fast beam chopper will also be placed ahead of the linac.

Because the linac is to serve the ZGS with high efficiency, the parameters chosen should be such as to meet all the minimum requirements without imposing stress on any components. The following parameters are based on this basic philosophy.

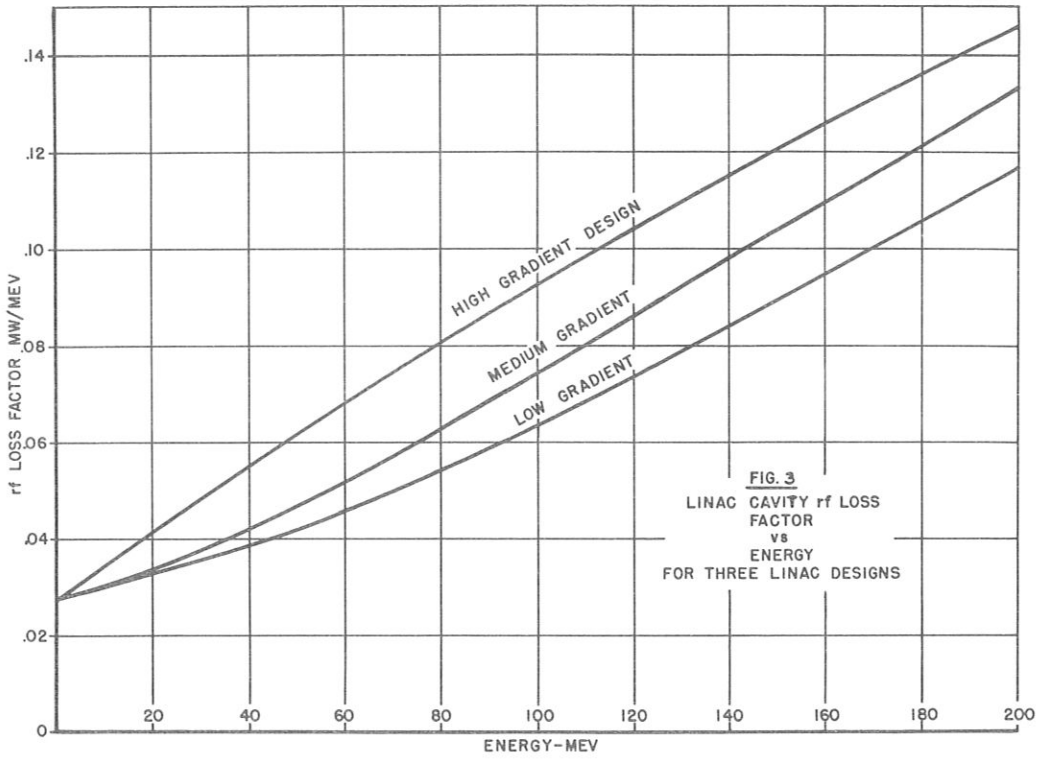

FIG. 3
LINAC CAVITY rf LOSS FACTOR vs ENERGY FOR THREE LINAC DESIGNS

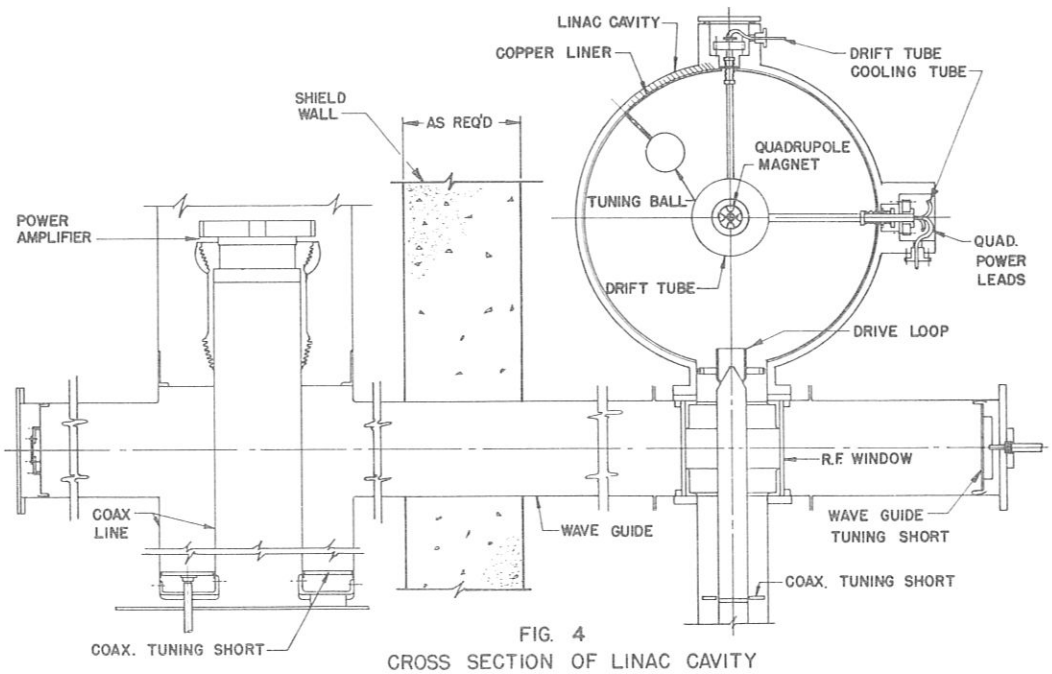

FIG. 4
CROSS SECTION OF LINAC CAVITY

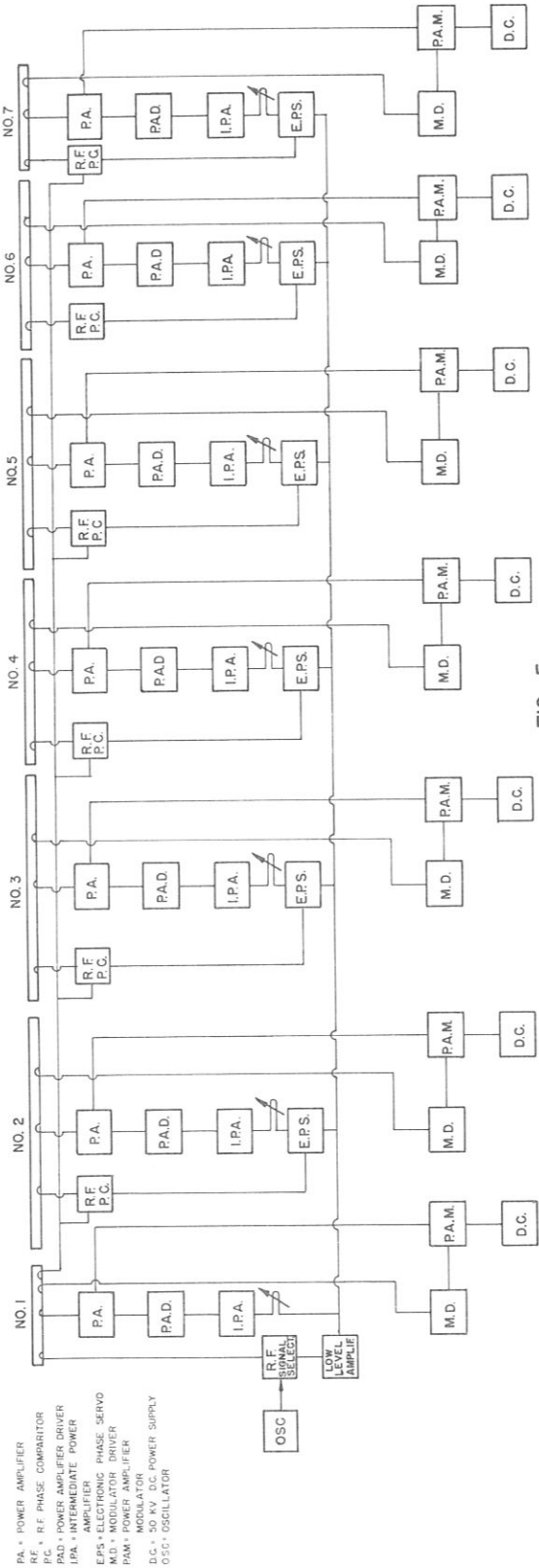

FIG. 5

BLOCK DIAGRAM OF THE R.F. SYSTEM FOR THE 200 MeV LINAC

Linac Parameters

Item	Value
Number of Cavities	7 - 8
Input Energy	750 keV
Final Energy	200 MeV
Input Current (protons)	150 mA
Output Current	100 mA
Transverse Phase Acceptance	17π cm-mr
Output Beam Emittance	4.6π cm-mr
Repetition Rate	5 per sec
Beam Pulse Length	400 - 500 μ sec
RF Pulse Length	1000 μ sec
RF Duty Factor	0.5%
RF Losses in Cavities	17 MW
RF Power for Beam Acceleration	16 MW
Temperature Stability	$< \pm 0.25^{\circ}$ C

The linac will be comprised of seven[2] separate cavities, each powered by a single rf amplifier capable of at least 5 MW peak rf power. The parameters of each cavity will be so chosen as to give the most efficient division of rf power, P_n, between cavity losses and beam power at the design beam current, I. The incremental energy gain, ΔW_n, for the n^{th} cavity when this condition is satisfied is given by

$$\Delta W_n = \frac{P_n}{L_n + I} \quad \text{(MeV)}$$

where $L_n \equiv$ average rf losses/MeV in the n^{th} cavity.

The rf loss factor, L_n, is a function of drift tube and cavity geometry. For a given cell it increases with drift tube diameter. It also increases with energy since drift tube lengths must increase with energy. It is also proportional to the square of the mean rf gradient, E_o, in the cavity. Figure 3 shows the general behavior of this factor as a function of energy for three different 200 MeV linac designs computed by MURA personnel who are cooperating with ANL in the design of the linac.

The linac cavities will be much like the present 50 MeV cavity. A cross section through the cavity and drive line is shown in Fig. 4. RF power from a power amplifier is coupled via a coax transition into a rectangular wave guide. At the linac end of the wave guide, power is

coupled through a cylindrical ceramic window into a short coaxial line which is terminated by a coupling loop at the linac cavity. The loop penetration is adjustable, and irises in the wave guide, together with tuning shorts at the ends of both wave guide and coax lines, permit impedance matching.

Drift tubes will be of the cylindrical type, which MURA people have computed, because of the simplicity of this design and the resultant economy of fabrication. However, the drift tubes for the first cavity may be of the Christofilos type, used in the existing injector, because the computer program is not yet capable of giving reliable results below 20 MeV. A dc quadrupole magnet will be installed in each drift tube although they may not all be necessary at the high energy end.

The type of tuner has not been established although ball tuners similar to those in the existing linac are being considered. It is believed from our experience in setting up the field distribution in the 50 MeV linac that a tuner in each cell may be very desirable, and this is presently being planned. For slow servo tuning of an entire cavity, an eccentric bar running along the cavity wall offers an interesting possibility.

Each of the cavities of the linac must be driven at the same rf frequency, and each must have the proper phase and amplitude. Because of the relatively large beam loading expected and the variation of cavity shunt impedance with energy, amplitude control must be either preprogrammed or servo controlled. Phasing also will require fast servo control.

The rf system is shown in block diagram form in Fig. 5. Each of the amplifier chains will be identical in operational requirements, and each will be separately controllable. The following table lists the specific requirements of the system.

Performance Specifications for the 200 MeV Linac RF System

Item	Value
Operating Frequency	201.25 Mc/sec
Pulse Length, Variable to	700 - 1000 μsec
Pulse Repetition Rate, Variable to	0.5 - 5 per sec
RF Duty Factor	0.035% - 0.5%
Number of Power Amplifiers	7 - 8
Peak RF Power per Amplifer	5 MW
Total Peak RF Power	33 - 37 MW

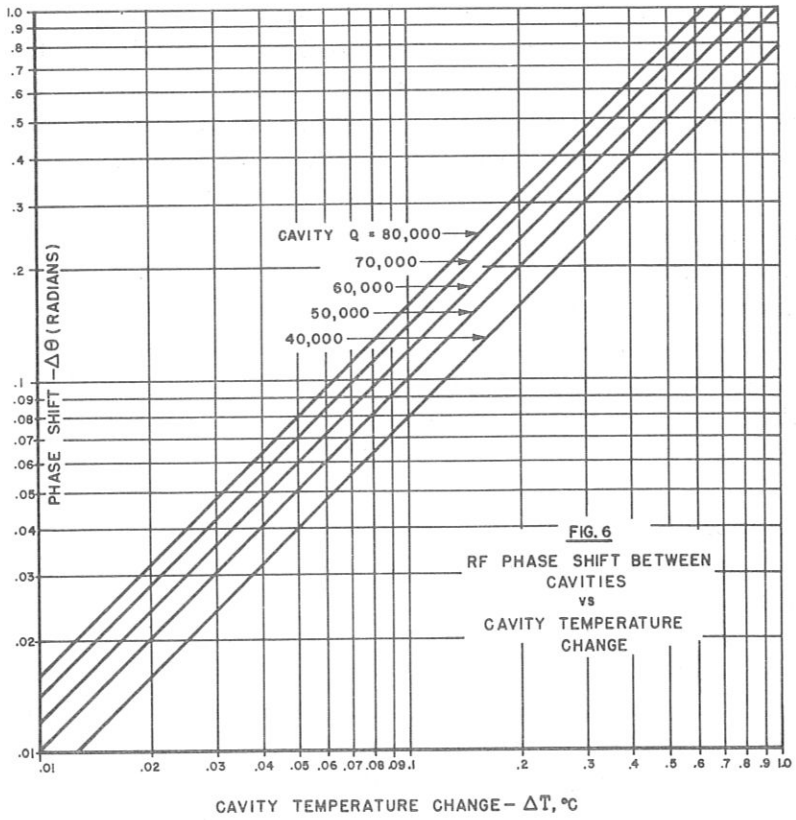

FIG. 6
RF PHASE SHIFT BETWEEN CAVITIES
vs
CAVITY TEMPERATURE CHANGE

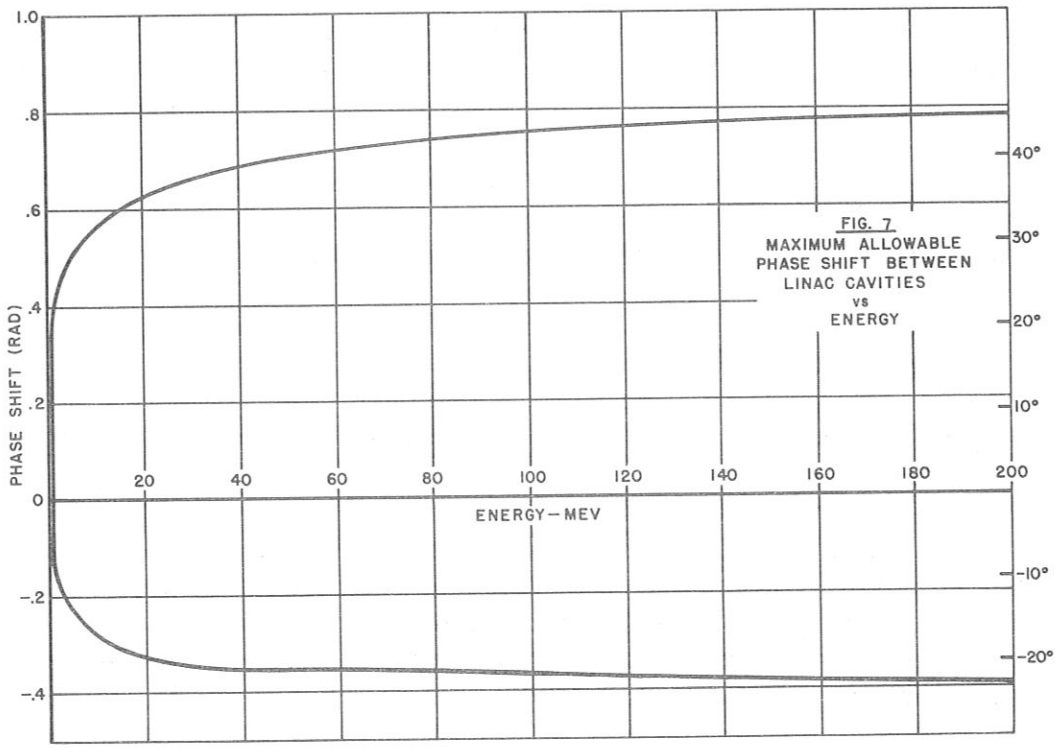

FIG. 7
MAXIMUM ALLOWABLE PHASE SHIFT BETWEEN LINAC CAVITIES
vs
ENERGY

The rf system, shown in Fig. 5, will consist of seven rf power amplifiers (PA's), one for each of the linac cavities. Each PA will use a single RCA 7835 super-power triode rated at 5 MW peak power and will be driven by an amplifier chain, capable of supplying approximately 160 kW peak drive power. The amplifier chains will be excited by a single low level oscillator-amplifier system so that all final amplifiers will be driven at a single frequency and at controllable relative phase, maintained by fast servo systems at the low level amplifier stages. This arrangement will permit independent testing of each of the rf amplifier systems and of the cavity it drives. It will also preclude interaction between one PA system and any other. Thus, from the standpoint of tune up and trouble diagnosis, this system will be most versatile. By eliminating interactions at the high power levels, it will be more reliable than with high level coupling.

A separate amplifier chain will drive the buncher and debuncher in order to avoid the effect of beam loading interactions on the amplitude and phase of these cavities.

It is proposed in the new system to use the same scheme that is presently in use on the 50 MeV linac in maintaining frequency stability; i.e., the rf system will be driven from an oscillator until the rf level in the linac cavity reaches approximately the accelerating gradient. At this time, a signal from No. 1 cavity will be gated on in place of the oscillator so that the No. 1 cavity will thereafter be driven at its resonant frequency. All other cavities would be driven at this same frequency, and all would, of course, require very good thermal stability in order to resonate at or near the same frequency, as $\frac{\Delta f}{f} = - \alpha \Delta T$, where α is the coefficient of thermal expansion for the cavity metal.

A further consequence of cavity temperature change is the phase shift resulting from driving a cavity at a frequency different from resonance. The magnitude of this phase shift is proportional to the Q of the cavity, i.e.,

$$\theta \simeq - 2 Q \alpha \Delta T .$$

Figure 6 shows the magnitude of the phase shift as a function of temperature for a few values of Q.

Taking into account the phase damping that can be expected, one can set an upper limit to the magnitude of phase shift between cavities that can be tolerated without loss of particles. As the phase damping is proportional to $\beta^{-3/4}$ one finds that the maximum allowable phase shift varies with energy, as shown in Fig. 7.

This in conjunction with Fig. 6 indicates that cavity temperature stability must be good to $\pm$ 0.25° C in order not to spill particles from the phase bucket in successive cavities. Considering energy spread and other factors, the thermal stability must be very much better than this.

The shape of the curves in Fig. 7 suggests that, since there is still considerable phase damping after the 10 MeV region, it would be desirable to design the first cavity of the linac for 20 MeV or even higher energy. In the ANL case, since we propose to use identical amplifier systems for each of the linac cavities, it will be advantageous to design the first cavity for 20 MeV or more in order to reserve more rf power for the remaining cavities. These are the two main reasons for designing the first cavity for 20 MeV rather than 10 MeV.

SYMON: I didn't see why this diagram that you have here really shows what the tolerance is on the phase shift. If you had one single phase shift that occurs, then I can see that this diagram is relevant, but if you suddenly jump the rf phase, then the packet moves over to where you have shown. If that situation lasts for on the order of a phase oscillation, you have smeared the packet around the boundary so that you no longer can tolerate another jump in phase. The packet is now equal to the full bucket size.

PERRY: Yes, what I showed on the curve was the maximum phase shift.

SYMON: Yes, but it would seem to me that what you are really interested in is a series of small phase errors from tank to tank, which occur at intervals that are short compared to a phase oscillation. Then I don't see that the diagram that you have drawn is relevant.

PERRY: In the case of which you are speaking, it is true, it is not relevant. I was looking only at the maximum phase shift allowable due to frequency shift or temperature change between the first and any successive cavity without loss of particles. This essentially places a maximum tolerance on frequency control or cavity temperature stability. The maximum allowable temperature variation of any cavity would be $\pm$ 0.25°C just to prevent particle spill, and in order to keep the phase spread, and thus the energy spread, to a minimum the temperature stability would have to be very much better than that.

REFERENCES

1. Expected Beam Intensities of the FFAG and ZGS Accelerators, Report to the Atomic Energy Commission of the Ad Hoc Committee, July 31, 1963.

2. Young, D. E. and Austin, B., "Design Study of 200 MeV Injector for ZGS," MURA Technical Note TN-469, April 7, 1964.

PRELIMINARY DESIGN OF A HIGH ENERGY HIGH DUTY CYCLE PROTON LINEAR ACCELERATOR

H. Leboutet, G. Guilbaud, Kervesic, Mangin, Tran
CSF - Compagnie Générale de Télégraphie Sans Fil - France

(Presented by G. Guilbaud)

One of the applications of proton linacs considered these days is the production of intense π meson beams. Roughly, this will be best achieved by use of protons of energies higher than 500 MeV. A high average current, of several hundred microamperes is desired, together with as high a duty cycle as possible.

The advantages of the linear accelerator for this application have been discussed at great length in many publications. The main one is extraction of the total beam current and the related absence of any induced radioactivity in the machine. Another is energy variation.

The Institut de Recherches Nucléaires of Strasbourg is planning to build such a meson factory and we have been attempting to evaluate the technical and financial implications of such a project. Work started about a year ago and this paper describes the present status of it.

Desired Performance

The performance we have been asked to take as an objective are the following: energy higher than 500 MeV, up to 800 MeV, average current: 200 μA, to be increased to 1 mA after some time of operation; duty cycle: 5%, this being essentially defined by the present state of the art for microwave tubes. These objectives are very similar to those of other projects and the following arguments are also the same. In short, the 200 Mc/s Alvarez structure cannot be used efficiently after some 150 or 200 MeV. One needs to look for other structures at higher frequencies, which implies a frequency jump at some point.

Our preliminary design has been guided by the following:

(a) Try and use a low voltage injector, to avoid pressurization.
(b) Limit the frequency jump to a minimum.
(c) Make the project as a whole as cheap as possible.

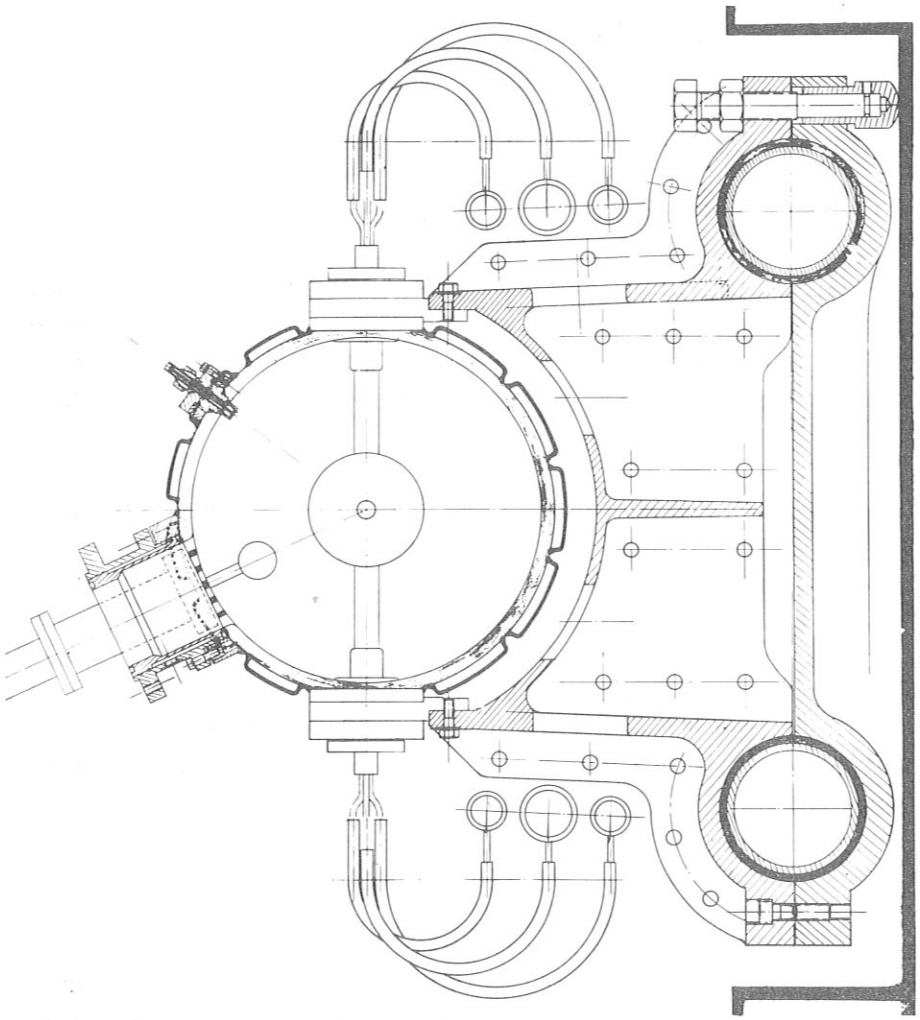

Fig. 2

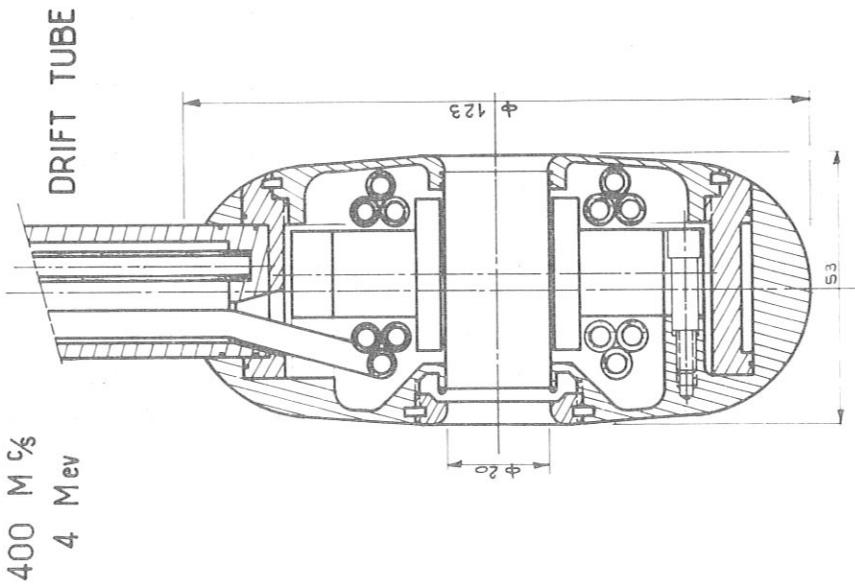

Fig. 1

Choice of the Accelerating Structures and Frequencies

A number of arguments make it desirable to operate at frequencies as high as possible at low energy: Shunt impedance is higher, the jump to the higher frequency will be smaller, and the filling time of cavities will be reduced, resulting in shorter pulses for the rf.

However, a number of practical reasons oppose this. The main one is the necessity to house, in the drift tubes, quadrupoles of a sufficient strength to compensate the rf defocusing effects.

Having looked into this with some detail, it appears that operation at 400 Mc/s at the low energy end of the machine is possible. Two possibilities have been considered.

(a) One is to inject 3 to 4 MeV protons. The general dimensions of the drift tube are then given by Fig. 1. The outer diameter is a little over 12 cm. The length is 5.3 cm. A model quadrupole is being built for magnetic testing. These figures, of course, are indicative. These lead to the general dimensions of the Alvarez structure, as shown on Fig. 2. It can be seen that the diameter of the cavity is of the order of 40 cm at most. The drift tube supports are shown here in alternate horizontal positions. This may not be final. One must position all parts so as to have enough perimeter for the water cooling which will have to be very efficient since dissipation will be of the order of 10 kW/m.

Models of 400 Mc/s Alvarez are being tested for shunt impedance requirements.

From the technological point of view, we are investigating the possibility of using an electrolytic copper tubing, supplied by a European firm who claims very good conductivity. The water pipes could be provided in the thickness of the copper, and the design of Fig. 2 could be greatly simplified.

Figure 3 shows the general structure of a tank and its support. The electrolytic tubing comes in 8 m lengths and, of course, tolerances being those of the mandril, a very precise tank can be obtained, avoiding the use of correcting bars.

(b) Another possibility is to operate on the $2\beta\lambda$ mode, at reduced rf electric field. At 500 kV/m, one is led to inject 750 kV protons into a 400 Mc/s Alvarez structure. These values correspond to the same quadrupole strength and drift tube size as before, so that Figs. 1, 2, and 3 give approximately the dimensions of a first cavity which could be used

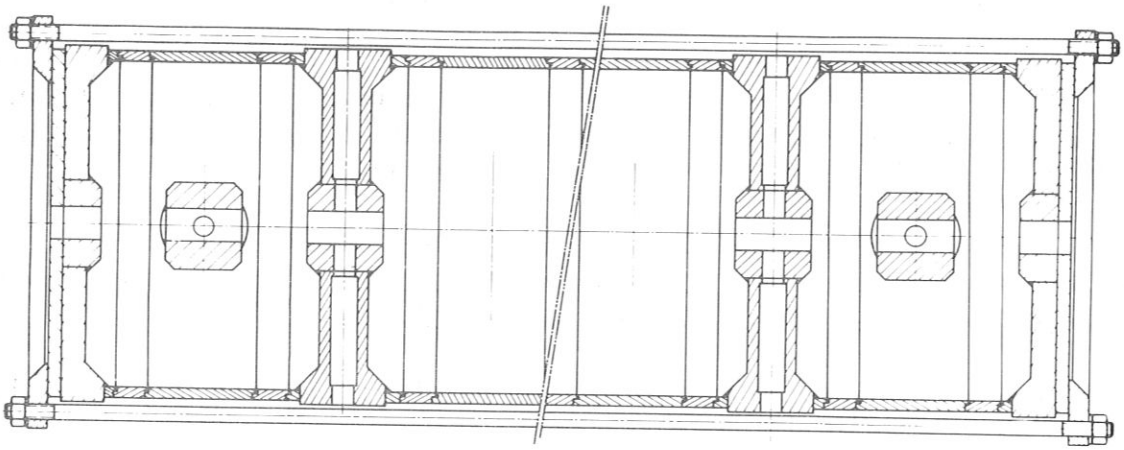

Fig. 3 400 Mc/s CROSS BAR EXPERIMENTAL MODEL

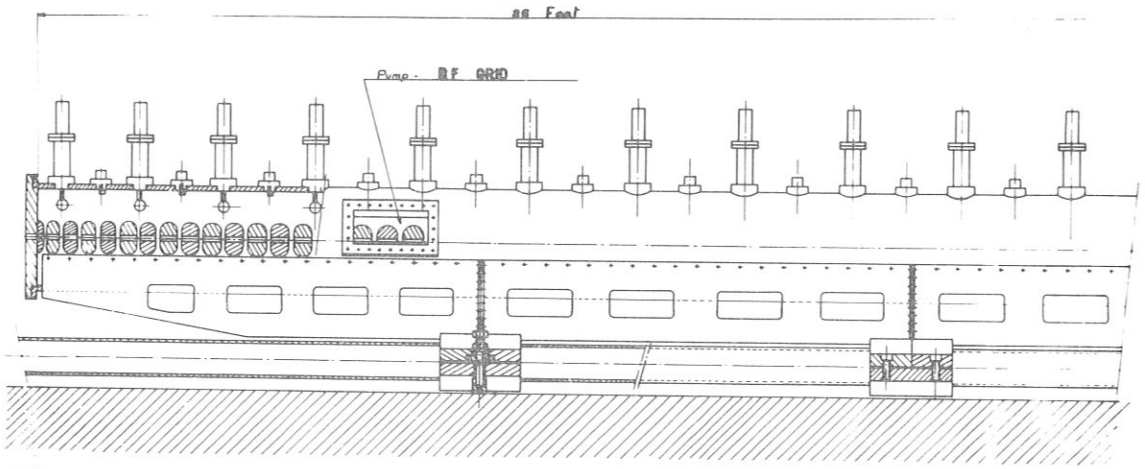

Fig. 4 400 Mc/s ALVAREZ CAVITY

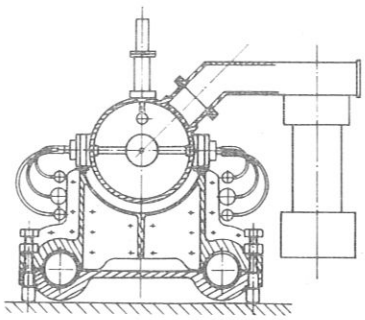

to take the protons from 0.750 to 4 MeV, where they would enter an ordinary $\beta\lambda$ Alvarez structure at 1.8 to 2 MV/m.

This low injection voltage is very attractive. Of course, it involves taking some precautions. The main one is to reduce the drift tube inner hole diameter, to limit transverse field variation effects. According to $\frac{2\pi A}{\gamma^2 \beta\lambda} \leq 1$, the hole should not exceed 1 cm in diameter. Since the peak current will be of the order of 10 A, this should not be a difficulty.

The 400 Mc/s Alvarez structure should be used for the first 100 MeV. After this, a number of other structures might prove useful, and we are presently investigating two main types.

(a) The first is the general class of bar structures. A model is presently being built according to the drawing of Fig. 4. The model will allow making measurements on X bar structure, on the interdigital structure, by suppressing half bars, and a number of intermediate ones, by varying the angle from one cell to the next. Measurement may be underway presently and results are expected in September or October.

(b) The second class is that of iris loaded structures. Our electron linear accelerator work has been done with the $\pi/2$ disc-loaded circular waveguide. Since a passband may be desirable here, variations of this guide should be used. We are investigating the one that was previously examined for backward wave oscillations at CSF; we call it the diabolo line. The discs are cut by two very wide slots, about 120^{o} wide, and the remaining sectors are not aligned from one cell to the next, but at an angle, which gives wide band characteristics. This circuit is about half way between the cross bar and the disc-loaded waveguide. Measurements made last fall with very low values of β are now extended to the region of β_s corresponding to 100 MeV. Such structures should be used after some 100 or 200 MeV, at an 800 or 1200 Mc/s frequency. The choice of the step energy will depend very much on the results of shunt impedance measurement. In any event, after 100 MeV, focusing can be made by magnetic doublets or triplets between short sections, of 4 to 5 m, so that the structure can be chosen without taking in account any focusing inside it.

Before turning to the general design of the machine, we should like to point out that beam-loading effects will bear heavily on the choice of the accelerating structure. We have just started an analysis of these, to understand them and determine their amplitude and ways of correcting them. It is our feeling that resonant π modes should be avoided because they lead to very large field amplitude variations and also to very large phase shifts along the structure, causing great difficulty during the beam-loading

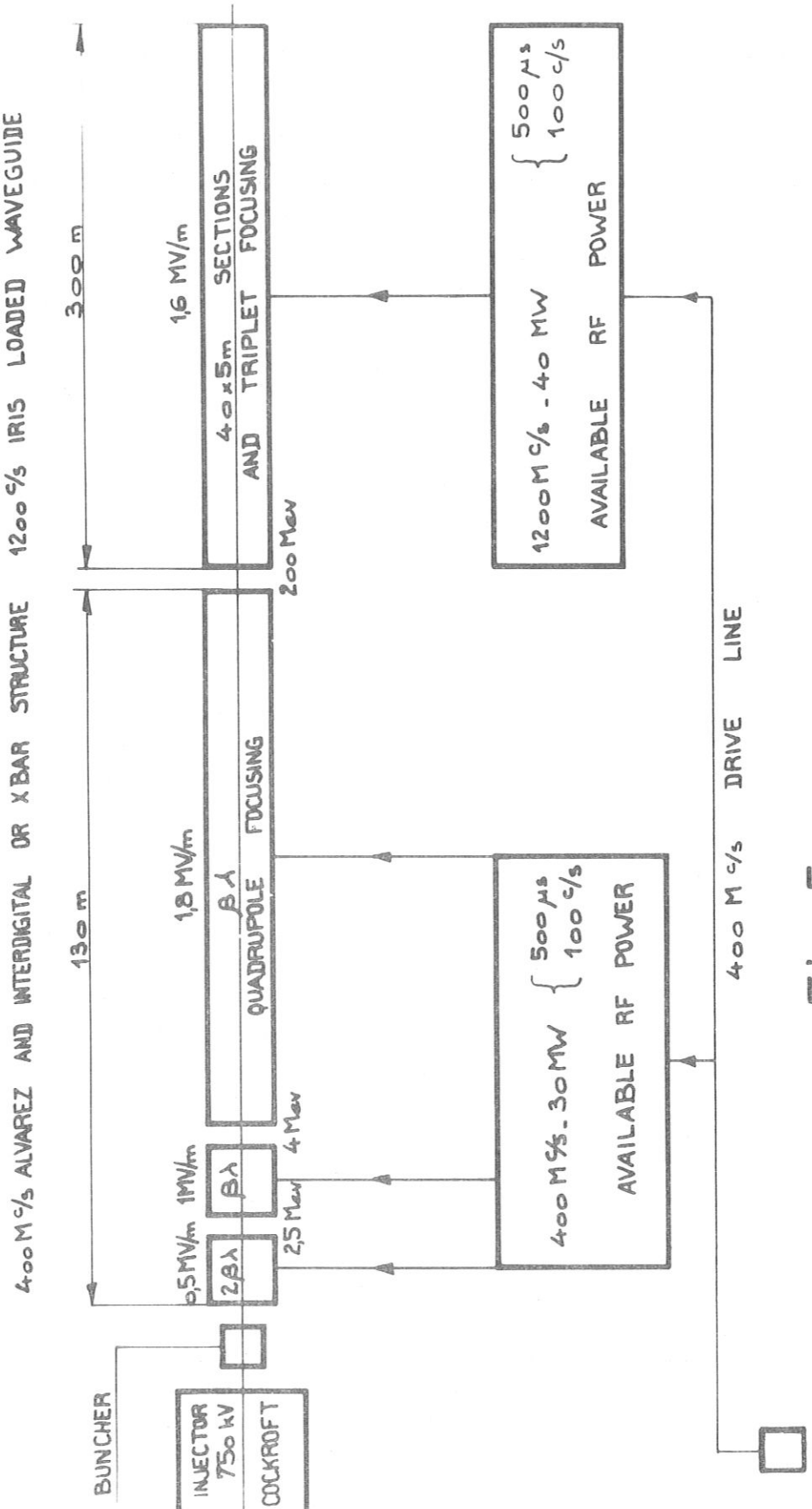
400 M c/s ALVAREZ AND INTERDIGITAL OR X BAR STRUCTURE 1200 c/s IRIS LOADED WAVEGUIDE
BUNCHER
INJECTOR 750 kV
COCKROFT
0,5 MV/m
2 βλ
1 MV/m
βλ
2,5 Mev
4 Mev
1,8 MV/m
βλ
QUADRUPOLE FOCUSING
130 m
200 Mev
1,6 MV/m
40 x 5m SECTIONS
AND TRIPLET FOCUSING
300 m
400 M c/s - 30 MW
500 μs
100 c/s
AVAILABLE RF POWER
1200 M c/s - 40 MW
500 μs
100 c/s
AVAILABLE RF POWER
400 M c/s DRIVE LINE

Fig. 5

transients. We would greatly favor the use of short travelling wave sections, where these effects will remain very small, at the cost of some complication in the use of residual power at the end of the sections. This subject will be studied in the next year; it may prove to be the most important criterion in the choice of the design.

General Design

As can be understood from above, we have not yet determined our exact choice for the circuit to be used at high energies. However, if we assume that the effective shunt impedance will average to 25 M Ω /m along the machine, one can fairly well determine its composition, including length, rf power, and later, the cost.

Figure 5 shows our present design, for the following performances:

500 MeV
4 ma peak accelerated current
5% duty cycle

Since the filling time at 400 Mc/s will be some 50 to 70 μs, 500 μs beam pulses can be used, which is very good for the higher frequency power tube.

First, we use a 750 kV Cockcroft, capable of 20 ma at 5% duty cycle. It is followed by a buncher, including beam transfer lenses. Next comes a 2 $\beta\lambda$-400 Mc/s - 0.5 MV/m cavity, either up to 4 MeV, or only to 2.5 MeV. In the latter case, a short section on the $\beta\lambda$ mode but at reduced electric field takes the protons from 2.5 to 4 MeV. After that, we have assumed that 400 Mc/s structures are used up to 200 MeV and 1200 Mc/s structures afterwards. The step energy is not determined. We have taken it to be 200 MeV here. The rf power has been estimated on the basis of an average shunt impedance of 25 M Ω /m and available evaluation of beam-loading effects. The length and rf power have been chosen by economical arguments: the product of rf losses and accelerator length is a constant, and consequently cost goes up with length for the waveguide and building and goes down with length for the rf power. The result is shown on Fig. 5. The breakdown of this over-all design in units has not been determined yet. At 400 Mc/s and up, good klystrons can be made, and some U. S. firms are already producing them. Units of 300 kW to 5 MW would lead to the lowest cost. However, these would feed about 20 m of accelerating structure each, and, according to what is known of beam-loading effects, this power would then have to broken down to feed several shorter sections. In that respect, the rf pool idea proposed by Berkeley is a very attractive solution.

Summary

As can be seen, the past year has been used to determine the main problems to be solved for the construction of such a machine and to lay the general design. The year to come will be used essentially to measure new structures and choose which one offers the best compromise at each energy, to get a good understanding of beam-loading effects, and to make as close a cost evaluation as possible, by going into detailed mechanical and electrical design.

HUBBARD: With respect to your drawing on the board, do you think there is any advantage in skewing the angles at other than 90°?

GUILBAUD: Well, I think varying this angle will give you different pass bands and we will have to play with that.

HUBBARD: You do not have any obvious advantage in mind then?

GUILBAUD: This line was done at a time when we were working on wide-band tubes and were looking for wide pass bands and certain slopes for tuning of oscillators. Measurements made last fall do not show any great dependence of shunt impedance on this angle, but only of pass band, which may be of definite interest.

PROGRESS REPORT ON THE STANFORD LINEAR ACCELERATOR CENTER*

G. A. Loew
Stanford Linear Accelerator Center

A. Introduction

This report describes some of the highlights of the present state of construction of the Stanford 20 GeV Linear Accelerator. Comprehensive descriptions, statistics and specifications of the two-mile linear electron accelerator have been given on numerous other occasions[1] and will not be included here. By the nature of progress in our construction schedule, hopefully a substantial fraction of the information and pictures given in this report will soon become obsolete.

B. Building Construction

Figure 1 shows a cross section of the accelerator layout. Two buildings are seen. The lower one, underground, called the accelerator housing, contains the accelerator structure proper, supported by a 24-inch aluminum girder which also provides the optical alignment vacuum pipe to be used to align the two-mile machine. Three jacks are used to adjust the position of each 40-foot girder in the transverse plane. The upper building, called the klystron gallery, is separated from the accelerator housing by 25 feet of earth shielding. The gallery contains all the equipment necessary to power the accelerator and includes the klystrons, their associated microwave equipment, the modulators, vacuum equipment, utilities and over-all instrumentation. In Stage I of the construction program, there will be 240 klystrons with their individual modulators, each feeding four 10-foot long accelerator sections. The vertical tube connecting the two buildings, shown in the picture, is one of the waveguide runs which feeds two accelerator sections. Extra modulators in the gallery are shown to illustrate the configuration foreseen for Stage II when there will be one klystron per accelerator section, hence 960 klystrons and modulators. Plans for this expansion are not firm at this date.

Initial excavations on the SLAC site for the housing started in December, 1962. The construction of the accelerator housing began in June, 1963. Figure 2 shows the concrete slab and the beginning of the

---

*Work supported by the U. S. Atomic Energy Commission.

accelerator housing construction. Figure 3 shows the same building after completion of the concrete housing, on July 3, 1964. The first parts of the water-cooling system installation can be seen. The Klystron Gallery construction was started in November, 1963 and Fig. 4 illustrates the first few hundred feet of construction of that building. Figure 5 shows the inside of the klystron gallery with some installed utilities as well as the klystron supporting frame structure.

C. Accelerator Structure

Figure 6 illustrates some of the slow-wave structures investigated three or four years ago to optimize the accelerator structure of the two-mile machine in terms of shunt impedance, pumping speed and ease of construction. This figure is included here only because of the renewed interest in more complex accelerator structures for high energy proton accelerators, such as the cross-bar structure, the slotted-disk structure and the cloverleaf structure. It should be restated here that for a phase velocity equal to the velocity of light, the highest shunt impedance was obtained with the simple disk-loaded structure operating in the $\frac{2\pi}{3}$ mode. Although a higher vacuum pumping speed could be obtained with the so-called ventilated structure, it was not adopted because of the difficulties in maintaining tolerances on the ventilating holes.

The specific design of the disk-loaded waveguide accelerator structure has been described in detail elsewhere.[2] The accelerator sections using the constant-gradient design are presently under fabrication at SLAC at the rate of about two sections per day. Figure 7 shows the layout of the waveguide circuitry, from the 24 MW klystron through a window, a vacuum pumpout, a waveguide valve, a 3-db coupler, the waveguide feeds, two additional couplers, the input to the accelerator sections, the accelerator sections themselves and the output loads. The configuration of the waveguide as it is shown in the lower part of this figure has recently been modified because the need was found to feed the accelerator sections alternately from right and left. This alternation, called "operation flip flop", was found necessary because it was not possible to cancel entirely the asymmetry in the longitudinal electric field present in the first and last cavities of each section. Microwave measurements showed that both an amplitude asymmetry in the field as well as a phase shift of this field exist across the cavity in the transverse plane. Since the net effect of this residual amplitude and phase asymmetry is to create a transverse force on the electron beam, it was believed safer to alternate coupler inputs. The final result of "operation flip flop" was the building of sections such as the one shown in Fig. 8 with input and output couplers on the same side. However, the mode of coupling into successive sections is to follow

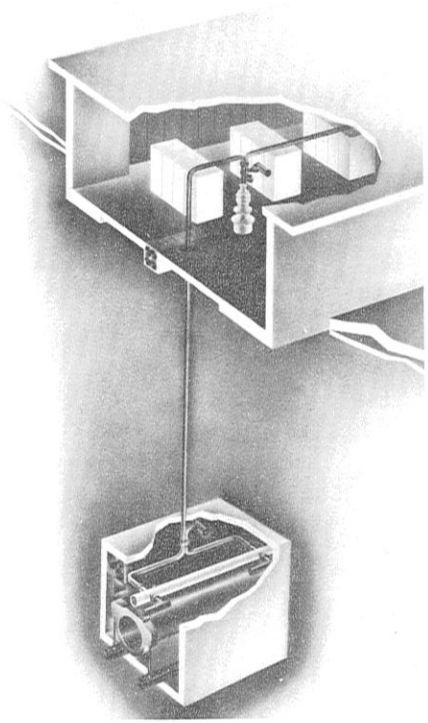

Fig. 1 Cross-sectional layout of klystron gallery (top) and accelerator housing (bottom).

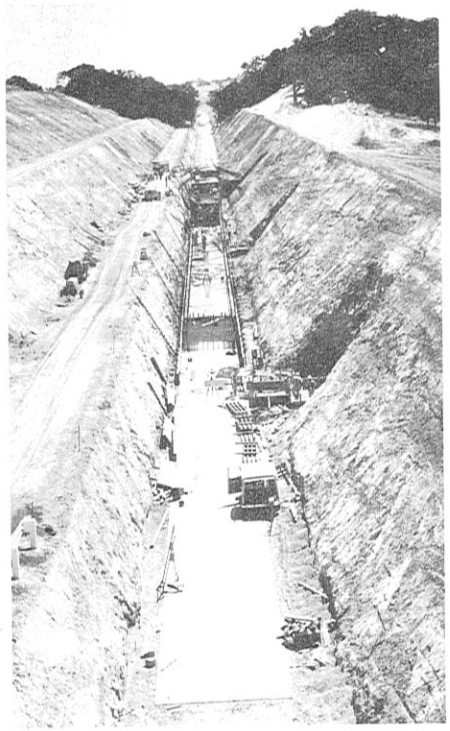

Fig. 2 Beginning of accelerator housing construction.

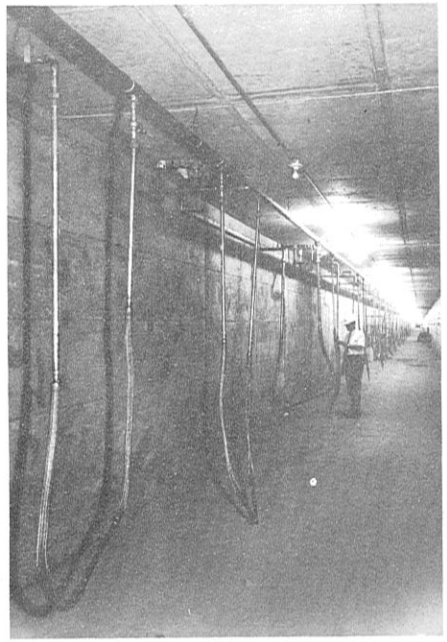

Fig. 3 Inside of accelerator housing shortly after completion.

Fig. 4 Beginning of klystron gallery construction.

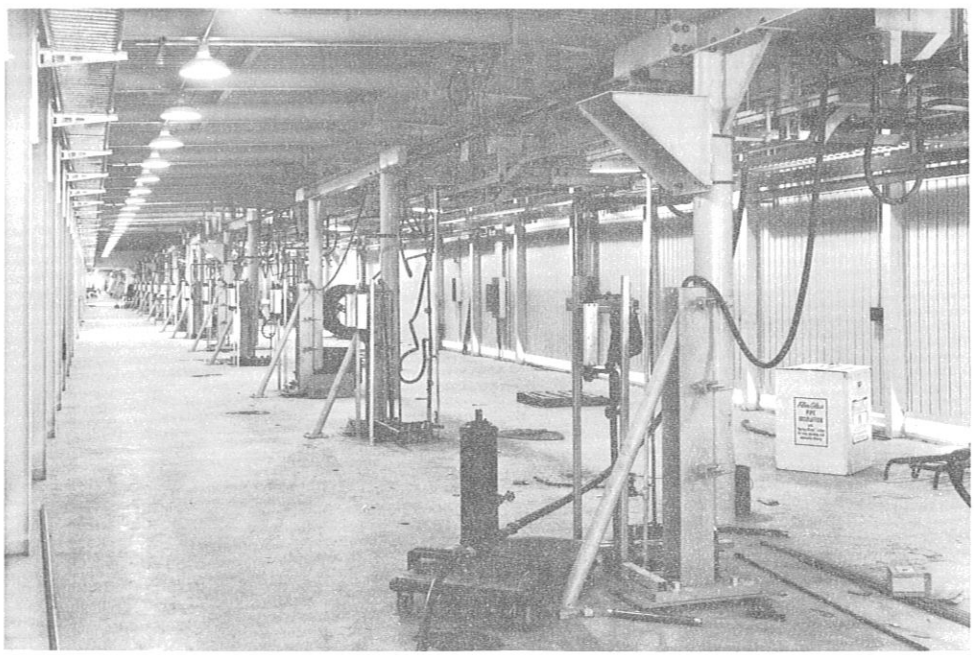

Fig. 5 Inside of first sector of klystron gallery showing utilities and klystron frame supporting structures.

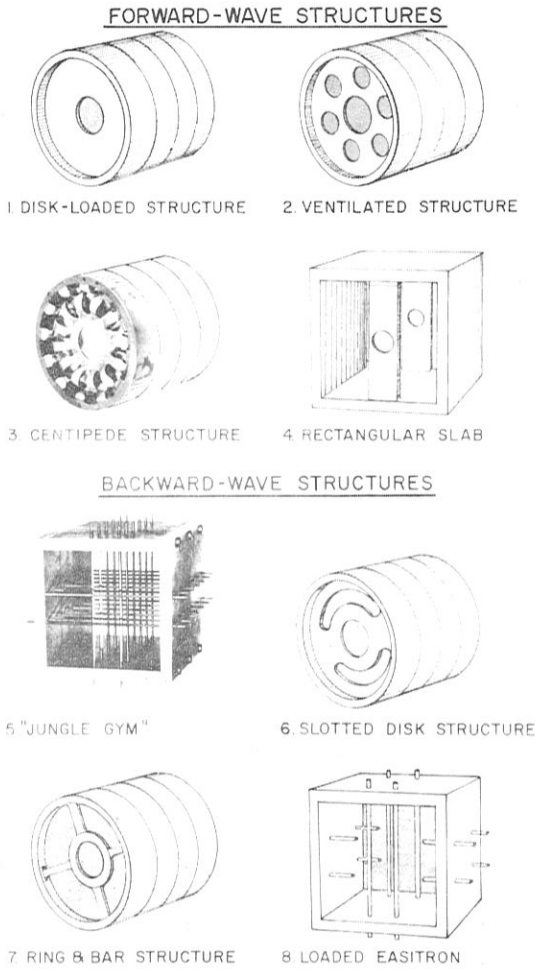

Fig. 6 Museum of forward- and backward-wave structures originally examined for use in the SLAC accelerator for $v_p = c$.

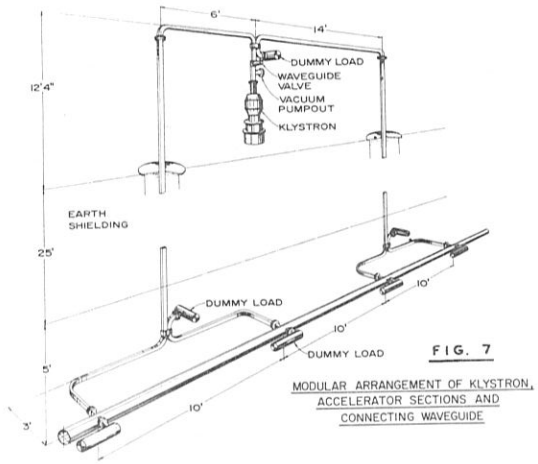

FIG. 7
MODULAR ARRANGEMENT OF KLYSTRON, ACCELERATOR SECTIONS AND CONNECTING WAVEGUIDE

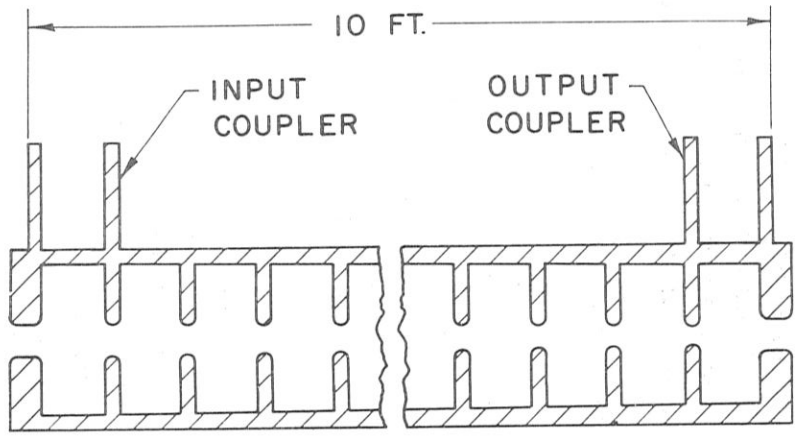

Fig. 8 Constant-gradient accelerator section.

the pattern right-left-right-left, followed by left-right-left-right. This is accomplished by rotating successive sections by 180 degrees. By this method, transverse deflections should cancel out. Over an 80-foot length, then, the beam should be back on axis and parallel to it without any increase in transverse phase space.

D. Drive and Phasing Systems

Figure 9 illustrates the microwave drive system from the master oscillator to the high-power klystrons. One main booster amplifier at 476 Mc/sec fed by a master oscillator powers the entire two-mile length of the drive system by means of a 3-1/8" coaxial line. Each of the 30 sectors into which the machine is divided obtains its rf power from a coupler in the main drive line. The frequency of the rf power is then multiplied by 6 by means of a varactor multiplier. The resulting 2856 Mc/sec rf power is then amplified by means of a sub-booster klystron to 60 kW of pulsed output power. Another coaxial line (1-5/8" diameter) feeds this rf power to each of the eight klystrons in a sector. The phase and amplitude of this signal is controlled by means of an isolator, a phase shifter, and an attenuator. A special protection attenuator is incorporated which automatically removes the rf drive power to the 24-MW klystron every time a major gas burst or modulator failure temporarily disables the klystron. The protection attenuator subsequently slowly restores this drive power to its former level, thereby preventing full output rf power from striking the klystron window instantaneously. As has been reported earlier, this procedure should prevent the frequency fractures and punctures of windows experienced in the Stanford Mark III accelerator.

Figure 10 illustrates the principle upon which the operation of the automatic phasing system for klystrons is based. It is known that when a klystron is correctly phased, the phase of the klystron output signal in the accelerator, E_W, is 180 degrees out of phase with the signal induced by the electron beam, E_e. Hence, maximum energy transfer is obtained from the klystron output wave to the electron beam, resulting in the resultant vector, E_R. On the other hand, if E_e is not 180 degrees out of phase with E_W, less than the maximum energy transfer takes place and one obtains a rotated resultant vector E_R as shown in the lower part of Fig. 10. This principle is used as follows. The klystron pulse is momentarily delayed in time, thereby allowing E_e to be compared in phase with a reference signal obtained from the drive line. A so-called "calibrating" phase shifter is used to null the output of a phase bridge under this condition. E_W is then compared with the reference signal and caused to be 180 degrees out of phase with E_e by means of the same phase bridge. This bridge consists of a magic T and is followed by a

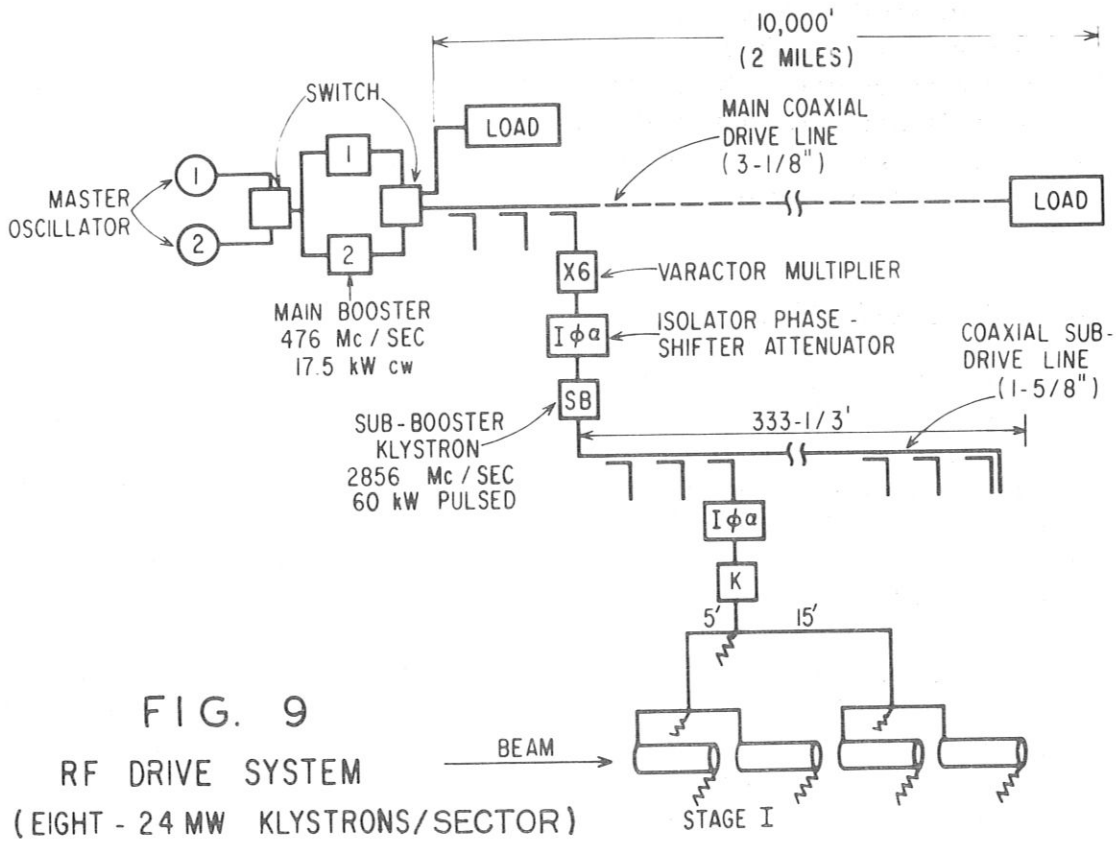

FIG. 9

RF DRIVE SYSTEM

(EIGHT - 24 MW KLYSTRONS/SECTOR)

ORIENTATION OF FIELD VECTORS
WHEN PHASING IS CORRECT

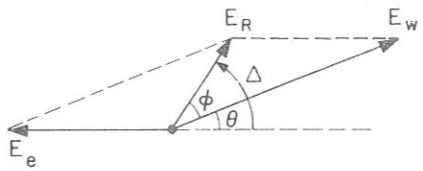

ORIENTATION OF FIELD VECTORS
WHEN PHASING IS INCORRECT

Fig. 10 Principle of automatic phasing system for klystrons using beam induction technique.

pair of linear thermionic diodes, a gated voltmeter, a phase wobbler and two servo amplifiers. These feed into the two windings of an ac motor which controls the rotation of the klystron phase shifter until a null is obtained. An automatic programmer causes all klystrons in a sector to be sequentially and automatically phased according to this technique. The operation should take no longer than one minute per sector.

E. Injection System

Figure 11 shows the main elements of the electron beam injection system to be used at the input to the accelerator. Briefly, this system will consist of a gridded gun, a prebuncher fed with approximately 1 kW of peak rf power and followed by a drift space, a constant velocity buncher (v_p = 0.75 c) and finally a standard accelerator section (v_p = c). The bunching process which results from this setup is illustrated in the lower part of the figure. An experimental injection system is presently being tested at SLAC and the various parameters including rf power levels, gun modulator settings, and magnetic focusing currents are being studied. It has been found by means of an rf deflector used as a bunch analyzer illustrated in Fig. 12 that 5 degree bunches can be obtained with this system. The structure used for the rf deflector is the same as that proposed for rf separators.[3] By varying the setting of the calibrated variable phase shifter which controls the phase to the input of the deflector, it is possible to study the charge density inside the electron bunch.

F. Beam Guidance

At the end of every sector, i.e. at 30 points along the machine, there will be a special drift space containing special devices to locate and to guide the electron beam. This drift space will include a set of quadrupole triplets, a set of two steering dipoles, a set of beam position monitors, a toroid to measure beam current, an insertable beam profile monitor, a beam scraper to protect the accelerator and to localize the radiation, and two vacuum valves enabling the operator to isolate one sector from the next. The principle of the microwave beam position monitors is illustrated in Fig. 13. The pickup cavity which is shown here as a structure similar to the beam deflector structure shown in Fig. 12, will, in fact, consist simply of a single cavity operating in the TM_{120} mode. Two such cavities will be used, one for x and the other for y position. Depending on whether the beam is up or down, left or right, the phase of the rf induced signal will flip by 180 degrees. This induced signal will be compared with a phase reference signal induced in a third cavity and compared by means of a magic T and two linear detector diodes. The information obtained from each of these drift spaces

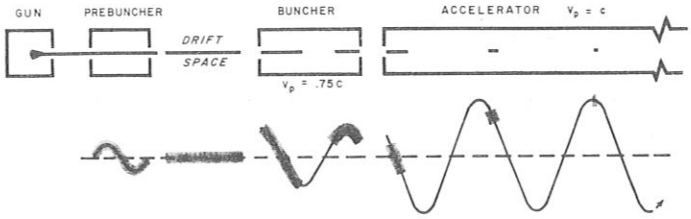

Fig. 11 Progressive bunching of electron beam.

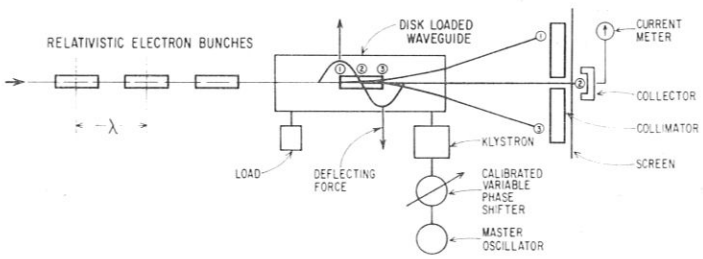

FIG. 12 DEFLECTOR-BUNCH ANALYZER

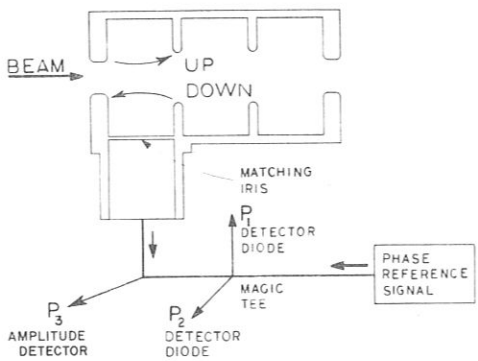

Fig. 13 Beam position monitor using TM_{11} mode structure and magic tee for phase comparison. For example, a maximum for P_1 indicates that the beam is up, a maximum for P_2 that the beam is down. The amplitude of P_3 indicates the distance from the axis.

will be sent to the Central Control Building by means of a base-band telemetry system and an FM system. There this information will be displayed on a set of oscilloscopes, allowing the operator to take corrective action by means of the remotely controllable steering dipoles and quadrupoles.

G. Support and Alignment

Figure 14 shows an expanded view of the support and alignment system. The three jacks which control the position of the beginning of each 40-foot support girder, are shown together with the accelerator tube and a retractable Fresnel lens mounted inside the girder. This Fresnel lens is part of the optical alignment system which will consist of three basic elements: (1) a laser mounted at the injector end of the accelerator, (2) 300 of these retractable lenses consisting of square copper and nickel plated targets perforated with an appropriate Fresnel pattern, and (3) at the end of the accelerator, a light intensity scanner and detector to determine the position of the image center. By determining the coordinates of successive spot centers formed by inserting successive lenses in the light path, it will be possible to measure the misalignment of each lens and hence of each corresponding girder. Corrective action can be taken accordingly. Because the focal length of the Fresnel lenses must change as a function of their position along the two-mile length, the hole pattern must change gradually from lens to lens. A special computer program has been used to determine the pattern pertaining to each lens position and a punched tape has been derived to control the ruling machine used to fabricate each target. Experiments with sample targets have already been conducted in an abandoned railway tunnel, not far from San Francisco, and it has been shown that over a 1,000-foot distance, displacements of a target of the order of 0.001 inch can be resolved.

H. Beam Switchyard

Figure 15 shows the layout of the array of magnets following the two-mile length of the machine which will be capable of switching the beam into the various experimental areas such as End Station A (for electron scattering experiments), and End Station B (for secondary beams, bubble chambers, etc.). A straight ahead beam is also provided. Before entering the beam switchyard, the beam will be steered onto and through an adjustable collimator. Electron energy of the deflected beams is measured in the switchyard by means of several momentum spectrometers.

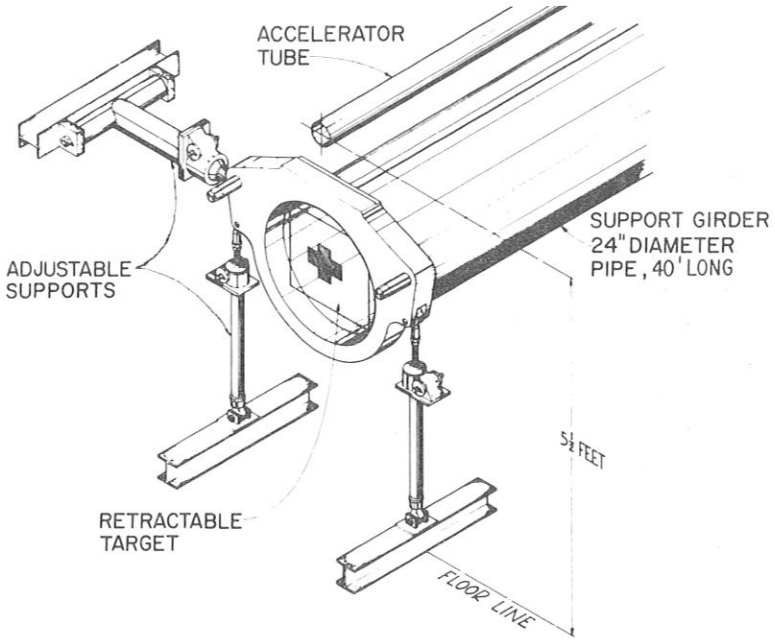

FIG. 14 SUPPORT AND ALIGNMENT SYSTEM

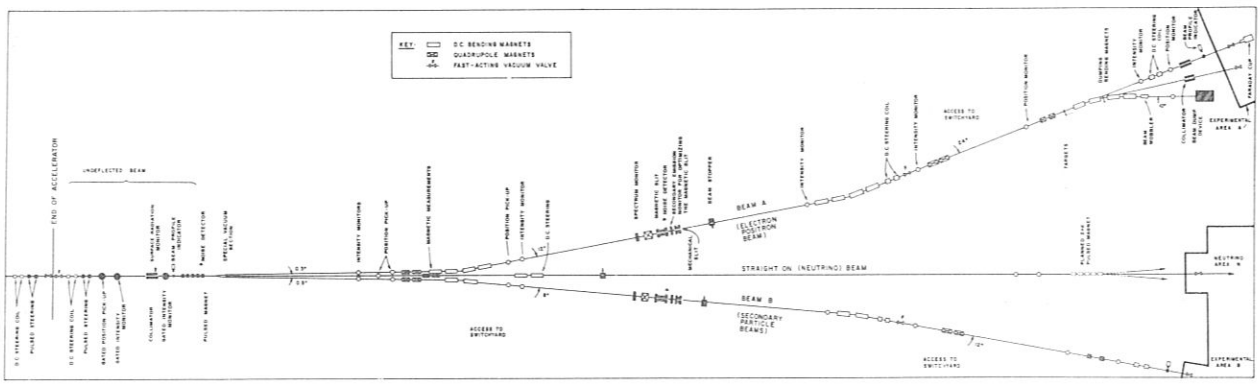

Fig. 15 Beam switchyard layout.

I. Instrumentation and Control

All essential instrumentation and control information will be available at the Central Control Building to be constructed close to the end of the machine. Several systems are being engineered and procured to permit monitoring and control of the accelerator, the switchyard, and some of the essential beam parameters in the experimental areas. These instrumentation and control systems include an "on-off" type status monitoring system based on the time-sharing multiplexing principle, an analog system to transmit information concerning certain analog signals available at each sector, a base-band telemetry system to transmit beam position and intensity information, a more accurate FM system to transmit accurate electron beam charge information and a remote control system consisting of a relay tree enabling the central control operator to actuate a number of devices along the machine, such as trigger delays, steering and quadrupole currents, gain controls, automatic phasing, etc. Because of the complexity of this instrumentation and control system and the difficulties foreseen in operating the accelerator with interlaced beams of different energies accelerated by different complements of klystrons on a pulse-to-pulse basis, it is now being contemplated to acquire at least one small computer to take over some of the control functions and many of the data logging functions which a human operator would not be able to perform. The first computer will be used to set up the magnet currents required in the beam switchyard for beams of specific energies. The next step may be to design a computer system capable of automatically controlling the beam guidance system along the two-mile length. Studies of these computer systems are presently beginning and will develop further in the near future.

J. Conclusion

While it outlines some of the highlights of the present construction status at SLAC, this report is by no means complete and several systems such as the modulators, the vacuum system, the cooling-water system, the variable voltage substations, and others have not even been touched upon. It is believed that the information on these systems can either be found in other SLAC reports or will be forthcoming at future conferences.

YOUNG: Can you tell us briefly what the situation is concerning klystron procurement and delivery.

LOEW: We are making klystrons at Stanford. In addition, we have two contracts, one with RCA and one with Sperry. We are now receiving tubes

from these suppliers which are meeting the specifications. To protect the project we have just signed two more study contracts, one with Eimac and one with Litton. These companies will make something like six tubes each in the next year with an incentive plan so that they will receive more for each additional megawatt output.

REFERENCES

1. W. K. H. Panofsky, et al., "Linear Electron Accelerator Progress at Stanford University", Proceedings of 1961 International Conference On High Energy Accelerators, Brookhaven; pp. 79-118; and W. K. H. Panofsky, "Progress Report on the Stanford Two-Mile Linear Accelerator", Proceedings of 1963 International Conference On High Energy Accelerators, Dubna; pp. 407-418.

2. A. L. Eldredge, G. A. Loew, and R. B. Neal, "Design and Fabrication of the Accelerating Structure for the Stanford Two-Mile Accelerator", SLAC Report No. 7, Stanford Linear Accelerator Center, Stanford University, Stanford California (November 1962).

3. O. A. Altenmueller, R. R. Larsen, and G. A. Loew, "Investitagions of Traveling Wave Separators for the Stanford Two-Mile Accelerator", SLAC Report No. 17, Stanford Linear Accelerator Center, Stanford University, Stanford, California (August 1963).

A GREEN'S FUNCTION APPROACH TO THE CALCULATION OF DRIFT TUBE CAVITIES*

M. Rich and W. M. Visscher
University of California, Los Alamos Scientific Laboratory
Los Alamos, New Mexico

I. Introduction

We report here on a calculation similar in spirit and method to that of Gluckstern[1] with some simplification and some generalization. Briefly, our method is to first use the symmetries of the drift tube calculation problem to reduce Maxwell's equations to a single one, which we solve by use of a cylindrical Green's function.[2] The Green's function gives directly and exactly the fields inside a cylindrical conductor for a prescribed dipole disc (or tube) source with sinusoidal time dependence of arbitrary frequency. By integrating this Green's function over a source distribution, we can in principle (and, with enough patience, in practice) obtain an exact solution for the fields due to an arbitrary internal current distribution. We have chosen a particular form for the internal current distribution, with which we hope to be able to mock up a variety of drift tube shapes.

Given a current distribution, the fields can be obtained exactly. If the fields have a mode on the transverse plane which bisects the current distribution, then one can start at that point to construct a surface which is everywhere normal to the electric vector. If this surface is found to stay outside of the current distribution, then the fields would be unchanged if the surface were made of a perfect conductor. If the conductor has a reasonable shape, we have designed a drift tube and can easily obtain the shunt impedance and transit time factor by numerical integration.

II. Equations

We define, in cylindrical coordinates

$$r\,B_\theta(r,z,t) = e^{i\omega t}\,F(r,z)\,. \tag{1}$$

Then for a current

$$\vec{j}(r,z,t) = e^{i\omega t}\,\vec{j}(r,z)\,, \tag{2}$$

Maxwell's equations reduce to

$$r\,\frac{\partial}{\partial r}\frac{1}{r}\,\frac{\partial F}{\partial r} + \frac{\partial^2 F}{\partial z^2} + \frac{\omega^2}{c^2}\,F = \mu_o\, r\left(\frac{\partial j_z}{\partial r} - \frac{\partial j_r}{\partial z}\right) \tag{3}$$

*Work performed under the auspices of the U. S. Atomic Energy Commission.

in MKS units. The Green's function for Eq. (3) satisfies

$$(\mathcal{L} + \lambda^2)\, G(r, z; r', z') = r\, \delta(r - r')\, \delta(z - z') \tag{4}$$

with

$$\mathcal{L} = r \frac{\partial}{\partial r} \frac{1}{r} \frac{\partial}{\partial r} + \frac{\partial^2}{\partial z^2} \quad .$$
$$\lambda^2 = \omega^2/c^2 \, . \tag{5}$$

Upon defining χ_k as a complete set of eigenfunctions of

$$\mathcal{L}\, \chi_k = -k^2 \chi_k \, , \tag{6}$$

G can be formally written down as

$$G(r, z; r', z') = \sum_k \frac{\chi_k(r, z)\ \chi_k^\dagger(r', z')}{\lambda^2 - k^2} \, , \tag{7}$$

which is verifiable by inspection of Eqs. (4) and (6) if the normalization of χ_k is such that

$$\int_o^R \frac{dr}{r} \int_o^L dz\ \chi_{k'}^\dagger(r, z)\ \chi_k(r, z) = \delta_{kk'} \, , \tag{8}$$

where R and L are the cavity radius and half length respectively (see Fig. 1). A complete set of χ_k's satisfying Eqs. (6) and (8) and the boundary conditions imposed by the physics of the problem, namely

$$\chi\Big|_{r=0} = 0$$
$$\frac{\partial \chi}{\partial r}\Big|_{r=R} = 0 \tag{9}$$
$$\frac{\partial \chi}{\partial z}\Big|_{z=0,\, L} = 0$$

is the two-parameter set

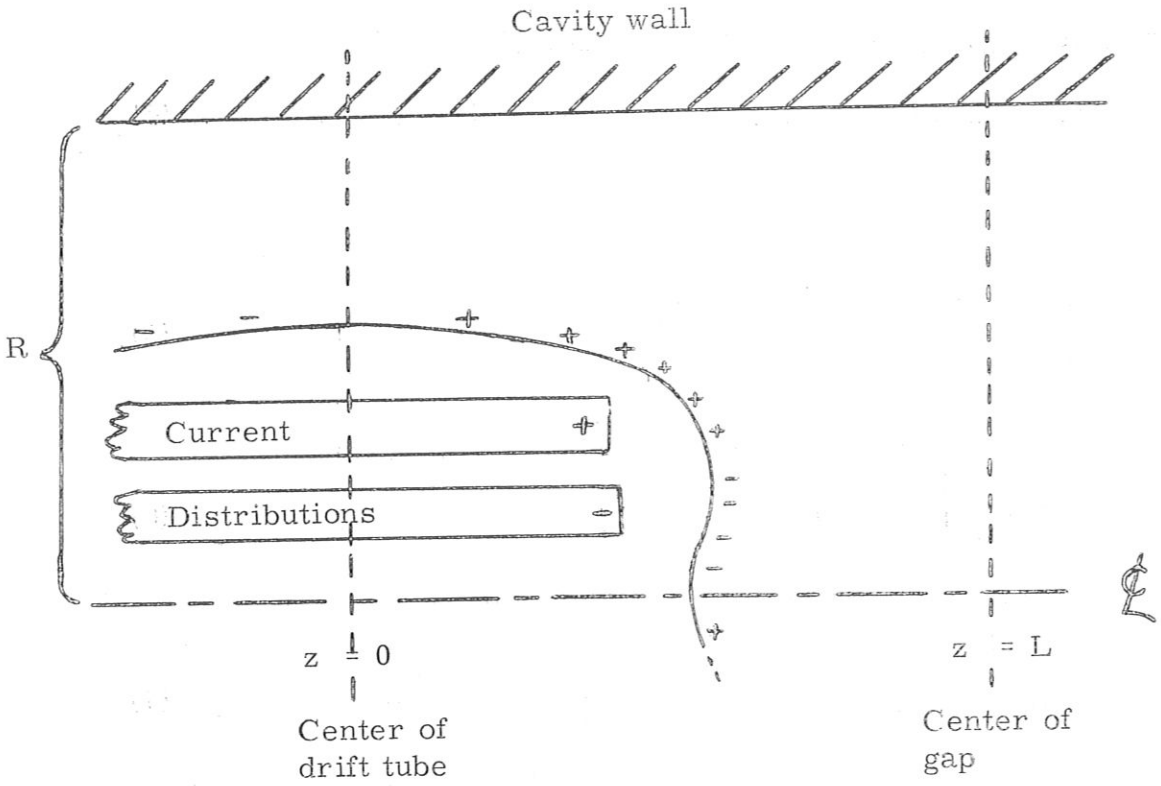

Fig. 1 Unit cell quadrant

$$\chi_{m,n} = \sqrt{\frac{2 - \delta_{m,0}}{L}} \cos \frac{m \pi z}{L} \frac{\sqrt{2}}{\rho_n \left| J_1 (\rho_n) \right|} \rho_n \frac{r}{R} J_1 \left(\rho_n \frac{r}{R} \right), \quad (10)$$

where m runs over all the non-negative integers and ρ_n is the n^{th} root of J_0.

Equation (7) is therefore a double sum, over n and m. Either, but not both, of them can be summed in closed form. One of the sums must be left for the computer to do numerically. The choice is made on the basis of speed of convergence; the more slowly converging sum always being done first, analytically. The relevant results are

$$\sum_n \frac{2 rr'}{R^2 J_1^2 (\rho_n)} \frac{J_1 (\rho_n r/R) J_1 (\rho_n r'/R)}{\kappa^2 - (\rho_n/R)^2} = \quad (11)$$

$$\frac{\pi rr'}{2} J_1 (\kappa r_<) \left[N_1 (\kappa r_>) - J_1 (\kappa r_>) \frac{N_0 (\kappa R)}{J_0 (\kappa R)} \right],$$

or, if $\kappa^2 = -\kappa'^2$ is negative,

$$\sum_n = -rr' I_1(\kappa' r_<)\left[I_1(\kappa' r_>)\frac{K_0(\kappa' R)}{I_0(\kappa' R)} + K_1(\kappa' r_>)\right], \quad (12)$$

where $r_>$ is the greater of r and r' and $r_<$ the lesser of the two. If one wishes to do the sum over m analytically, it is

$$\sum_{m=0}^{\infty} \frac{2-\delta_{m,0}}{L} \frac{\cos\frac{m\pi z}{L}\cos\frac{m\pi z'}{L}}{\beta^2 + \left(\frac{m\pi}{2}\right)^2} = \frac{\cosh\beta(z_> - L)\cosh\beta z_<}{\beta \sinh\beta L}. \quad (13)$$

The solution F (r, z) of Eq. (3) is found from the Green's function according to

$$F(r,z) = \mu_0 \int_0^R dr' \int_0^L dz' G(r,z;r',z')\left(\frac{\partial j_z(r'z')}{\partial r'} - \frac{\partial j_r(r',z')}{\partial z'}\right). \quad (14)$$

Here we must specify the form of $\vec{j}$. We stipulate that only j_z differs from zero, and that it has the form

$$j_z(r;z') = \frac{1}{\mu_0}\sum_\mu j_\mu \cos k_\mu z' \,\theta(r' - a_\mu)\,\theta(b_\mu - r')\,\theta(y_\mu - z') \quad (15)$$

where θ is the unit step function $\theta(x) = \frac{1}{2}(1 + \frac{x}{|x|})$. Since the derivative of θ is a δ function, the integral over r' in Eq. (14) can be performed by inspection, and the integral over z' is elementary. The task remaining is then to perform either the n or m sum and the μ sum (which we have never yet taken to have more than two terms).

III. Calculations

A Fortran code for the IBM 7094 has been written to calculate drift tube shapes using Eq. (14) for F. The input consists of the parameters of Eq. (15) describing the current distribution, the frequency, the cavity radius, the proton energy (length of the cavity), the surface resistivity of the structural material, and a number to provide a convergence criterion for the Bessel function sums. Since the metallic boundary condition for Maxwell's equations specifies that the normal derivative of F vanish at the surface

$$\frac{\partial F}{\partial n} = 0, \tag{16}$$

and since at $z = 0$ the surface of the drift tube is parallel to the axis, F must satisfy

$$\frac{\partial F}{\partial r} = 0 \tag{17}$$

at the point r_d where the metal cuts the median plane. The code searches r at $z = 0$ for a point satisfying Eq. (17); if one is found, it then integrates Eq. (16) to find the surface along which one can put a metallic drift tube without altering the fields. The method used to integrate Eq. (16) is the same as that used by Gluckstern; briefly, it approximates the curve of the surface by a series of circular arcs of constant chord. By reducing the chord length one can increase the accuracy indefinitely; we find 1/2 cm to be usually adequate.

The transit time factor is formed by a Simpson's rule integration of the E field along the axis

$$T = - \frac{\int_0^L \left(\frac{1}{r}\frac{\partial F}{\partial r}\right)_{0,z} \cos\frac{\pi z}{L}\, dz}{\int_0^L \left(\frac{1}{r}\frac{\partial F}{\partial r}\right)_{0,z} dz} . \tag{18}$$

The shunt impedance is found by a Simpson's rule integration of B^2 over the metal surfaces of the drift tube and the outer cylinder:

$$ZT^2 = \frac{(\text{numerator of Eq. (18)})^2}{L\,\omega^2\,\epsilon^2\,\pi\,R_s \int \frac{F^2}{r}\, d\ell} , \tag{19}$$

where $R_s = 3.6 \times 10^{-3}$ ohms for copper at 200 Mc, $\epsilon^{-1} = 36\pi \times 10^9$, and the integral is a line integral over all the metal surfaces in a quarter cell as shown in Fig. 1.

Other output available from this code includes the maximum electric field on the drift tube, the electric fields everywhere in the cavity, and the fraction of the total power dissipation which occurs on the drift tube.

IV. Results

The form of Eq. (15) allows the construction of distributed charge distributions for excitation of a cavity. Except for comparisons with some cases of Gluckstern,[1] the problems which have been run with the present code were done with two charge distributions of opposite sign running parallel to the cavity axis, the lower one usually carrying less charge than the upper. This choice was made with the hope that it would more nearly approximate the charge configuration which must be produced in the metallic surface of a real drift tube, as illustrated by the + and - signs in Fig. 1, in order to result in an interior shielded region. In this we have only been partially successful. Axial indentations in the drift tubes can be accomplished with such dipole charge distributions and the axial fields interior to the drift tubes can be made approximately zero, but the electric fields near the end of the charge distribution and close to the axis vary rapidly in such a way that formation of a true hole seems impossible. Presumably a more complicated charge distribution would produce a drift tube with an axial hole.

No exhaustive study of drift tube shapes has been made with the present code. Some problems have been run at 10, 50, 100, and 150 MeV in an effort to obtain relatively cylindrical drift tubes with reasonable values of $Z\,T^2$, G/L, and radius. Because of the large number of parameters involved with these distributed "dipole" charge distributions and the restriction to reasonable shapes, optimization of the drift tubes becomes very difficult.

Running times with 0.5 centimeter integration stop and a maximum of sixty sum terms are about three minutes per problem. These use a single sinusoidal form for the Z-dependence of each of two distributions. The phase of the cosine function at the end of the distribution was kept the same for both in each case. For similar drift tube sizes and shapes in the neighborhood of what appeared to be optimum, ZT^2 values were not overly sensitive to changes in the parameters of the charge configurations, as would be expected. Relative to an arbitrary configuration in this neighborhood, increasing the cavity radius decreases the drift tube radius, generally with a resultant increase in ZT^2. An increase of the length of the charge distribution would decrease the drift tube radius while slightly increasing its length. As the phase of the sinusoidal charge distributions were made to approach 90^o, distributing the charge more uniformly, the drift tube radius would in general increase, reducing ZT^2. Finally, making the magnitude of the charge on the lower distribution approach that of the upper tended to result in a reduction of the drift tube radius and the formation of an indentation at its front, the beginnings of a hole.

Figures 2, 3, 4, and 5 show some typical results for drift tube shapes and axial electric fields within the gap for energies of 10, 50, 100, and 150 MeV, respectively. Pertinent data with respect to cavity radius, g/L, T, ZT^2, etc., are contained in the figures. These results are consistent with those of Gluckstern[1] and with MURA MESSYMESH calculations,[3] although there seems to be a tendency to obtain lower ZT^2 values than do the latter.

In conclusion, we would like to emphasize that the material presented here is very preliminary. It is hoped that as more detailed parameter studies are made and more "realistic" charge distributions used, a closer approach to drift tube optimization will be achieved.

YOUNG: I have two questions. The first is: How much effort have you put into making a drift tube hole and are you going to devote more attention to this? The second is: Have you checked your program against the results of other programs?

VISSCHER: To the first question: We have made an effort to achieve a drift tube hole. I don't think that it is practical for us because we have so many parameters to change to optimize the drift tube shape. By adding one or more current distributions close to the point where the drift tube contour intersects the axis when these currents are not present, we can get a deep depression in the nose of the drift tube, but not a real hole.

As far as our agreement with other calculations that have been done, we have tried to reproduce some of Gluckstern's single-charge drift tube shapes. We were able to do that all right with the agreement in shunt impedance to within a couple of percent. The difference may be due to the fact that we didn't quite duplicate his shape. We can't really duplicate the shapes calculated by the MURA MESSYMESH program but our results are in general agreement considering this fact.

REFERENCES

1. R. L. Gluckstern, Proceedings of the International Conference on Accelerators, Brookhaven National Laboratory, 1961.

2. P. M. Morse and H. Feshbach, Methods of Theoretical Physics, McGraw-Hill Publishing Company, 1953.

3. See, for example, MURA reports 622 and 642.

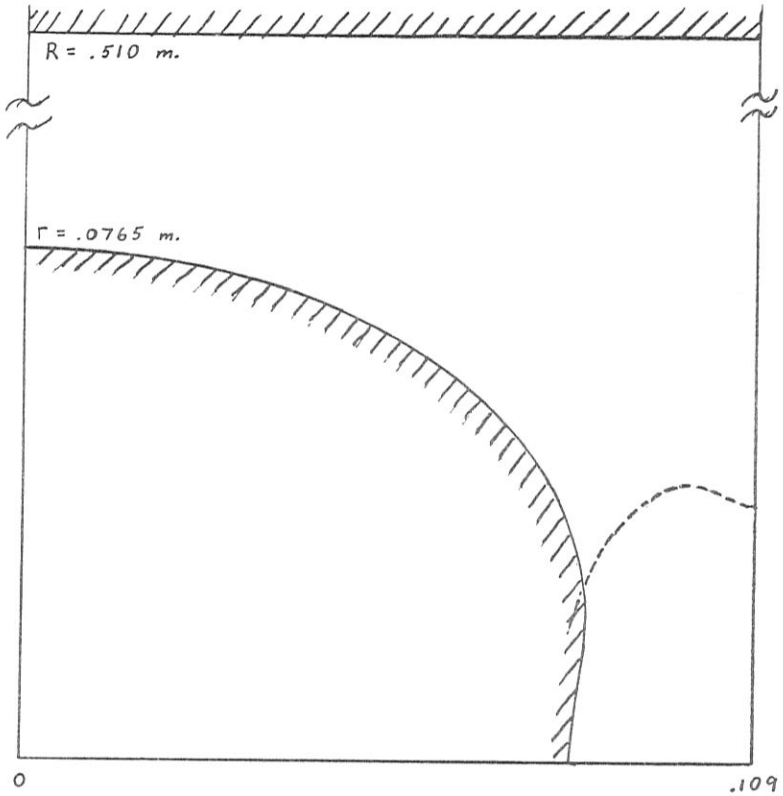

$g/L = .226$

$T = .908$

$ZT^2 = 78.1\ M\Omega/m$

$E_{max} = 1.26$

$f = .195$

Fig. 2: Example of a 10 Mev drift tube shape and axial E field. E_{max} is the maximum field on the drift tube in units of the field at the center of the gap; f is the fraction of the total RF power dissipated on the drift tube.

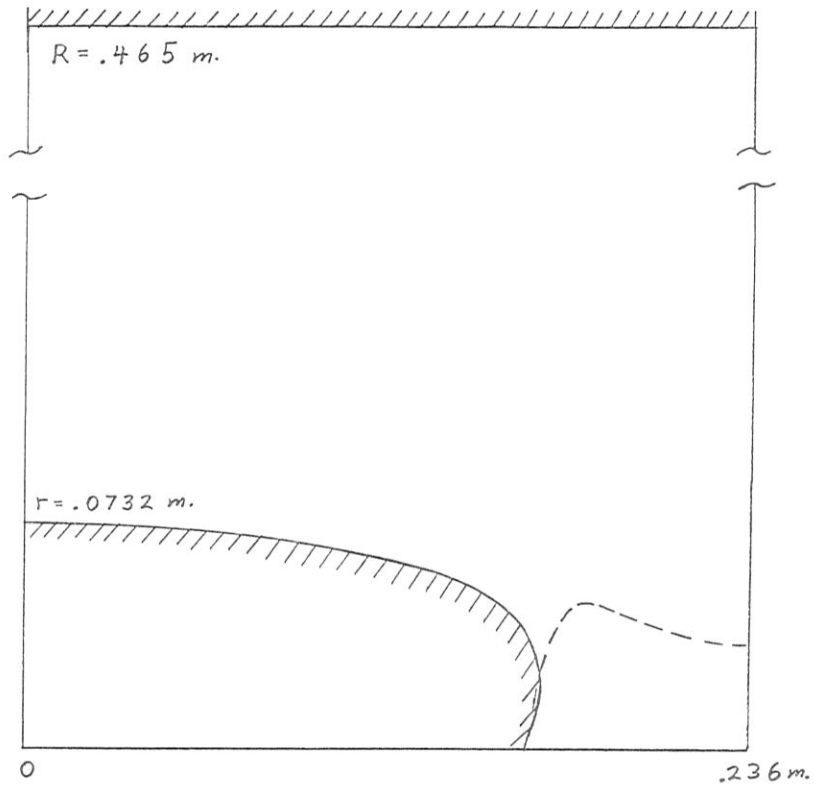

$g/L = .285$

$T = .849$

$ZT^2 = 53.3\ M\Omega/m.$

$E_{max} = 2.26$

$f = .398$

Fig. 3: Example of a 50 Mev drift tube shape and axial E field.

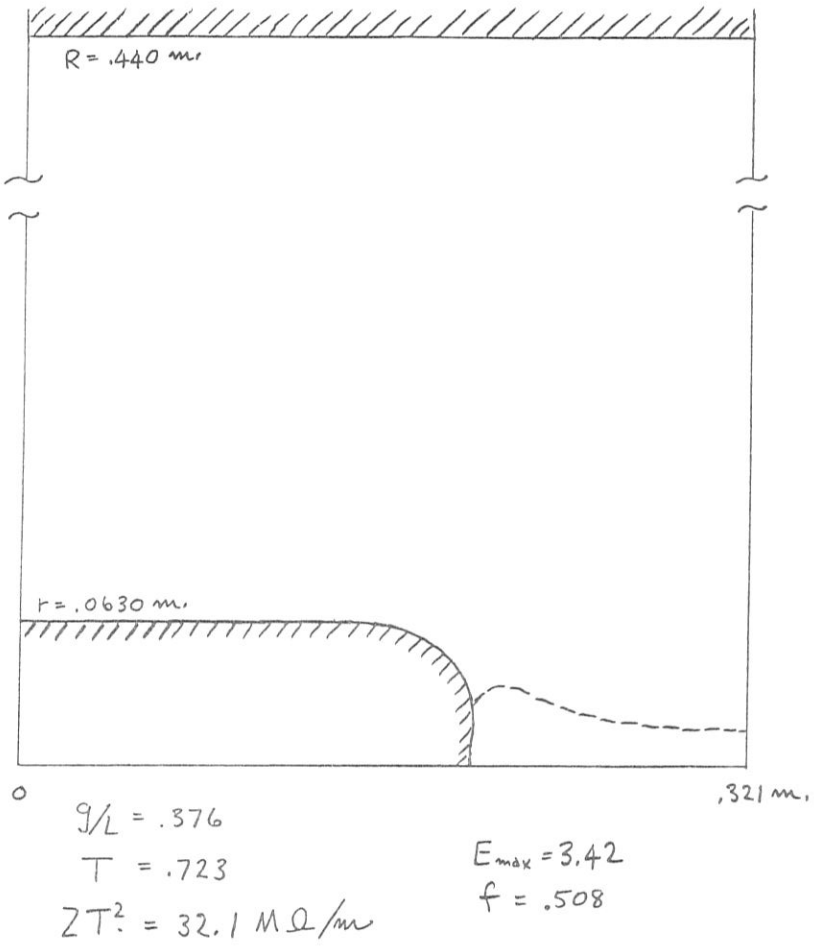

Fig. 4: Exampie of a 100 Mev drift tube shape and axial E field.

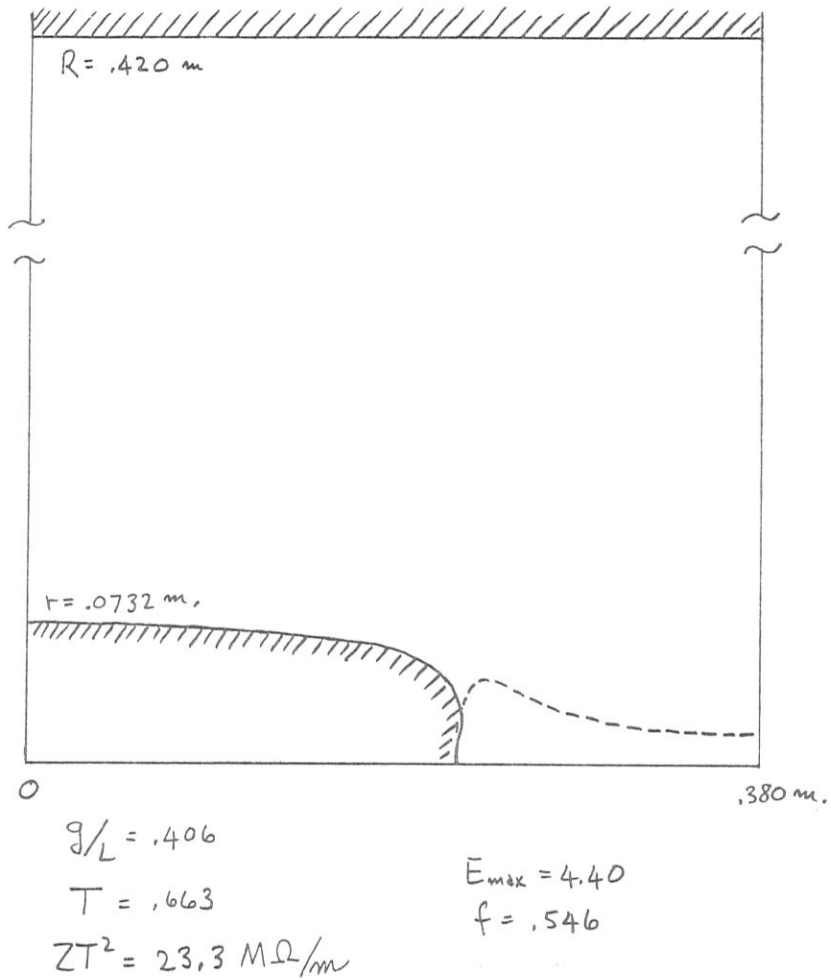

Fig. 5: Example of a 150 Mev drift tube shape and axial E field.

DRIFT TUBE CALCULATIONS*

Harry C. Hoyt
Los Alamos Scientific Laboratory, University of California
Los Alamos, New Mexico

I would like to talk about the mesh calculation that we are trying to set up at Los Alamos for the calculation of resonant cavities. I know quite a number of you have heard about these mesh calculations before, and I hope that you will bear with me as I go through some of the more elementary details. Our calculation divides the resonant cavity into a mesh containing a finite number of points, and then uses a finite difference scheme for computing the values for the magnetic field strength at the points in the mesh. Once we know the magnetic field we can compute other quantities of interest, such as the frequency, shunt impedance, transit time factor, and so on. The voltage is also computed, but is used to determine the normalizing factor needed to get rid of an arbitrary constant which multiplies all the values for the magnetic field strength.

My reasons for wanting to do this mesh calculation are two in number: First, I wanted to learn how to do this type of calculation, and second, there seemed to be a need for a mesh calculation which could be used for a cavity having any arbitrary boundary shape. Consequently our mesh calculation has been set up to allow any boundary shape; in this respect it is different from those calculations which have been done previously. The freedom that we might gain from having a calculation in which we can easily draw in new boundaries will allow us to actually do some comparisons between a lot of strange ideas which are not easily adaptable to other methods of calculation. Also, the mesh calculation is readily adaptable to parameter studies if one has a man who has the time to look at several million numbers.

A resonant cavity which can be handled by our mesh calculation has symmetry with respect to an axis, that is, such a cavity is a figure of revolution. Because of the symmetry, the calculation is carried out for points in a plane which contains the axis, and we have a two-dimensional problem. The calculation may cover either the entire cavity or, if the two halves of the cavity are identical, only half of the cavity. Figure 1 shows the sections used for half-cavity and full-cavity calculations. In Fig. 1 the holes in the drift tubes have not been shown; the calculation, however, can treat the holes.

---

*Work performed under the auspices of the U. S. Atomic Energy Commission.

The mesh used in a given calculation is chosen so that there are an integral number of spaces along the axis, or z-direction. The mesh interval is the same in the radial direction or r-direction, as in the z-direction; that is, we have a square mesh. The outer surface of the cavity does not have to coincide with a mesh line. Figure 2a shows how a mesh might look for a half-cavity calculation. The curved lines show a drift tube and a curved outer wall. The principal difference between MURA's MESSYMESH code and the Los Alamos program is in the way in which we treat the boundary. Since we decided to allow for any boundary shape, we abandoned the idea of doing our calculating on the actual boundary. Instead we compute at points on a zig-zag approximation to the actual boundary. Figure 2b illustrates different ways of determining a zig-zag boundary. The curved line represents an actual boundary, say a metallic surface. One can draw a zig-zag boundary which is the closest approximation to the actual boundary, or one can draw a zig-zag boundary either completely inside the actual boundary or completely outside the actual boundary. How one chooses which zig-zag boundary to use can depend on the type of difference equations one decides to use for the boundary points. Other considerations also may indicate a preference for a particular way of drawing the zig-zag boundary. Hopefully we will be able to choose the zig-zag boundary and the difference equations for the boundary points so that we will get the greatest accuracy for the boundary equations.

We have decided to use the zig-zag boundary which lies completely outside the actual boundary. One of the original reasons for this choice was that it allowed us to choose a set of boundary point equations with nice mathematical properties; however, we have since abandoned that particular set of boundary point equations. Another reason for choosing the zig-zag boundary outside the actual boundary is that we can find field values on the actual boundary by interpolation, rather than by extrapolation. In setting up our difference equations for the boundary points, we do insist that the boundary conditions are satisfied on the actual boundary. Thus, although the mathematical properties of our set of difference equations are not ideal, the physics is correct. Figure 2a shows how the zig-zag boundary would be drawn for the configuration shown.

The partial differential equation for our problem is given below. In

$$\frac{\partial^2 F}{\partial r^2} - \frac{1}{r}\frac{\partial F}{\partial r} + \frac{\partial^2 F}{\partial z^2} + \lambda^2 F = 0 \qquad (1)$$

equation (1), $F = r H_\theta$ and $\lambda^2 = \omega^2/c^2$, where H_θ is the only component of the magnetic field present. Equation (1) is the equation which remains after the time dependence has been removed from the wave equation. The boundary conditions are

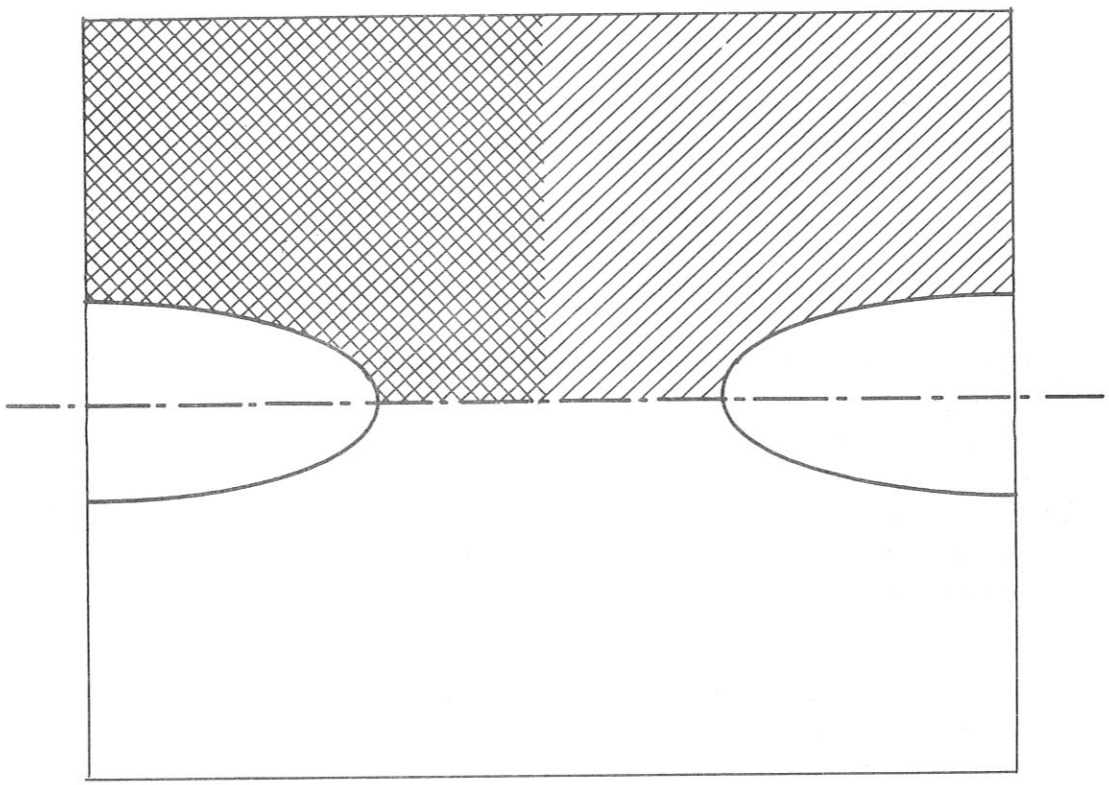

Drift tube Cavity (holes not shown)

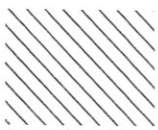

Section used for Half-cavity calculation

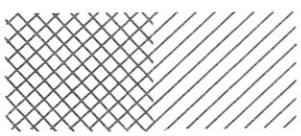

Section used for Full-cavity calculation

Figure 1.

$$F = 0 \qquad \text{on the axis, and}$$
$$\frac{\partial F}{\partial n} = 0 \qquad \text{on the remainder of the boundary.} \tag{2}$$

$\frac{\partial F}{\partial n}$ is the derivative of F normal to the boundary. These conditions are equivalent to the following conditions on the electric field:

$$E_r = 0 \qquad \text{on the axis, and}$$
$$\vec{n} \times \vec{E} = 0 \qquad \text{on the remainder of the boundary.} \tag{3}$$

Equations (3) say that there can be no radial component of the electric field on the axis because of symmetry, and that on the remainder of the boundary the electric field must be perpendicular to the boundary either because of the presence of a conducting surface or because of symmetry. The second condition of (2) is called a Neumann condition, and it is the difficulty in treating this condition numerically which is a major problem in a mesh calculation of this type.

Our method for getting the difference equations is somewhat different from that used by others, at least insofar as the interior points of the mesh are concerned. Our original intention was to obtain a set of difference equations which would have a positive definite matrix, since this would assure convergence to a solution. To get such a set of equations, one uses a variational principle. Consider the following integral:

$$I = \frac{1}{2} \int\int \frac{1}{r^2} \left[\left(\frac{\partial F}{\partial r} \right)^2 + \left(\frac{\partial F}{\partial z} \right)^2 - \lambda^2 F^2 \right] r \, dr dz \, . \tag{4}$$

If we take the variation of (4) and require it to be equal to zero, i.e.,

$$\delta I = 0 \, , \tag{5}$$

we find that the condition for (5) to be satisfied is that the differential equation (1) be satisfied. Equation (5) says that the integral (4) will be either a maximum or a minimum. Substitution from Maxwell's equations into (4) shows that

$$I \propto \int (\epsilon E^2 + \mu H^2) \, dV \, , \tag{6}$$

that is, I is proportional to the energy in the cavity. Equation (5) then requires that the energy be a minimum. The procedure for obtaining the

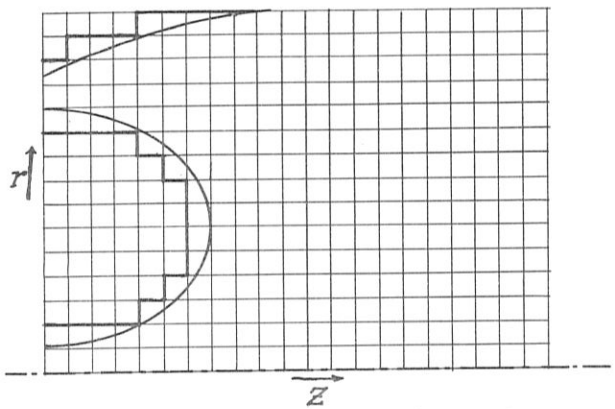

(a) Actual and Zig-Zag Boundaries for Mesh Calculation

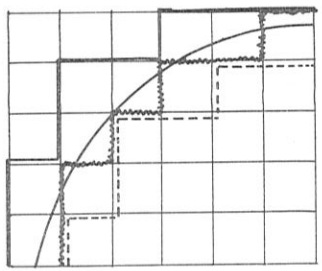

(b) Ways of Drawing Zig-Zag Boundary
Closest approximation
Inside
Outside

Figure 2.

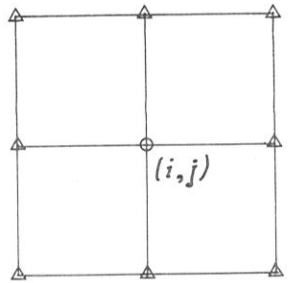

(a) Points used in 9-point difference equation for interior point (i,j)

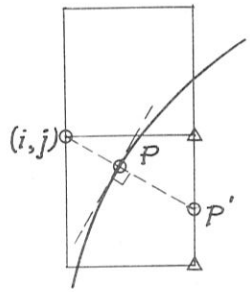

(b) Points used for difference equation for one type of boundary point.

Figure 3

difference equations is to substitute our difference approximations in (5) rather than in the differential equation (1). We then perform the process of taking the variation of I and setting it equal to zero. The result gives us our difference equations, both for interior points and for points on the zig-zag boundary. However, the difference equations for the points on the zig-zag boundary say that the normal derivative of F on the zig-zag boundary--not the actual boundary--is zero. Because we want the condition to apply on the actual boundary, we have substituted a new set of equations for the boundary points.

Figure 3 shows the points which are involved in the resulting difference equations. For the interior points we have a 9-point difference equation. In Fig. 3a, we wish to compute a value of F for the point (i, j), where i and j are integers giving the location of the point. The illustration shows the other points which are referred to in the difference equation. Figure 3b shows an example of how the equation for a boundary point can be obtained. We wish to compute the value of F at point (i, j). However, the boundary point equation must say that $\frac{\partial F}{\partial n} = 0$ on the actual boundary at P, the intersection of the actual boundary with the normal to the boundary which passes through (i, j). The first approximation satisfying the boundary condition is to say that F at (i, j) equals F at point P'. The value of F at P' is found by interpolation from the values at the adjacent mesh points. Figure 3b shows what points will be referred to in the difference equation.

Once we have a complete set of difference equations for the mesh, we would like to compute the F values for the mesh points. We also would like to compute the lowest eigenvalue for the system of equations; this will give us the frequency of the cavity. The eigenvalue, λ^2, is computed from equation (7). This

$$\lambda^2 = \frac{\iint \frac{1}{r^2}\left[\left(\frac{\partial F}{\partial r}\right)^2 + \left(\frac{\partial F}{\partial z}\right)^2\right] r\, dr\, dz}{\iint \frac{1}{r^2} F^2\, r\, dr\, dz} \qquad (7)$$

equation can be shown to give the eigenvalue we want by taking

$$\delta \lambda^2 = 0 . \qquad (8)$$

Again we can find that the condition (8) for an extremum is that the differential equation (1) be satisfied.

The input data required to describe the boundary have been chosen as follows: For each point where the actual boundary crosses a line of

the mesh, three numbers are given. These three numbers are the coordinates, r and z, of the point and the slope m of the actual boundary at that point. Any given problem may require several thousand input numbers to describe the boundary, but the data handling problem can be reduced considerably by considering each problem as a modification of a previous problem. Then the input for the previous problem can be used, together with the necessary information which shows the changes from the previous problem. In addition to data describing the boundary, we must provide input, or guessed, values for the F's at the mesh points and the eigenvalue λ^2. Once you have a backlog of problems, the values for the solution of one problem can be used as the input for the next one. One cannot start a problem without this "mesh loading" of F's because F = 0 everywhere is a solution to the differential equation, and the program would get nowhere.

The calculational procedure used is point-by-point relaxation. This allows us to compute a new value for F at a given point on the basis of the values at adjacent points, regardless of whether they are new or old values. We proceed through the mesh systematically, starting at the bottom where r = 0 and going from left to right. When we finish one row, we go to the next row above and repeat the process. When we finish computing the F values, we compute a new value for λ^2 using equation (7). Then the process is repeated. The result is a kind of double iteration: you iterate with a given value for λ^2 until the F values settle down, then you calculate a new λ^2. Finally when both the F's and λ^2 have settled down, you can declare that the solution has converged. Once the F's and λ^2 have been computed, we can calculate Q, shunt impedance, transit time factor, and so on.

The status of our program is as follows: We have completed programming and check-out on the input program and the parts computing the F's and the eigenvalue, and we are in the process of programming the calculations for Q, Z, transit time factor, and so on. We have done some checking out on problems. Our first check-out problem was a spherical cavity, for which we have an analytic solution; this problem works very well. The F values for points in the interior (and some distance from the boundaries) agree with the analytic solution to 0.1 or 0.2 percent. Near the axis, F values seem to be within 2 percent, and near the outside boundary they are within 3 or 4 percent. Better values might be obtained by running the problem longer. Boundary point equations, however, do not have the same degree of accuracy as the equation for interior points, and some of the error near the boundary may be a more or less permanent feature. We are now trying to run a drift tube problem for a 50 MeV cavity. This is a problem which has been computed by

Bill Visscher and Marvin Rich using the methods described in the previous paper.

A word about the computer time involved might be in order. A problem with a 100 x 100 mesh, or 10,000 points, will take about 8 minutes on the IBM 7094 if we make reasonable guesses for the initial values of the F's and λ^2. By "reasonable guess", I mean that these values should be within 10 percent of the final values. As I mentioned before, this is not too difficult, since each problem is a slight variation from a previous problem. The calculation currently can handle a mesh having up to 40,000 points; this means mesh spacing of a few millimeters for the drift tube cavities we are now interested in. Our current estimate of the time required to complete the program is two to three months. If we are successful, perhaps we can answer some of the questions which have been the subject of many arguments.

EDWARDS: Do you use the technique of overrelaxation? We find here at MURA that it speeds up the convergence immensely.

HOYT: I set the calculation up in such a way that we can use overrelaxation. I found that on the spherical problem overrelaxation was not as fast as using a relaxation factor of one. One gets the answer in half to two-thirds the time required when a larger value for the relaxation factor is used. I also checked to see what theoretical estimates one can make for the relaxation factor, and found to my surprise that the estimate is very nearly one. The relaxation factor depends on the frequency of the cavity, so this might not be true for frequencies other than 200 Mc.

GLUCKSTERN: Didn't the numbers you gave as estimates of the accuracies of interior points also apply to the electric field on the axis?

HOYT: I don't know about this yet. We have not computed any electric field values on the axis yet. The procedure we plan to follow is this: One can compute the voltage across the cavity using Faraday's Law, which should be more accurate than obtaining it by computing the electric field on the axis. We would then also, using the best curve fitting methods, try to compute the electric field on the axis, integrate along the axis to get the voltage, and compare with the Faraday's Law value to estimate the accuracy. I feel this estimate is necessary, because E_z on the axis must be used in the calculation for the transit time factor, and we should know all we can about the accuracy. I might explain to those of you who are not familiar with the problem that E_z is proportional to $\frac{1}{r}\frac{\partial F}{\partial r}$, and so when r approaches zero, E_z is given by $\frac{\partial^2 F}{\partial r^2}$. Determining second derivatives

with accuracy is very difficult in numerical calculations. One must do some curve fitting, or use some other approximate methods. We are going to reflect into the axis for two or three points out and then do a curve fit which will give F as a function of r for fixed z. We will differentiate this to obtain E_z on the axis. With the spherical problem and some of Bill Visscher's problems, we should be able to determine the accuracy.

EDWARDS: We have done much the same thing in calculating the axial E field. We find that the difference between the two methods is of the order of 4 to 5 percent, if my memory is correct.

HOYT: I have a feeling that most of the errors which I have mentioned here, like the ones near the conducting surfaces and those near the axis, may well turn out to be systematic errors. If it can be established that they are systematic errors, and if someone can furnish good measurements, then we can correct for them. Then the errors would not be serious when we compare and evaluate different types of structures.

THE SACLAY DESIGN STUDY OF PROTON LINEAR ACCELERATORS

M. Promé
C. E. N. -Saclay

I. Introduction

A team* from Saclay has been dealing with proton linacs for about two years. The purpose is to design, with the collaboration of the Compagnie Générale de Télégraphie sans Fil (C. S. F.),** a 200 MeV linac capable of injecting a 100 milliamp beam into a future synchrotron.

Another purpose of these studies is to design a 20 MeV linac to replace the 3.6 MeV Van de Graaf injector of Saturne. In this case the required beam is about 20 milliamp.

The purpose of this talk is to present some information about the studies undertaken in connection with these projects: theoretical work, models, design of the preinjector, and a general survey of the 200 MeV project in its present form.

II. Theoretical Studies

Theoretical studies have proceeded in two different ways. On the one hand, a computation program for individual cells is being written at Saclay. This program will be similar to the MESSYMESH program of MURA. It will give the values of the resonance frequency, Q factor, shunt impedance, and will allow one to choose accurate dimensions for the linac.

On the other hand, studies have been made to find out if there is any interest in choosing a variable accelerating rate along the linac, from the point of view of an easy trapping of particles by the accelerating process. For instance, a small accelerating rate at the input end of the linac, and gradually increased over a few MeV up to a final value, increases the useful acceptance area for the axial motion. We are now investigating whether this does not implicate a growth in the energy spread of the beam at the exit of the linac.

---

* This team consists of MM. M. Gouttefangeas, M. Promé, G. Rastoix, under the direction of M. Levy-Mandel, and to whom M. P. Lapostolle (CERN) gave a lot of fruitful ideas.

** MM. F. Girard, G. Guilbaud, R. Jean, H. Leboutet, Tran Duc Tien.

Computations have been performed for particles on the axis with a simple program. It will be determined later whether such a variable accelerating rate damages the radial acceptance or not. This will be done by using a program taking into account the six phase coordinates, similar to the PARMILA program of MURA.

III. Experimental Program

The purpose of the experimental program undertaken at Saclay is to get some experience in the field of proton linac cavities.

A two-cell model at 50 MeV has been built and some experiments have already been performed. The 150 kW required to set the rf field to its nominal value inside this model are supplied by a 10 kW C. S. F. television transmitter. C. S. F. has reached the 150 kW level easily by improving the power tube anode insulation, and by adding a 200 μs, one pulse per second modulator.

It is planned to build a 3 m long model at 750 keV. Profiting from the experience acquired with the first model, this one will be closer to the final design.

Experiments performed or planned with these models involve measurements of the Q factor, measurements of the fields and determination of shunt impedance by the perturbation method, and the behavior of the cavity at full power.

IV. Preinjector*

A 750 keV injection energy has been chosen for the linac. The preinjector, a Cockcroft-type machine, offers the possibility of being pressurized. Such an injector has the advantage of being small, 2.5 m long and 2 m in diameter. With such technology, one can avoid setting the classical storage capacitor between the high voltage electrode and earth. Such a capacitor can be damaged when a breakdown occurs. This capacitor is replaced by a pulsed liner, which permits balancing the voltage decrease during the 200 milliamp pulsed beam. Such a liner already exists on the Van de Graaff injector of Saturne, with the different purpose of producing $\frac{dV}{dt} > 0$, and works in a satisfactory manner. The pulse to be applied to the liner will be supplied by a beam intensity transformer, and will be monitored by the beam itself.

The preinjector voltage will be controlled by a continuous beam of about 50 microamp. This beam, which is deflected by an electrostatic

*Preinjector design has been performed by MM. R. Vienet and J. Faure.

device at the exit of the preinjector, passes through a regulation slit which provides a control signal. This signal feeds back on the one hand to the Cockcroft (slow regulation), and on the other hand to the liner (fast regulation).

The behavior of the beam at the exit of the ion source remains to be checked experimentally. However, the focusing device has been computed for a 200 milliamp beam. Calculations have proceeded far enough to take into account the aberrations. In this scheme the beam is accelerated quickly up to 200 keV; the focusing process operates at this level. The whole column, between the ion source and zero potential, is 80 cm long. Moreover, there is a cross-over at about 50 cm after the exit of the preinjector tube. This will make the adjustment and tuning of the beam easier (Fig. 1).

It is estimated that the time spent to reach the ion source with such a pressurized device will be increased by about half an hour with respect to a nonpressurized device. It is planned to have at one's disposal two similar preinjectors, the time spent to switch from one to the other will be five minutes. Of course, one can repair the first one while the second one is running.

V. Design of the 200 MeV Linac

Cavities

The structure considered in this project is the conventional one, with drift tubes. Copper-clad technology, which seems to be cheaper than the separate vacuum tank solution, has been chosen. Elementary sections would be 3 m long.

It has been shown after some difficulty that it would be possible to manufacture copper-clad linac cavities in Europe; copper being either an American OFHC copper from "American Metal", or a European one, such as the BE58 copper, from Norddeutsche Affinerie, Hambourg, whose qualities are close to the OFHC one. The German Company, Phoenix Rheinrohr, will be able to perform the cladding by hot lamination without brazing compound. Rolling and welding operations could be made either by the same company with an accuracy of $\pm$ 5 mm on the diameter, so that it would be necessary to inlay copper at the ends of each section in order to machine an accurate circle, or in France by "Les Chantiers Navals de La Ciotat", in which case tolerances would be $\pm$ 8/10 mm on the diameter, thanks to encircling rings left afterwards on the cavities. In the latter case, it would be unnecessary to inlay copper at the end of the sections.

The mechanical tolerances are important from the point of view of the joining of two sections, not from the point of view of having cavities tuned exactly to the chosen frequency of 200 Mc/s. The coarse tuning will be made with auxiliary rods similar to Brookhaven. The fine tuning of the local frequency will be obtained by means of classical ball tuners which will also be used for setting the accelerating field law chosen along the cavity.

The accelerating structure will be about 125 m long. The temperature control system has been designed so that the linac temperature will be within 0.1° C along the machine, whatever the operating conditions.

Rf Power Supply

In the present design we are considering a short first cavity of 6 m maximum length and 4 to 6 cavities 20 to 30 m long (Figs. 2 and 3), each cavity being fed by a power tube. This choice results from the power available in one tube. Power estimations have been based on the shunt impedance values published by MURA. A conservative interpretation leads one to predict 65 kW/m at the input end of the linac and 130 kW/m at the output end, with a linear decrease. Calculations made on beam loading have shown that these figures have to be overvalued by about 55% during the beam acceleration process. A good security coefficient will be obtained by providing an rf power pulse of 5 MW maximum for each cavity during 200 μs for the filling up of the cavities, and 10 MW maximum during 20 μs to balance the beam loading. Either the well known RCA 7835 tube or the RCA 4617 tube will be used. The latter tube, which requires lower plate voltage, should lead to a simpler modulator (Fig. 4). The modulator is of the hard tube type and is more easily operated than a delay line when it is a question of nonrectangular pulses. The RCA 7835 tube leads to the design of a modulator with two sets of capacitors and a switching system from one to the other. The RCA 4617 tube allows the use of a single set of capacitors, with a hard tube grid controlled system.

It must be pointed out that according to the results of the experiments being performed on the PS linac at Geneva one will perhaps find it preferable to feed each cavity with two tubes, the first one working during 220 μs, the second one during 20 μs. This should lead to simpler modulators because each tube would have a quasi-rectangular pulse. Moreover, cheaper tubes than the RCA tubes previously mentioned could be employed if need be by dividing the accelerator into a large number of cavities. Another advantage would be to set free a new parameter, the rf phase angle between the two tubes.

Radial Focusing

Radial stability will be insured by magnetic quadrupoles in the ++-- pattern (Fig. 5). Quadrupoles will be fed by dc current; the first 20 could be made with 5-turn windings of a hollow 6 x 6 mm wire, with a 4 mm diameter hole for water cooling. Maximum current density will be then about 27 amp/mm^2. The other quadrupoles will be made with ordinary conductor windings and will be molded in plastified araldite. They will be cooled by a water jacket. Induction on the pole faces nowhere exceeds 6250 gauss (Figs. 6, 7, 8 and 9).

Vacuum System

Primary pumping will be in two steps: 20 minutes to reach 10 Torr starting from atmospheric pressure (the required pumping speed is 325 m^3/hr for a 30 m long cavity), then one hour to reach 10^{-4} Torr (the required pumping speed is then 600 m^3/hr). In the present state of this project, secondary pumping will be turned on at 10^{-4} Torr; later, it may be thought preferable to turn on the secondary pumping at a lower pressure. 1000 l/s VacIon pumps will be used for the secondary pumping. We are considering providing one pump every 3 m along the linac (Fig. 10).

Alignment

The method being considered is the following one: cavities lay on a main girder by means of wheels dependent on an adjusting system; each 3 m long section is machined at its ends in order to define its axis; the drift tubes are aligned along this axis. The sections are joined together to form a 20 or 30 m long cavity. A slight rectification of the drift tube position is sufficient to balance the lack of parallelism of the end faces of each section. Outside references allow checking the slow displacements of the drift tubes following a possible distortion of the main concrete girder. Stem attachment devices have been designed so that it is possible to correct the drift tube positions without opening the cavities (Fig. 11).

Planning

The planning has been conceived in order to keep in line with the building time of the synchrotron (Fig. 12). The critical path appears to be linked to the quadrupole studies, machining and controls; it is therefore planned to carry out special studies on this feature. From another point of view, copper-clad cavity models will be tested in conditions as close as possible to the operating conditions of a particle accelerator.

OHNUMA: I would like to ask about your choice of quadrupole magnet strength. I noticed that the magnet strength reduces very drastically as the energy increases. Are you always taking the optimum point at each energy? The solid line comes down rather rapidly and I don't believe those are optimum points.

PROMÉ: With reference to Fig. 5, one can choose lines inside the stability limits such that the beam keeps a constant size. These lines fall rather quickly and starting from the input point, you can choose such a line for the operating line so that the size of the beam does not increase. It is perhaps not the best, but is at least feasible.

OHNUMA: How far do the nonsynchronous particles penetrate into the unstable region?

PROMÉ: Not far and this is only at the beginning of the machine. Very quickly the nonsynchronous particles enter the stable area. Of course, this has to be checked with a computer program using the six coordinates.

FEATHERSTONE: I was interested in your reference to the possibility of using large power tubes of less cost than the RCA tubes that you have also considered. Is there anything concrete that you can say about this matter at this time?

PROMÉ: There is nothing new, to my knowledge, about these tubes.

FEATHERSTONE: F. T. H. has not done something interesting we should know about?

PROMÉ: Perhaps Colin Taylor will say something about this.

TAYLOR: I will give some information about this during my talk.

FEATHERSTONE: You referred to using a variable rate of acceleration at the injection end to improve capture. Would this be used in conjunction with conventional bunching or to the exclusion of an ordinary buncher?

PROMÉ: This does not exclude a buncher.

FEATHERSTONE: Would one inject a continuous stream of protons?

PROMÉ: No, you would need a buncher as well.

FEATHERSTONE: Do you have an estimate of the efficiency of capture that you should obtain with the combination of buncher and variable acceleration rate?

PROMÉ: I am afraid that I cannot give a number because we have not finished the calculation. However, we saw that we gained something.

CURTIS: You mentioned the use of a liner in your preinjector Van de Graaff. How much of a voltage droop do you have to correct for when you are drawing 200 milliamps?

LAPOSTOLLE: I think it was a few 10's of kilovolts. It depends on the capacity of the machine.

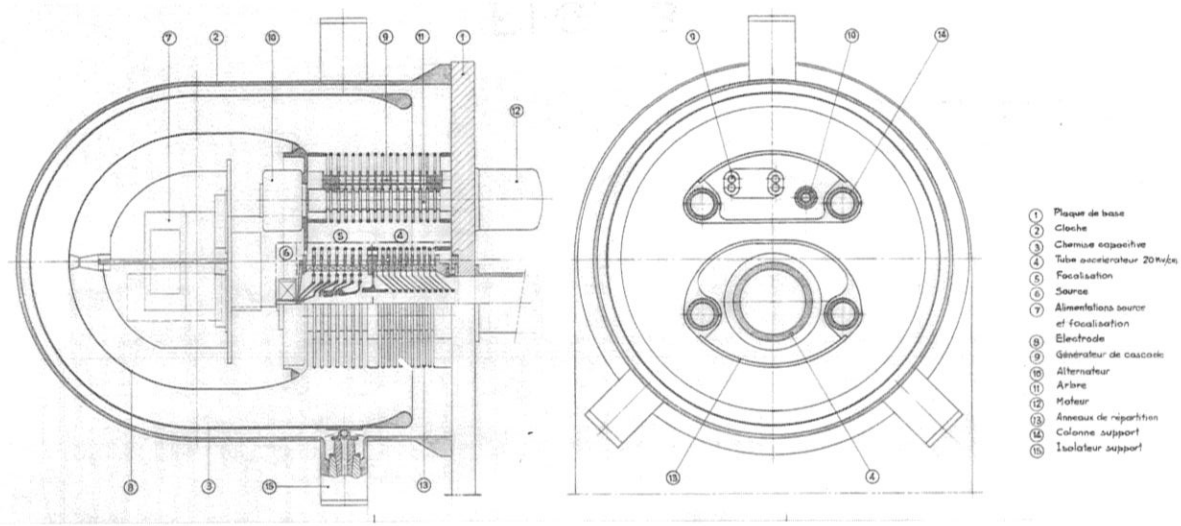
① Plaque de base
② Cloche
③ Chemise capacitive
④ Tube accelerateur 20 m/m
⑤ Focalisation
⑥ Source
⑦ Alimentations source et focalisation
⑧ Electrode
⑨ Générateur de cascade
⑩ Alternateur
⑪ Arbre
⑫ Moteur
⑬ Anneaux de répartition
⑭ Colonne support
⑮ Isolateur support

FIG. 1

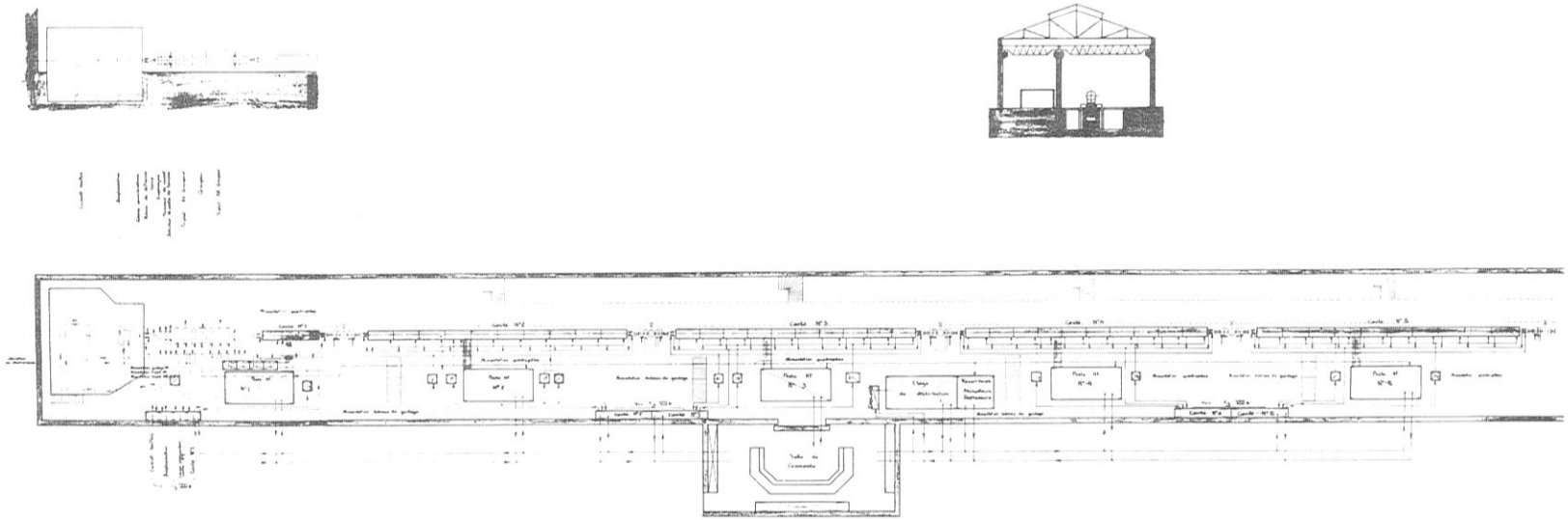

FIG. 2

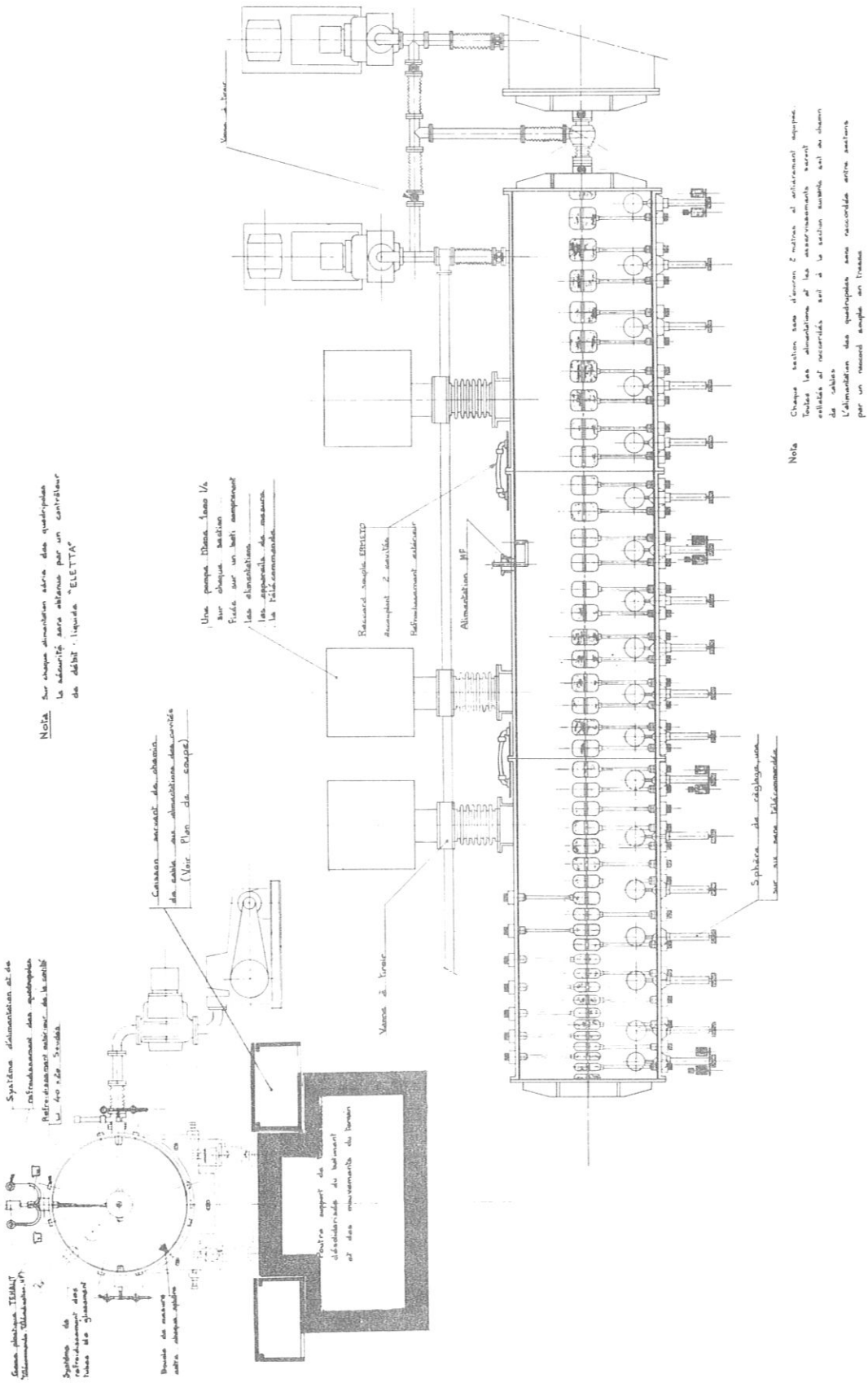

FIG. 3

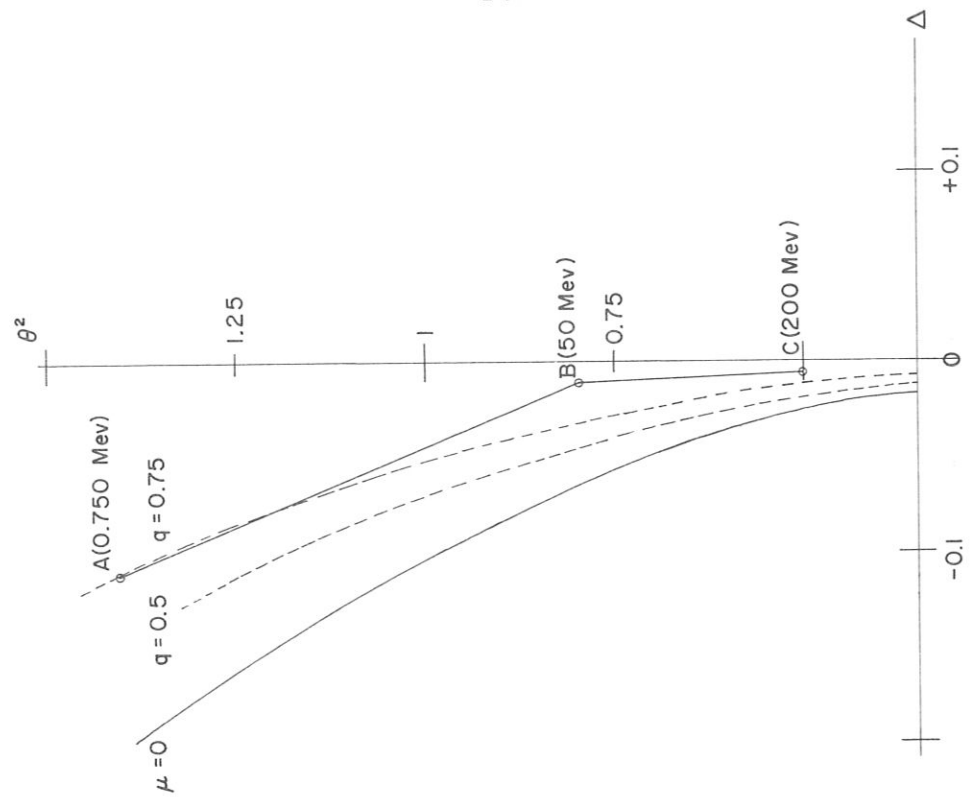

FIG. 5 DIAGRAMME DE STABILITÉ
ABC points de fonctionnement

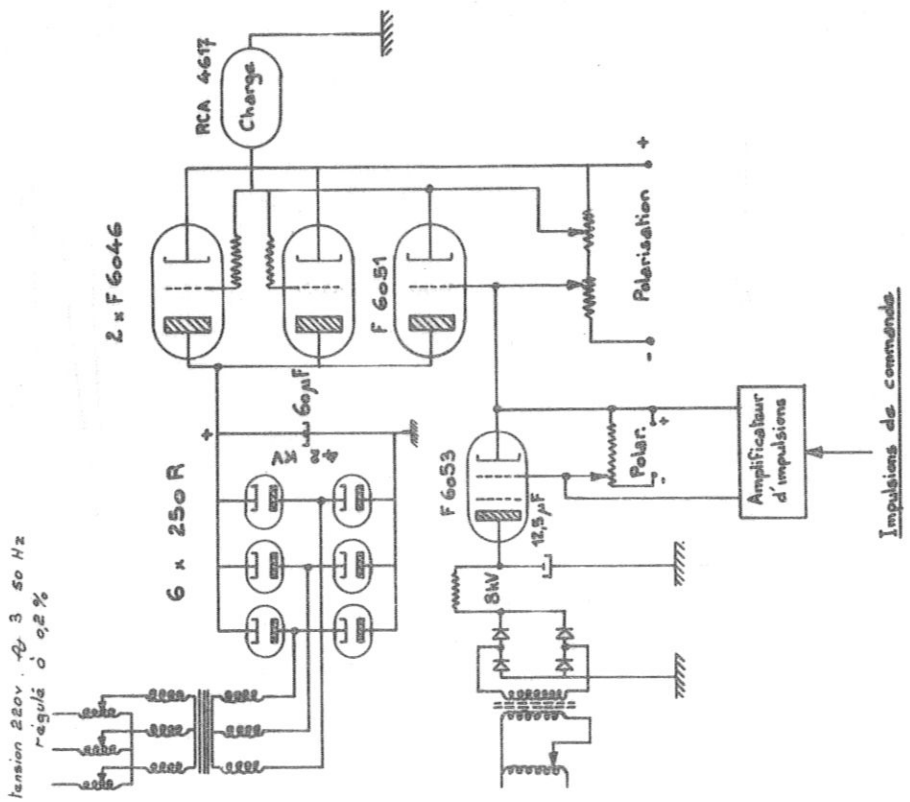

FIG. 4 Schéma du modulateur pour tube RCA 4617

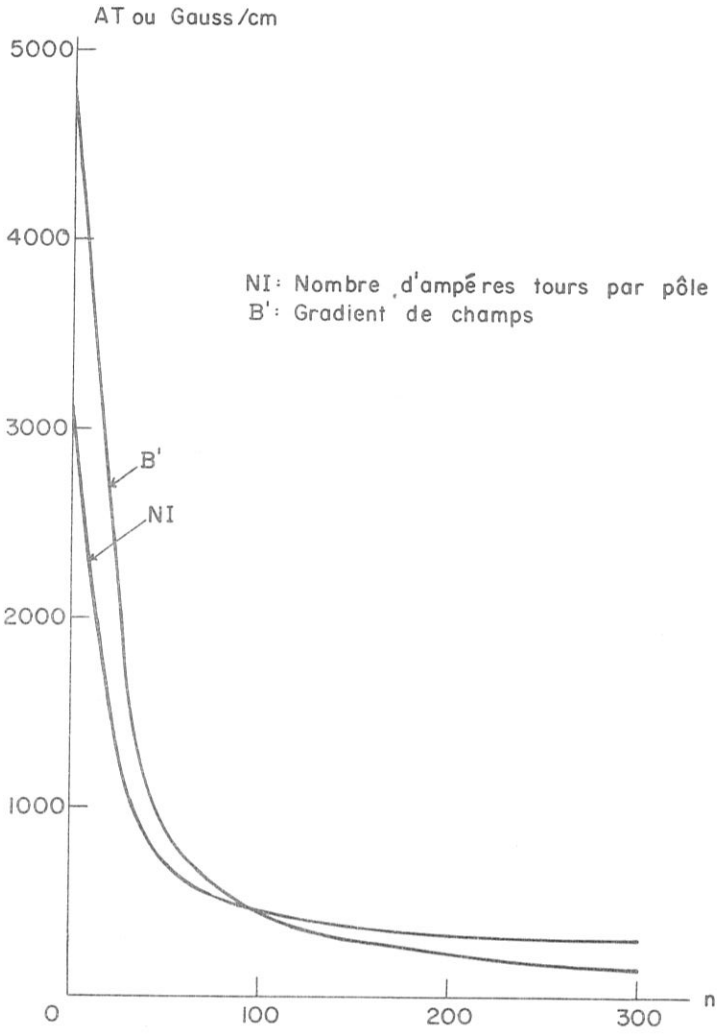

FIG. 6 Nombre d'ampéres tours par pôle et gradient de champ

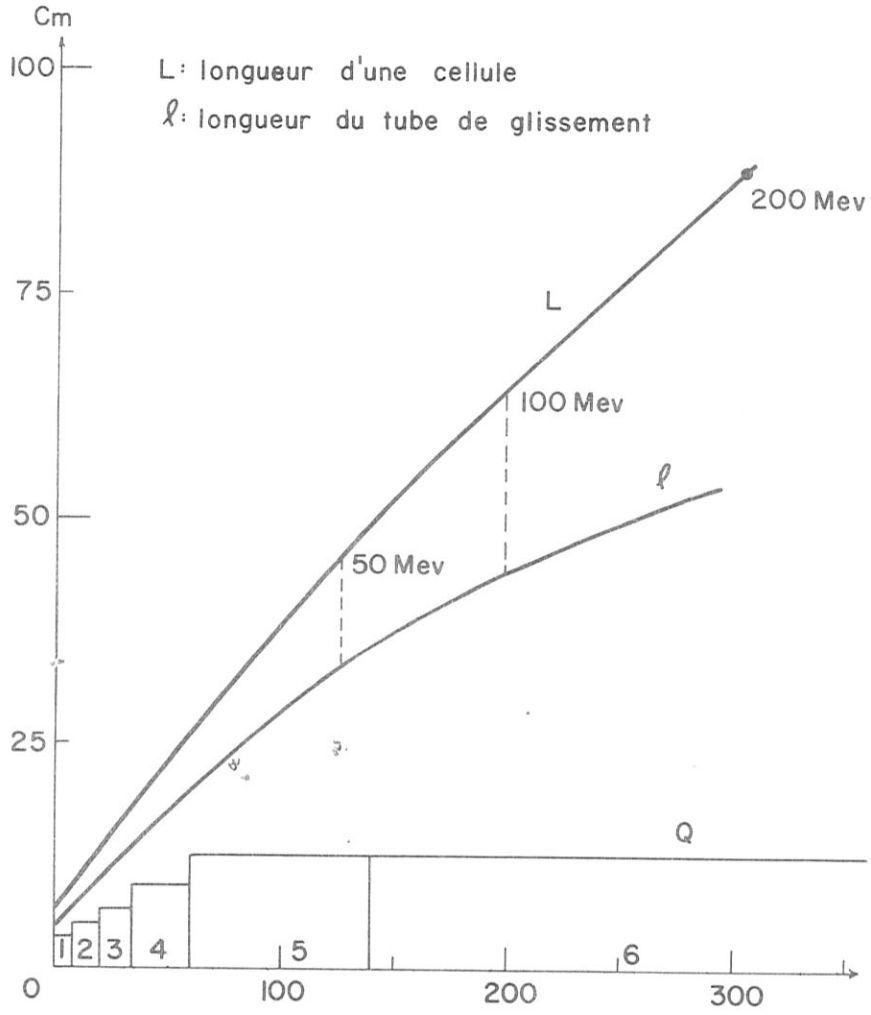

FIG. 7 Caracteristiques dimensionnelles de l'accelerateur

Type de section	Type I		Type II		Type III	Type IV
Type de bobine	Type 1	Type 2	Type 3	Type 4	Type 5	Type 6
Numéro de quadrupole	1 à 10	11 à 20	21 à 34	35 à 40	41 à 140	141 à 285
Type de Fil	creux $6x6mm^2$ $\phi 4mm$	creux $6x6mm^2$ $\phi 4mm$	plein $1x4mm^2$	plein $1x4mm^2$	plein $1x4mm^2$	plein $1x4mm^2$
Nombre de tours	5	5	80	80	60	40
Epaissaur. acier	3cm	4,5cm	6,5cm	9cm	13cm	13cm
Resistance 4 bob. en seria			0,420Ω	0,52Ω	0,368Ω	0,224 Ω
Densité de courant	$\leqslant$ 27 A/mm^2	$\leqslant$ 15 A/mm^2	$\leqslant$ 5 A/mm^2	$\leqslant$ 3 A/mm^2	$\leqslant$ 2 A/mm^2	$\leqslant$ 2 A/mm^2
tension oux bornes			5 à 7,5 v	$\sim$ 6 v	2,5 à 5 v	$\sim$ 2 v

PARAMETRES DES QUADRUPOLES

Fig. 8

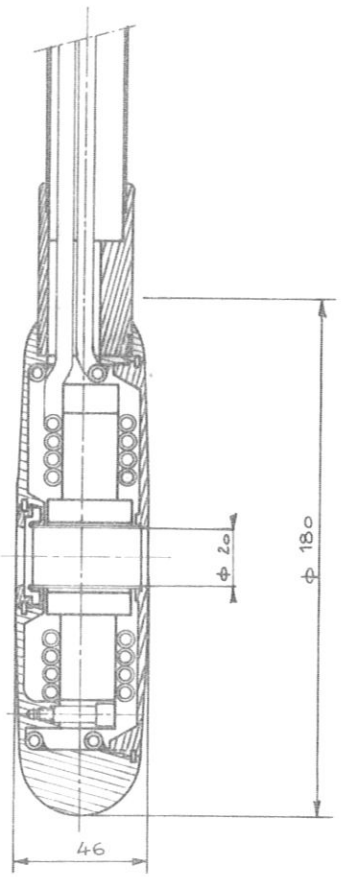

FIG. 9

PROJET JUPITER
Premier tube de glissement

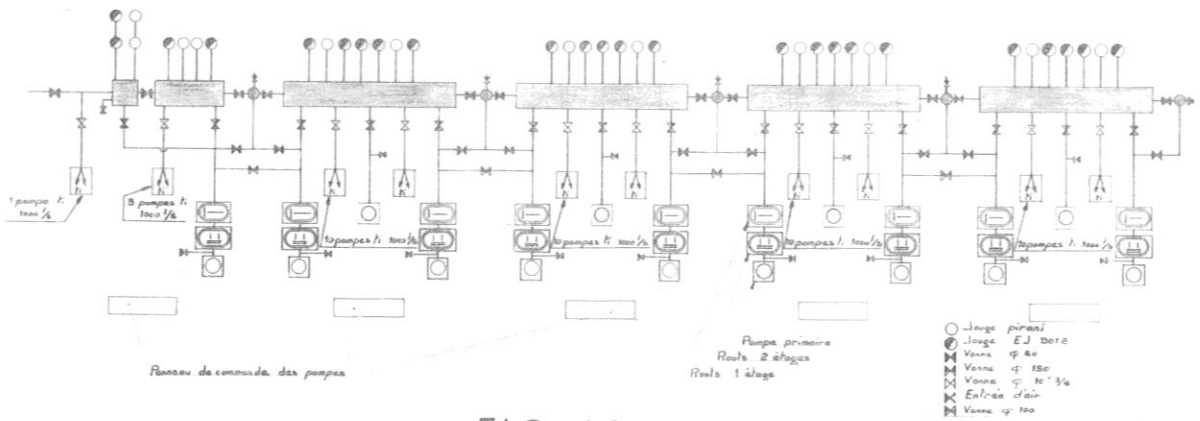

FIG. 10

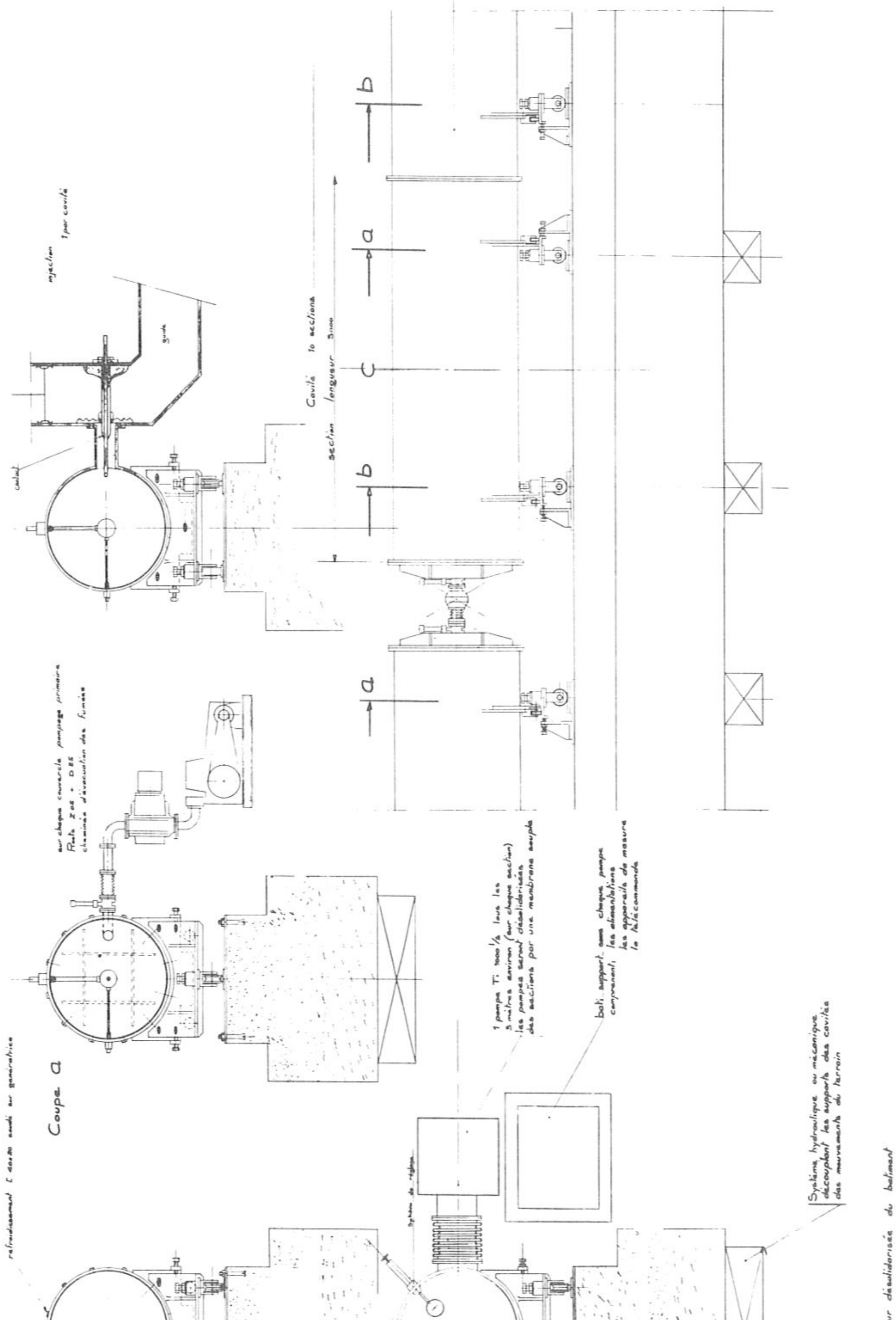

FIG. 11

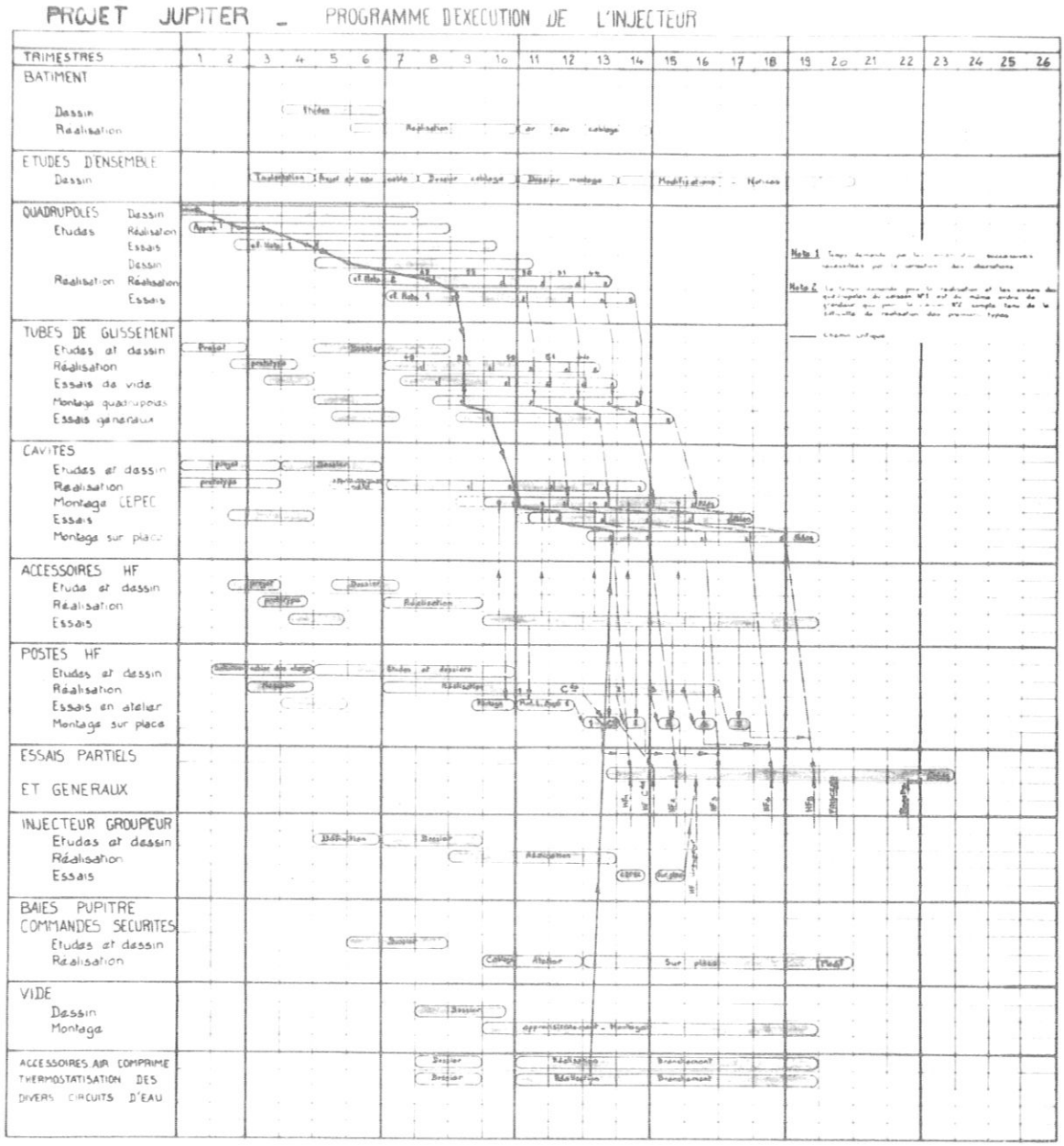
PROJET JUPITER - PROGRAMME D'EXECUTION DE L'INJECTEUR
TRIMESTRES 1 2 3 4 5 6 7 8 9 10 11 12 13 14 15 16 17 18 19 20 21 22 23 24 25 26
BATIMENT
Dessin
Réalisation
ETUDES D'ENSEMBLE
Dessin
QUADRUPOLES
Etudes
Dessin
Réalisation
Essais
Réalisation
Dessin
Réalisation
Essais
TUBES DE GLISSEMENT
Etudes et dessin
Réalisation
Essais de vide
Montage quadrupoles
Essais généraux
CAVITES
Etudes et dessin
Réalisation
Montage CEPEC
Essais
Montage sur place
ACCESSOIRES HF
Etudes et dessin
Réalisation
Essais
POSTES HF
Etudes et dessin
Réalisation
Essais en atelier
Montage sur place
ESSAIS PARTIELS
ET GENERAUX
INJECTEUR GROUPEUR
Etudes et dessin
Réalisation
Essais
BAIES PUPITRE
COMMANDES SECURITES
Etudes et dessin
Réalisation
VIDE
Dessin
Montage
ACCESSOIRES AIR COMPRIME
THERMOSTATISATION DES
DIVERS CIRCUITS D'EAU

FIG. 12

DRIFT TUBE AND PARAMETER SELECTION FOR LINEAR ACCELERATOR STRUCTURES BELOW 150 MEV

D. E. Young
Midwestern Universities Research Association

With three linac proposals being submitted to the USAEC this year, the question has arisen whether money could be saved by cooperation between the different groups. Savings could be realized in research and design, engineering, and in procuring similar items in greater quantities. Since each of these linacs have different basic design parameters such as the duty factor, beam current, energy, etc., the question arises whether a common design is really feasible. Certainly below 200 MeV where a drift tube loaded Alvarez structure is proposed there are many similarities. However, if one looks at the basic parameters which are to be met by each and tries to fit a common design to these parameters, one soon realizes that this is not possible. Wheeler has looked at this problem in detail[1] and concludes that if LASL agrees to derate their power supply so as to require an additional power module for the extra tank needed, which is the same as having the capability of accelerating a larger current but not doing so, and which of course would raise the cost of their proposal, then a common design is possible. If all three linacs were built, the saving in the common design might more than offset the added cost to LASL. I do not want to get too involved in this question. Rather I would like to point out that it is still possible to meet the basic parameters of each laboratory without adding greatly to fabrication costs if decisions can be reached on drift tube and tank structures which are fabricated of similar modules.

In order to reach agreement between the different laboratories on drift tube shapes, a committee was formed whose purpose was to try to enumerate the problem areas in adopting a particular drift tube shape and to try to expedite work in these areas. This committee made certain recommendations which I shall relate and work is proceeding in other areas. Since the committee was formed, its activities have been extended to a selection of parameters for the 200 Mc portion of the linac. If agreement can be reached, then savings should be realized in design and in larger volume purchases of similar components.

So far, the following recommendations have been made by the drift tube subcommittee:

1. Since sparking is mostly confined to the first gaps in operating linacs, it is desirable to design a short first section which can

be operated at reduced gradients. At 750 keV an average gap field of 8 MV/m or less should prevent excessive sparking for conventional shaped drift tubes. Above 10 MeV an average gap field of 12 to 13 MV/m is considered conservative.

2. An operating frequency of 201.25 Mc should allow design requirements to be met and give minimum interference with existing FCC allotted bands.

3. A drift tube hole of 2 cm has been achieved in the first drift tube at 0.75 MeV with a dc quadrupole and without unduly affecting the radial transit time factor. A linear increase from this size up to 4 cm at 200 MeV is recommended.

4. Satisfactory dc quadrupoles for drift tubes have been built and could be used in future design without major modifications.

5. A single drift tube stem is adequate even though a large diameter is required to accommodate four cooling leads.

6. The current computer programs for the calculation of drift tube shapes are sufficiently accurate so that extensive modelling is unnecessary.

7. Cylindrical shaped drift tubes at the higher energies can be chosen which are not far from an optimum shape and which, in addition, can be more easily fabricated.

In order to choose a drift tube shape, it is necessary to arrive at figures concerning the cost of rf power, the cost per unit length of the linac, the diameter of drift tubes which allow quadrupoles and adequate cooling, the maximum value of the accelerating rf gradients, the operating costs of the linac, as well as many other interacting requirements. In the months ahead many of these items will be better evaluated. To attempt to optimize the rf structure, including drift tube shape, clearly requires these considerations to be adequately assessed. However, even with the present knowledge it is instructive to understand the way these parameters affect the structure.

The total cost for building and operating a linac in terms of the power and length may be written as:

$$C = C_f + C_p P + C_{op} P t + C_L L + C_{oL} L t$$

where:

C_f = fixed costs
C_p = power costs per unit of power
C_{op} = power operating cost per unit of power per unit time
C_L = length costs per unit length
C_{oL} = length operating cost per unit length per unit time

A great deal of effort is being expended on an evaluation of the cost coefficients at the present time. The operating cost coefficients are difficult to assess, but after some searching through records of laboratories with operating linacs, we have found that if one takes t = 10 years, a possible lifetime of such a linac, then (within the error of determining these coefficients):

$$C_p \approx C_{op}\, t$$
$$C_L \approx C_{oL}\, t \ .$$

Now rewriting the formula in such a way as to give prominance to the factors which influence the structure

$$\frac{C - C_f}{2} = C_p P + C_L L$$

with the power P per energy gain ΔW given by

$$\frac{P}{\Delta W} = \frac{E_o T}{Z T^2 \cos\varphi}$$

and the length L per energy gain by

$$\frac{L}{\Delta W} = \frac{1}{E_o T \cos\varphi}$$

where E_o is the average peak axial accelerating field, T the longitudinal transit time factor, and φ the stable phase angle. In practice the power has to be increased, (a) to allow for losses on drift tube stems, tuners, and end plates as well as additional losses accounting for a lower Q value than the calculated value , and (b) reserve power to take care of beam loading. The power will be increased by a factor k to take care of the former, and a term $C_p I_B \Delta W$ added to allow for a beam I_B. With these considerations, the cost formula becomes:

$$\frac{C - C_f}{2} = \frac{C_p k E_o T \Delta W}{Z T^2 \cos\varphi} + C_p I_B \Delta W + C_L \frac{\Delta W}{E_o T \cos\varphi}$$

or

$$\frac{1}{\Delta W}\left[\frac{C - C_f}{2}\right] - C_p I_B = C_p\left[\frac{k E_o T}{ZT^2 \cos\varphi}\right] + C_L\left[\frac{1}{E_o T \cos\varphi}\right]$$

where the terms on the right are related to the choice of geometry. For any particular description of the geometry which specifes a value for Z and T, a cost can be calculated. The lowest cost will correspond to the largest value of Z and T. However, this alone does not allow one to choose a geometry that will allow the desired accelerating gradient to be achieved without excessive sparking. An accelerating gradient which will minimize this cost equation can be determined and is given by

$$E_o = \left[\frac{Z\, C_L}{k\, C_p}\right]^{1/2} .$$

This value of E_o is shown plotted in Fig. 1 as a function of Z. For any description of the geometry which gives a value of the shunt impedance Z, the value of E_o can be determined which gives a cost minimum. However before this information can be used in linac design, it is necessary to know what gradient can be maintained without problems due to sparking. Attempts are now being made to set safe sparking limits by accumulating data on operating linacs and by experimental measurements on a sparking cavity at this laboratory. Some preliminary results on the sparking cavity will be mentioned later. In the absence of a suitable explanation of sparking, one can use a value for the maximum field on the surface, such as the Kilpatrick criteria.[2] The MURA field computational program, MESSYMESH, can calculate the maximum value of the field on the surface of a drift tube. Actually what is calculated is a factor α, where

$$\alpha = \frac{E_{max}\ (\text{on surface})}{E_o} .$$

For some peak value on the surface, the value E_o can be calculated for the geometry considered. This value of E_o may be less than the optimum value of E_o obtained from the cost function for that particular geometry. If this is so, then to go to the optimum value would clearly cause maximum fields in excess of the chosen peak value on the surface and a danger of sparking. However, if it turns out that this value is greater than the optimum E_o, then sparking is not a problem because power is too expensive to go to the sparking level anyhow.

Using the MURA field computational program, we have investigated nearly 2000 different geometries for cylindrical shaped drift tubes. A

large number of runs have been done at energies of 50, 100, 150, and 200 MeV. When these runs are evaluated using the cost formula, it is possible to choose an optimum set of parameters that describe the geometry. This optimizing procedure using a specified value of the maximum field on the surface was described at the Yale Linac Conference.[3] If each run is plotted on the Z, E_o diagram with the value Z corresponding to the geometry and the value E_o calculated on the basis of an upper limit for the maximum field on the surface, one can observe the importance of the sparking restriction. At 50 MeV the cluster of points lie to the left of the curve of optimum gradient; at 100 MeV the cluster of points lie closer to the curve; and as the energy increases, the cluster moves closer to the curve. At 50 MeV, clearly money can be saved by raising the gradient to more nearly approach the optimum. At the higher energies where the value of Z is lower, it is not as definite and depends on the diameter of the drift tube which may be specified from engineering considerations.

Any practical drift tube must allow space for quadrupoles and cooling. This places an additional restriction on the diameter of a drift tube. Our studies indicate that a diameter of 15 or 16 cm is necessary especially for a high duty factor linac at energies of about 200 MeV. The latest popular cost data indicate that this diameter is a departure from the cost minimum and that it is unwise from sparking considerations to raise the accelerating gradient to the optimum value. However, it should be pointed out that the cost minima are rather flat so that the departure from the minimum may not be a great penalty. When one considers raising the gradient to reduce cost, one must also consider the limitation on the power amplifier tube. A shorter linac with a greater multiplicity of tanks and power amplifier tubes, phasing systems, and poorer reliability may not be a suitable way to save money.

When the specifications of the 200 Mc linacs at the three laboratories are considered, it is found possible to arrive at a design which uses many similar components. In particular, it is possible to maintain a constant drift tube diameter from 50 or 60 MeV upwards. Thus cylindrical drift tubes could be fabricated out of stock material with similar end caps. Quadrupoles might also be alike. The tank diameters can be similar, although of different lengths. By mass procurement of these similar components or pieces overall cost reductions can be realized when two or more linacs are constructed simultaneously without the necessity of requiring a departure from the basic design parameters.

To gather more information on the sparking restriction we have fabricated a one unit-cell cavity, with movable end plates so that geometry from 5 MeV to 150 MeV can be investigated under full power conditions.

This cavity is driven by an RCA 2515E (2041) power amplifer capable of approximately 300 kW at pulse lengths of about 500 μsec and about 30 pulses per second, and at a frequency of 200 Mc. Our initial operation was at 50 MeV with a drift tube diameter of 16 cm, 3 cm hole, and 4 cm curvature on the outer corner (the cavity diameter is 79 cm). At the present time we have operated up to 125 kW in the cavity. This power level corresponds to an average accelerating gradient (E_o) of 2.7 MV/m, an average gap field of 10 MV/m, or a peak field on the surface of 16 MV/m. At this level there was not a single spark detected, it was just a matter of running the power up. We are now trying to get more power out of the power supply to go to a level where we can see a few sparks. However, the next step will be to go to 5 MeV where sparks should occur at a lower power level. Here hopefully we can study the phenomena.

WHEELER: This type of expression for cost, which both Don and I have used, leaves out a very important consideration especially for the injectors, that is, there is nothing in the equation which says anything about the reliability of the accelerator. The constant k, which comes from experience, can be used to contribute to the reliability and one should consider very seriously keeping k a fairly large number. Experience with most of the proton linacs to date certainly shows that they have been underpowered. By increasing k one can design for lots of reserve power and this of course will greatly improve the reliability. The other matter is the choice of E_o with respect to sparking limit. In the MURA sparking cavity I am told that the x-ray background at the 125 kW level is rising very rapidly and I would predict that, at 16 MV/m on the surface, you are very close to the sparking limit. We have observed in the heavy ion machine that the x-ray background rises very steeply just before the sparking level is reached. So again in terms of reliability for the machine, one should be very conservative in keeping the value of the maximum field safely below the sparking limit. These two factors are very important in terms of achieving highly reliable machines.

LEISS: People have been using cost formulas for years and have systematically left out what is really in many projects the biggest cost of all, that is the project salaries. Have you thought how to integrate some of this into guessing what is the best to do? This would be particularly advantageous, although difficult, if examining the desirability of a common design.

YOUNG: The rules are becoming clearer now on how you estimate cost, even the salary costs. MURA has a technical note on their experience on

cost estimation and other people have discussed these things with the AEC to see how salaries should be integrated into the total project cost. This has not been put into the cost formula used here; this is a bigger operation research project than has been undertaken so far.

HUBBARD: As Wheeler pointed out, when you get somewhere near the sparking limit, you get a large amount of x-rays out of the machine which you must shield against. If you just lower the gradient slightly, the x-rays go down rapidly. Have you given any consideration to the amount of shielding necessary if you operate close to the sparking limit or have you put this into the cost formula?

YOUNG: We have not put the cost of shielding into the cost formula as a function of the gradient, only the cost of shielding as a part of the building costs which is part of the length costs. We intend, however, to make some measurements on the sparking cavity of the radiation background as a function of the voltage across the gap. We would like to get some good values for these quantities.

FEATHERSTONE: For the benefit of those of you who have not been paying close attention to the argument about sparking, I would just like to say a couple of words that I think should be repeated again and again. Mr. Kilpatrick wrote his "criterion", as it is so often referred to, in an attempt to integrate a great deal of data from many different sources and to account for it in an approximate way. I do not believe that he himself has ever given it the degree of authority that one would think it had by listening to the use of "Kilpatrick's criterion." Second, it was not intended as a working upper limit, but rather as a threshold level below which no sparking at all is expected to occur. Third, at 200 Mc a great many of the terms of his equation drop out and one arrives at something which is related only to the maximum field strength at the surface of the electrode. I think there is an accumulating body of evidence which indicates this is not adequate to account for the sparking we have observed in practical machines. I am very glad to hear Don say that they are going to try the spark cavity down in the equivalent of the 5 MeV energy region. What was the equivalent energy range of the present drift tube size?

YOUNG: 50 MeV.

FEATHERSTONE: The experience with the Brookhaven and Argonne linacs suggests strongly that something different is going on at the low energy end of the machine where there seem to be lower gradients and more sparking than at the high energy end. I don't think the gradient alone is enough to account for what we see. Of course, everybody knows

that sparking is affected by surface conditions and vacuum quality, but we presume that the surface conditions and vacuum conditions are pretty uniform from end to end.

REFERENCES

1. G. W. Wheeler, "The Unified Drift Tube Linac", Yale University Internal Report, G.W. 16 (June 3, 1964).

2. W. D. Kilpatrick, "A Criterion for Vacuum Sparking Designed to Include Both RF and DC", UCRL-2321 (1953).

3. D. E. Young, "Drift Tube Structures", Minutes of the Conference on Proton Linear Accelerators at Yale University (1963).

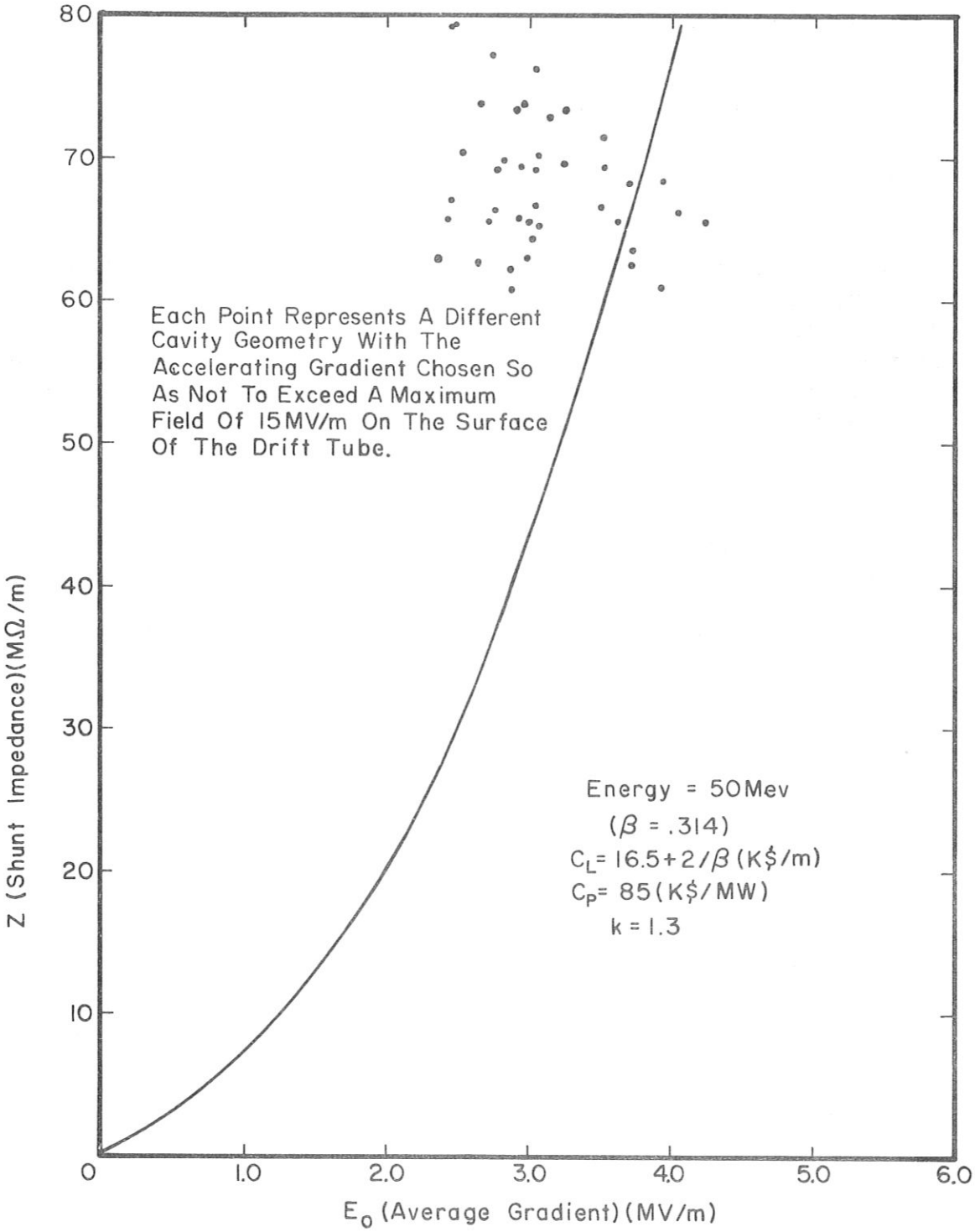

OPTIMUM ACCELERATING GRADIENT AS A FUNCTION OF SHUNT IMPEDANCE AT 50 MEV

Fig. 1

TRANSVERSE BEAM BLOW-UP IN STANDING WAVE LINACS

R. L. Gluckstern
Yale University and Brookhaven National Laboratory

I. Introduction

The phenomenon of beam blow-up in traveling wave electron linear accelerators[1] has caused concern as one has attempted to increase the beam current and pulse length. Among the explanations of the observed phenomenon is one presented by Wilson[2] in analogy with the theory of backward wave oscillators for accelerating-type fields. This explanation suggests that means exist to reduce the serious consequences of the blow-up by modifying the synchronism of the beam and backward wave deflecting mode. The effect discussed by Wilson takes place for bunched or unbunched beams.

A similar concern has been expressed by Leiss and Schrack[3] who point out that a bunched beam may have a harmonic which resonates with that component of the deflecting mode traveling with the beam velocity. For conventional iris-loaded guides, the deflecting mode frequency band is approximately 50% above that for the accelerating mode. If the beam bunching is, for example, at the 4th subharmonic of the accelerating mode (as it is at present for the AGS improvement program), then the 6th harmonic of the beam will be approximately resonant with the deflecting mode. This phenomenon clearly depends on the details of the mode spectrum for different values of β and can probably be influenced by transverse focusing and by perturbation of the deflecting modes where necessary.

The present work is an attempt to formulate the two corresponding effects for the case of a standing wave accelerator (proton linac in the case of the AGS improvement program). We will not treat here the additional serious effect of beam loading on the accelerating mode. (In this case the steady state effect can presumably be compensated for by adjusting the power source to supply additional power at high beam currents; the transient effect will require beam injection while the fields are rising in an appropriate way.)

II. Cavity Fields

We shall consider an iris-loaded guide of length $L = NL_o$, where L_o is the cell length, as shown in Fig. 1. The deflections will be assumed to be confined to the x - z plane, where z is taken as the longitudinal direction. In this plane the j^{th} normalized standing wave

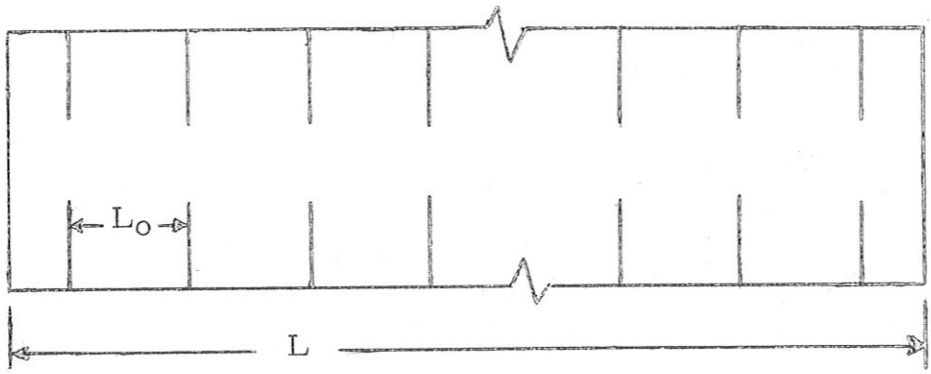

Fig. 1

deflecting mode can be written, because of Floquet's theorem, as

$$E_x^j(x,o,z) = \sum_{n=o}^{N-1} P_{jn}(x) \sin k_{jn} z ,$$

$$H_y^j(x,o,z) = \sum Q_{jn}(x) \cos k_{jn} z , \qquad (2.1)$$

$$E_z^j(x,o,z) = \sum R_{jn}(x) \cos k_{jn} z ,$$

where

$$k_{jn} = k_j + 2n\pi/L_o , \quad k_j = j\pi/L . \qquad (2.2)$$

If we define the space harmonic of concern as that for $n = 0$, the important components of the fields in the vicinity of the axis may be written as

$$E_x^j \cong P_j \sin k_j z$$
$$H_y^j \cong Q_j \cos k_j z \qquad (2.3)$$
$$E_z^j \cong x R_j \cos k_j z .$$

The fields are normalized such that

$$\nabla \times \vec{E}^j = (\omega_j/c)\,\vec{H}^j\,, \qquad \nabla \times \vec{H}^j = (\omega_j/c)\,\vec{E}^j\,,$$

$$\int dv\, \vec{E}^i \cdot \vec{E}^j = \int dv\, \vec{H}^i \cdot \vec{H}^j = \delta_{ij}\,, \tag{2.4}$$

and the actual fields are written in terms of the normalized fields as

$$\vec{E} = \sum_j C_j(t)\, E^j(\vec{x})\,, \qquad \vec{H} = \sum_j D_j(t)\, H^j(\vec{x})\,, \tag{2.5}$$

where C_j and D_j are related in the absence of beam by

$$D_j = (\epsilon c/\omega_j)\,\dot{C}_j\,, \qquad C_j = -(\mu c/\omega_j)\,\dot{D}_j\,. \tag{2.6}$$

Relations can be obtained between P_j, Q_j, R_j via Maxwell's equations. One must, however, take into account the component H_z in obtaining these relations, since the modes are not purely TE or TM, but are hybrid modes.[4] Let us write:

$$Q_j = F_j R_j\,, \qquad P_j = K_j R_j\,. \tag{2.7}$$

In the presence of a current pulse of the form

$$\vec{J}(\vec{x}, t) = \int_{-\infty}^{\infty} \vec{j}(\vec{x}, \omega)\, e^{i\omega t}\, d\omega \tag{2.8}$$

it can be shown that $C_j(t)$ satisfies a differential equation whose solution can be written in the form

$$C_j(t) = \frac{-i}{\epsilon} \int d\omega\, \frac{\omega\, e^{i\omega t}}{\omega^2 - \omega_j^2} \int \vec{j}(\vec{x}, \omega) \cdot E^j(\vec{x})\, dv\,. \tag{2.9}$$

The poles are moved into the upper half ω-plane because of losses. Assuming the losses to be small, one can write for late times (after the beam pulse has passed through the cavity)

$$\begin{aligned} C_j(t) &= -(\pi/\epsilon)\left[e^{i\omega_j t} \int \vec{j}(\vec{x}, \omega_j) \cdot \vec{E}^j\, dv + \text{c.c.}\right] \\ &\equiv -(\epsilon c)^{-1} D_j \cos(\omega_j t + \phi_j) \\ D_j(t) &= -\pi c\left[i\, e^{i\omega_j t} \int \vec{j}(\vec{x}, \omega_j) \cdot \vec{E}^j\, dv + \text{c.c.}\right] \\ &\equiv D_j \sin(\omega_j t + \phi_j)\,. \end{aligned} \tag{2.10}$$

In the presence of losses these fields will decay at the rate

$$e^{-\frac{\omega_j}{2Q_j}t} . \tag{2.11}$$

The transverse angular impulse given to a particle entering the cavity at $t = t_m$ in the presence of deflecting fields can be calculated in the approximation that the trajectory is along the longitudinal axis. One then has

$$\Delta\theta_x = (e/pv)\int_0^L dz \left[E_x - \mu v H_y\right]_{t = t_m + z/v} \tag{2.12}$$

$$= (e/\epsilon pc)\sum_j \omega_j^{-1}\int_0^L dz\, R_j \cos k_j z\, D_j \sin(\omega_j z/v + \psi_j) ,$$

where

$$\psi_j = \omega_j t_m + \phi_j . \tag{2.13}$$

Since one is interested only in those modes for which k_j and ω_j/v are almost equal (phase velocity of deflecting mode approximately the same as beam velocity), one may write

$$\Delta\theta_x \cong (eL/\epsilon pc)\sum_j (\omega_j \alpha_j)^{-1} D_j R_j \sin(\alpha_j/2)\sin(\psi_j - \alpha_j/2) , \tag{2.14}$$

where

$$\alpha_j \equiv (k_j - \omega_j/v)L \tag{2.15}$$

is the slip of beam relative to the wave in its transit through the cavity. If one adds angular impulses due to all effects, the beam will be lost when

$$\Lambda_x \Delta\theta_x \sim 2\pi a , \tag{2.16}$$

where Λ_x is the wavelength of the transverse oscillation and a is the bore radius.

The remaining quantity needed for our analysis is $\vec{j}(\omega)$. Assuming a single bunch of spatial dependence f (z) (symmetric about z = 0

for convenience) whose center follows the trajectory $z = vt$, $x = x(t)$, one has

$$\vec{J}(\vec{x}, t) = I_o \Delta t\, \delta\left[x - x(t)\right]\ \delta(y)\, f\left[z - v(t - t_m)\right]\ \left[\vec{i}\,\dot{x}(t) + \vec{k}\, v\right]$$

where $\Delta t = 2\pi / \omega_o$ is the separation of beam bunches and I_o is the average current. Writing

$$f(u) = \frac{1}{2\pi v}\int d\omega\ e^{-i\frac{\omega}{v}u}\ g(\omega), \quad g(\omega) = \int_{-\infty}^{\infty} du\ e^{i\frac{\omega}{v}u}\ f(u) \tag{2.17}$$

one finds, for narrow bunches,

$$\vec{j}(\vec{x}, \omega) = \frac{I_o}{\omega_o}\, g(\omega)\ \delta\left[x - x(t_m + z/v)\right]\ \delta(y)\left[\vec{i}\,\dot{x}(t_m + z/v)/v + \vec{k}\right] e^{-i\omega t_m - i\omega z/v} \tag{2.18}$$

The normalization is such that for a delta function bunch $g(\omega) = 1$; that is, $g(\omega)$ is the relative harmonic content of the beam pulse. The relevant integral in (2.10) is therefore

$$\int \vec{j}(\vec{x}, \omega_j) \cdot \vec{E}^j\, dv =$$

$$(I_o / \omega_o v)\, g(\omega_j)\, e^{-i\omega_j z/v}\left[\dot{x}(t_m + z/v)\, E_x^j(x(t_m + z/v), 0, z) + v\, E_z^j(x(t_m + z/v), 0, z)\right] \tag{2.19}$$

In the limit of small transverse displacements, one then finds from (2.3), (2.7):

$$\int \vec{j}(\vec{x}, \omega_j) \cdot \vec{E}^j\, dv =$$

$$(I_o / \omega_o)\, g(\omega_j)\, e^{-i\omega_j t_m} R_j \int_o^L dz\, e^{-i\omega_j z/v}\left[K_j(\dot{x}/v)\sin k_j z + x\cos k_j z\right] \cong (I_o/2\omega_o)\, g(\omega_j)\, e^{-i\omega_j t_m} R_j \int_o^L dz\, e^{i\alpha_j z/L}$$

$$\left[x(z) - K_j\, i x'(z)\right] . \tag{2.20}$$

III. Nonresonant Beam Blow-up

If one considers that the beam has transverse displacement and velocity unaffected by the cavity fields in calculating the contribution to (2.20), then the contribution of successive bunches will depend on their relative phase, and build-up will be serious only if there is a resonance between a beam pulse harmonic and a defelcting mode. This phenomenon is treated in Section IV. If no resonance exists, one must consider the effect of the field itself on the trajectory in order to get a significant contribution to (2.20). This is the effect considered by Wilson, and the one we shall treat in Section III for a standing wave linac.

In order to evaluate (2.20), we must find the trajectory of that particle entering the cavity which is oscillating with fields

$$C_j(t) = -(\epsilon c)^{-1} D_j \cos(\omega_j t + \phi_j)$$
$$D_j(t) = D_j \sin(\omega_j t + \phi_j), \tag{3.1}$$

at the time t_m. According to (2.12) one has

$$\Delta\theta_x = x'(z) = (e/pv)\int_0^z dz \left[E_x - \mu v H_y\right]_{t = t_m + z/v}. \tag{3.2}$$

Keeping only those wave components traveling at approximately the same velocity as the particle, one finds

$$x'(z) \cong -\sum_k (e/\epsilon p c \omega_k)\left\{\left[D_k(t_m + z/v) E_x^k\right]_0^z - \int_0^z dz\, D_k(t_m + z/v)(\partial E_z^k/\partial x)\right\}$$

$$\cong (e/2\epsilon pc)\sum_k (D_k R_k/\omega_k)(L/\alpha_k - K_k)\left[\cos(\alpha_k z/L - \psi_k) - \cos\psi_k\right], \tag{3.3}$$

$$x(z) = (e/2\epsilon pc)\sum_k (D_k R_k/\omega_k)(L/\alpha_k - K_k)(L/\alpha_k)\left[\sin(\alpha_k z/L - \psi_k) + \sin\psi_k - (\alpha_k z/L)\cos\psi_k\right], \tag{3.4}$$

where

$$\psi_k = \omega_k t_m + \phi_k. \tag{3.5}$$

The nonresonant character of the values of t_m implies that only the $e^{i\Psi_k}$ component of (3.3) and (3.4) is needed with the factor $e^{-i\omega_j t_m}$ in (2.20). In this approximation one has

$$\int \vec{j} \cdot \vec{E^j}\, dv = (e I_o / 8 \omega_o \epsilon\, pc)\, g(\omega_j) \sum_k e^{i(\omega_k - \omega_j) t_m + i\phi_k} (D_k R_j R_k / \omega_k)(L/\alpha_k - K_k)$$

$$\times \int_o^L dz\, e^{i\alpha_j z/L} \left[(L/\alpha_k)(i\, e^{-i\alpha_k z/L} - i - \alpha_k z/L) - K_j\, i\, (e^{-i\alpha_k z/L} - 1)\right]$$

$$\equiv \sum_k M_{jk}\, e^{i m_{jk}}\, e^{i(\omega_k - \omega_j) t_m}\, D_k\, e^{i\phi_k}, \qquad (3.6)$$

where M_{jk} and m_{jk} are the amplitude and phase of all the factors not appearing explicitly in the last form of (3.6). From (2.10), the pulse entering at t_m contributes an increment to the field already present, which is given, including the decay of the field already present, by

$$\Delta D_j(t) \cong 2\pi c \sum_k D_k M_{jk} \sin\left[\omega_j t + (\omega_k - \omega_j) t_m + \phi_k + m_{jk}\right]$$

$$- (\omega_j \Delta t / 2 Q_j) D_j \sin(\omega_j t + \phi_j). \qquad (3.7)$$

This is our result. It is, of course, dependent on the mode spectrum (ω_j vs j), the timing of the pulses* (t_m), the slip (α_j vs j), and all the other nonexponential factors appearing in M_{jk}. Particularly in cases of low group velocity (ω_k close to ω_j), one should proceed directly from (3.7) on a numerical basis.

We shall try to reduce (3.7) analytically by making further assumptions. In particular we shall assume a steady state solution for which the contributions for $k \neq j$ in (3.7) average to zero. In this case

$$\Delta D_j(t) = 2\pi c\, M_{jj} D_j \sin(\omega_j t + \phi_j + m_{jj}) - (\pi \omega_j / \omega_o Q_j) D_j \sin(\omega_j t + \phi), \qquad (3.8)$$

---

*We have already assumed that the pulses are nonresonant and have ignored the term in $(\omega_k + \omega_j) t_m$. If they are resonant, the present considerations are modified by a factor of order 2.

which is equivalent to the relations

$$\frac{\Delta D_j}{D_j} = 2\pi c M_{jj} \cos m_{jj} - \frac{\pi \omega_j}{\omega_o Q_j} \tag{3.9}$$

and

$$\Delta \phi_j = -2\pi c M_{jj} \sin m_{jj} . \tag{3.10}$$

From (3.6), one finds

$$M_{jj} \cos m_{jj} = (e I_o / 8 \omega_o \epsilon pc)\, g(\omega_j)\, (R_j^2/\omega_j)(L/\alpha - K)\, L$$

$$\times \mathrm{Re} \int_0^1 dx \left[i (L/\alpha - K)(1 - e^{i\alpha x}) - \alpha x e^{i\alpha x} L/\alpha \right]$$

$$= (e I_o / 4 \omega_o \epsilon pc)\, g(\omega_j)\, (R_j^2/\omega_j)(L/\alpha - K)\, L/\alpha \left[L/\alpha \left(1 - \cos\alpha - \tfrac{\alpha}{2}\sin\alpha\right) - \right.$$

$$\left. - K (1 - \cos\alpha)/2 \right] . \tag{3.11}$$

In the approximation of small coupling holes it can be shown that

$$\frac{L}{\alpha} \gg K . \tag{3.12}$$

Equation (3.11) then becomes

$$M_{jj} \cos m_{jj} = (e I_o / 2\pi^3 \omega_o \epsilon pc)\, g(\omega_j)(R_j^2/\omega_j)\, L^3\, g_2(\alpha_j) \tag{3.13}$$

where

$$g_2(\alpha) = \frac{1 - \cos\alpha - (\alpha/2)\sin\alpha}{2(\alpha/\pi)^3} \tag{3.14}$$

is the same function as that defined by Wilson, and has a maximum value of 1.04 when $\alpha = 2.65$.

The "starting current" for the beam blow-up is therefore given by the vanishing of (3.9), that is for

$$e I_o = \frac{\pi^3 \epsilon p \omega_j^2}{g_2 g L^3 R_j^2 Q_j} . \tag{3.15}$$

The quantity $Q_j R_j^2$ is related to the ratio of the square of the electric field gradient along the axis to the power loss and therefore has the general form of a shunt resistance per unit length for the deflecting mode. Specifically, if one defines r_ℓ as

$$r_\ell = \frac{\left[(c/\omega_j)\int_o^L dz\ (\partial E_z^j/\partial x)\cos k_j z\right]^2}{L \times \text{Power Loss}}\ , \qquad (3.16)$$

and notes that Q_j may be written as

$$Q_j = \frac{(\omega_j \epsilon/2)\int |\vec{E^j}|^2\, dv}{\text{Power Loss}} = (\omega_j \epsilon/2\ \text{Power Loss}) \qquad (3.17)$$

one has

$$\frac{r_\ell}{Q_j} = L R_j^2 (c/\omega_j)^3 Z_o/2\ , \qquad (3.18)$$

where

$$Z_o = \sqrt{\mu/\epsilon} = 377\ \text{ohms}\ . \qquad (3.19)$$

This leads finally to

$$e I_o = \frac{\pi^3 Mc^2 (c/\omega_j)\beta\gamma}{2 g_2 g r_\ell L^2}\ . \qquad (3.20)$$

As an illustration of the order of magnitude of (3.20), we shall apply it to the first iris cavity in the proposed new AGS injector where we use the following parameters:

$$\begin{aligned} Mc^2 &= 940\ \text{Mev} \\ 2\pi c/\omega_j &= 0.25\ \text{m} \\ \beta &= 0.6 \\ \gamma &= 1.25 \\ g_2 &\sim g \sim 1 \\ L &\sim 3\ \text{m} \\ r_\ell &\sim 20\ \text{megohms/m} \end{aligned} \qquad (3.21)$$

leading to

$$I_o \simeq 2\ \text{amp.} \qquad (3.22)$$

Several comments should be made at this time:

1) The value of r_ℓ has been chosen typical of accelerating modes. It will probably be considerably smaller since the square of a transit time factor should be included to correspond to the particular space harmonic used. This will lead to an even higher "starting current."*

2) Resonance between the deflecting mode and the beam bunch frequency will lead to a reduction of order of a factor 2 in (3.20) and (3.22).

3) If the current is higher than the limit in (3.20), the build-up time can be estimated from (3.9) with an assumption for the order of magnitude of the "noise" in the cavity. The result will be of the form

$$T_B = \frac{\text{Const.}}{I_o - I_{o,\,\text{starting}}} . \tag{3.23}$$

4) Although the present calculation is for a standing wave linac, the form of Wilson's result for a traveling wave linac can be obtained by going to the limit of large L in (3.6). The sum over k becomes an integral over k and a sum over beam pulses (m) leads to

$$\sum_m e^{i(\omega_k - \omega_j)m\Delta t} = 2\pi\,\delta\left[(\omega_k - \omega_j)\,\Delta t\right]$$

$$\cong \left(\frac{d\pi}{dk}\right)^{-1} \frac{\omega_o L}{\pi}\,\delta(k-j) = \frac{\omega_o L}{\pi v_g}\,\delta(k-j) . \tag{3.24}$$

The factor M_{jj} in (3.6) must then be multiplied by the factor $(\omega_o L/\pi v_g)$ and the self-consistent condition $\Delta D/D = 1$ leads to (3.20) multiplied by the factor $v_g Q_j/\omega_j L$. This factor, which is the ratio of the decay time to the filling time, is not surprising when one goes from a standing to a traveling wave linac. The net result for the starting current is an expression of the form

$$e I_o{}^{T.W.} \sim \frac{Mc^2 \beta\gamma (v_g/c)(c/\omega)^2}{g_2\, g\, L^3} \left(\frac{Q}{r_\ell}\right) , \tag{3.25}$$

which is identical in its dependence on the parameters with Wilson's result.

*An estimate of r_ℓ has been made for a model of independent cells. This leads to $r_\ell \sim 1$ megohm/m and gives a starting current of 40 amp. See Appendix.

5) The contributions from $k \neq j$ in (3.7) may not be negligible, as indicated by the traveling wave result. However, the factor M_{jk} has a structure which confines contributions to the vicinity $\alpha_j \sim \alpha_k \sim \pi$. An estimate of the effect of the term

$$(\omega_k - \omega_j)\, t_m \tag{3.26}$$

for an adjacent mode can be made by taking t_m to be the build-up time, which is assumed to be of the same order as the decay time, i.e.,

$$t_m \sim Q/\omega_j \,. \tag{3.27}$$

For this choice

$$(\omega_k - \omega_j)\, t_m \approx v_g\, Q_j/\omega_j\, L \,. \tag{3.28}$$

The contributions will therefore be confined to the mode $k = j$ or will extend to the neighboring modes according to whether the parameter in (3.28) is greater than or less than 1. If it were not for the factor M_{jk}, one would then multiply (3.20) by the factor $v_g\, Q/\omega_j\, L$ as we did in (3.25) for the traveling wave case.

6) Proper numerical investigation of this phenomenon should be performed starting with (3.7), with an appropriate deflecting mode spectrum.

7) Motion in the y direction has been neglected. If this is taken into account, the cavity oscillations may be induced with rotating polarization. This can, of course, be prevented by destroying the azimuthal symmetry.

IV. Resonant Beam Blow-up

The other possible serious effect previously mentioned occurs if one of the harmonics of the beam frequency resonates with one of the deflecting modes. In this case the transverse motion of the bunches induces cavity fields which may then build up from successive pulses. Since the build-up leads to deflections, this phenomenon involves not only the transverse focusing system, but the entire transverse history of the beam in preceding cavities.

According to (2.20), the m^{th} beam bunch, traversing a cavity with average transverse displacement and angle given by x_m and x'_m, gives a contribution to the current of

$$\int \vec{j}\,(\vec{x},\ \omega_j) \cdot \vec{E}^j \, dv \ =$$

$$= (I_o\, g/2\,\omega_o)\, R_j\, (L/\alpha)\, e^{-i\omega_j t_m} (x_m - K_j\, i x'_m)(e^{i\alpha} - 1)\ . \quad (4.1)$$

The contribution to the field is therefore

$$\Delta D_j\,(t) = (\pi c\, I_o\, g\, L\, R_j\, g_3/\omega_o)\ \mathrm{Re}\left\{e^{i\omega_j(t - t_m) + i\alpha/2} (x_m - K_j\, i x'_m)\right\}\ . \quad (4.2)$$

The factor $g_3 = \dfrac{\sin(\alpha/2)}{\alpha/2}$ indicates that the effect is appreciable only for those deflecting modes with phase velocities close to the beam velocity. The factor $e^{-i\omega_j t_m}$ indicates that the contributions of successive bunches will be out of phase unless

$$\omega_j\, \Delta t/2\pi = \omega_j/\omega_o \simeq s\ , \quad (4.3)$$

that is, unless the ratio of deflecting mode frequency to beam frequency is close to an integer.

The angular deflection due to the presence of deflecting modes is given by (2.14). If one also includes the effects of the focusing forces, the coupled set of equations (2.14) and (4.2) allow one to follow the progress of the effect from cavity to cavity and from pulse to pulse numerically. [The effect treated in Section III may even be included by adding (3.8) to (4.2).] It is clear that in this case the effect depends even more sensitively on the deflecting mode spectrum.

An order of magnitude estimate of the effect can be made in the steady state condition (constant values of x_m, x'_m from pulse to pulse) by including the field decay due to losses. The field after the entrance of the n^{th} bunch is then

$$D_j\,(t) = (\pi c\, I_o\, g\, L\, R_j\, g_3/\omega_o)\ \mathrm{Re}\left\{e^{i\omega_j\,(t - t_n) + i\alpha/2} (x - K_j\, i x')\right.$$

$$\left.\sum_{m=o}^{\infty} e^{2\pi m\left[i\,(\omega_j/\omega_o - s) - (\omega_j/2\omega_o Q_j\right]}\right\}$$

$$\simeq (c\, I_o\, g\, L\, R_j\, g_3/2\,\omega_o)\ \mathrm{Re}\left\{\frac{e^{i\omega_j(t - t_n) + i\alpha/2}\ (x - K_j\, i x')}{(\omega_j/2\ \omega_o Q_j) - i\,(\omega_j/\omega_o - s)}\right\}. \quad (4.4)$$

Since Q_j will normally be much larger than $\left|\omega_j/\omega_o - s\right|$, (4.4) can be reduced to

$$D_j(t) \simeq (\pi c I_o g L R_j g_3)\left[\frac{K_j x' \cos \chi_j - x \sin \chi_j}{\omega_j - s\omega_o}\right], \qquad (4.5)$$

where

$$\chi_j = \omega_j (t - t_n) + \alpha/2 . \qquad (4.6)$$

The deflection of the n^{th} bunch in this field is given by (2.14). The $\cos \chi_j$ term in (4.5) corresponds to $\psi_j = \alpha_j/2 + \pi/2$ in (2.13), while the $\sin \chi_j$ term corresponds to $\psi_j = \alpha_j/2$. One therefore has, using (3.18),

$$\Delta x' \simeq x' \sum_j (e\pi I_o g g_3^2 L/p)(r_\ell/Q_j)/(\omega_j - s\omega_o) K_j (\omega_j/c)^2 . \qquad (4.7)$$

The increase in transverse amplitude due to this angular deflection is

$$\Delta A_x \simeq \sum_j \frac{\Lambda_x e I_o g g_3^2 L \omega_j r_\ell K_j (\omega_j/c)}{2 Mc^2 \beta\gamma Q_j (\omega_j - s\omega_o)} . \qquad (4.8)$$

For the independent cell model used before, and the AGS improvement program parameters, including I_o = 100 mA, one finds (see Appendix)

$$\Delta A_x \sim \frac{3 \times 10^{-7}}{s\omega_o (1 - \frac{\omega_o}{\omega_j})} \text{ meters} . \qquad (4.9)$$

Thus, for a resonance accurate to 10^{-3}, the increase in transverse amplitude from this cavity is ~ 0.03 cm. Since it is unlikely that this resonance will persist to an accuracy of 10^{-3} for several cavities, the effect appears not to be serious. If it should turn out that the resonance is more serious in one of the cavities, a perturbation of the deflecting modes of order 10^{-3} can undoubtedly be readily provided for.

In summary, therefore, it appears that the transverse motion of the beam can lead to a build-up of the deflecting mode if there is a resonance between the beam and deflecting mode frequencies. A rough estimate of the effect indicates that it is small, but numerical estimates

using (3.8), (4.2) and (2.14) are desirable. For these and other reasons it is recommended that both the accelerating and deflecting mode spectrum be measured carefully at several values of β.

We have of course neglected the variation of cell geometry within a cavity. This should reduce the effects discussed in this paper even further.

V. Summary

We have calculated the build-up of deflecting modes due to two separate causes. The first (Section III) is the nonresonant effect that comes from the deflection of the beam by the transverse fields already present. These deflections induce further transverse fields which have a component in phase with the original field. The appropriate equation governing the behavior of a bunched beam due to this effect is (3.7), with M_{jk} and m_{jk} defined in (3.6). For an approximate treatment of the steady state behavior, (3.20) is relevant. A further approximate calculation of r_ℓ is contained in the Appendix, and the corresponding current limit is given in (A-12).

The second effect treated (Section IV) is the resonant build-up of the deflecting modes due to the transverse oscillations of the beam. The average displacement and angle of a beam bunch with respect to the longitudinal cavity axis induces a transverse field. Successive bunches can build up this field if there is a resonance between the transverse mode and one of the harmonics of the beam. The appropriate equations governing the build-up of these coupled "displacement-field" oscillations are (4.2) and (2.14). For an approximate treatment of the steady state behavior, (4.5), (4.7) and (4.8) are relevant. A further approximate calculation of r_ℓ/Q_j is contained in the Appendix, and the corresponding limit is given in (A-10).

Numerical computation of the combination of the above two effects can also be performed. For this purpose the field increment per pulse is the sum of (3.8) and (4.2).

It is clear that both effects limit the contributions to those modes which slip no more than 180° behind the beam. In addition, the second effect is significant only if the resonance exists. For these reasons it is important to measure the mode spectrum for the cavities accurately for both the accelerating and deflecting bands at several values of β.

Estimates of the magnitudes of the two effects discussed have been made for the AGS improvement program parameters. Although these

are extremely crude, the values obtained are not at all serious and should not prove troublesome.

We have not treated the case of two transverse dimensions, nor have we considered the effects of the induced fields on the bunching of the beam pulses. Moreover, we have treated each cavity as having a constant value of v and a uniform cell geometry. These effects will hopefully not be serious. Besides, one always has the possibility of perturbing the transverse modes to modify transverse effects. We have also not considered the possibility of longitudinal beam blow-up.

VI. Acknowledgements

It is a pleasure to acknowledge several helpful conversations with Dr. T. Nishikawa of the University of Tokyo, and with Dr. W. Walkinshaw of the Rutherford Laboratory.

APPENDIX

We shall estimate r_ℓ and Q for the deflecting modes under the assumption that the cells are approximately uncoupled. In this case the fields in the m^{th} cell are TM_{110} of the form

$$\begin{aligned} E_z^j &= A_m^j \, J_1 (p_{11} \, r/b) \cos \theta \\ H_\varphi^j &= A_m^j \, J_1' (p_{11} \, r/b) \cos \theta \\ H_r^j &= A_m \, \frac{J_1 (p_{11} \, r/b)}{p_{11} \, r/b} \sin \theta , \end{aligned} \tag{A-1}$$

where

$$A_m^j = A_o^j \cos (m \, k_j \, L_o) , \qquad b = p_{11} \, c/\omega_j , \tag{A-2}$$

and p_{11} is the first zero of J_1. The Fourier decomposition of E_z^j can be shown to be

$$E_z^j = J_1 (p_{11} \, r/b) \cos \theta \, A_o^j \sum_{n=o}^{N-1} \frac{\sin k_{jn} \, L_o}{k_{jn} \, L_o} \cos k_{jn} \, z, \tag{A-3}$$

where k_{jn} is given by (2.2). The relevant deflecting mode (n = 0) in the vicinity of the axis is therefore given by

$$E_z^j = x \, (p_{11} \, A_o^j \, g_1/2 \, b) \cos k_j \, z . \tag{A-4}$$

Comparison with (2.3) indicates that

$$R_j = \omega_j \, A_o^j \, g_1/2 \, c , \tag{A-5}$$

where

$$g_1 = \frac{\sin k_j \, L_o}{k_j \, L_o} . \tag{A-6}$$

The quantity A_o^j is obtained from the normalization condition (2.4). It can be shown to be

$$A_o^{j2} = \left[4 \, \omega_j^2 / \pi \, L \, p_{11}^2 \, c^2 \, J_o^2 (p_{11}) \right] \simeq \left[2 \, \omega_j^2 / L \, p_{11} \, c^2 \right] . \tag{A-7}$$

From (3.18) one has

$$\frac{r_\ell}{Q_j} = L R_j^2 (c/\omega_j)^3 Z_o/2 \simeq \frac{\dot{Z}_o g_1^2 (\omega_j/c)}{4 p_{11}} . \qquad (A-8)$$

For small holes one can show that

$$K \omega/c \sim (p_{11}^2/4\beta) (a/b)^2 \qquad (A-9)$$

where a is the hole radius. Equation (4.8) can then be written as

$$\Delta A_x \simeq \sum_j \frac{\Lambda_x e I_o Z_o L g g_1^2 g_3^2 (\omega_j/c) p_{11} a^2}{32 Mc^2 (1 - s \omega_o/\omega_j) \beta^2 \gamma b^2} . \qquad (A-10)$$

In order to obtain r_ℓ or Q_j independently, one must calculate the power loss. This is obtained from the square of the tangential magnetic field on both the guide and cell walls, and turns out to be

$$r_\ell \simeq \left(\frac{Z_o}{\delta}\right) \left(\frac{g_1^2}{8}\right) \left(\frac{L_o}{L_o + b}\right) , \quad Q_j^{-1} = \frac{2 \delta(\omega_j/c)}{p_{11}} \left(\frac{L_o + b}{L_o}\right) \qquad (A-11)$$

where δ is the skin depth. Equation (3.20) then becomes

$$e I_o = \left(\frac{4 \pi^3}{g g_1^2 g_2}\right) \left[\frac{\delta \beta \gamma Mc^2 (c/\omega_j)}{Z_o L^2}\right] \left(\frac{L_o + b}{L_o}\right) . \qquad (A-12)$$

LEISS: Does not the resonant beam blow-up always contribute in a serious way?

GLUCKSTERN: It does in the sense that the nonaxial component of the beam current can be increased by the response of the cavity. However, this depends on a resonance between the transverse mode and a multiple of the beam frequency. In addition the presence of transverse forces may modify the build-up.

E. KNAPP: Isn't the value of shunt impedance used (20 Megohms/meter) high?

GLUCKSTERN: Yes. As a first conservative calculation I took a value comparable with the accelerating mode. However, for the transverse one should take the appropriate space harmonic with a phase velocity equal to that of the particle. In this case the "starting" current is increased by a factor of order 10.

WALKINSHAW: Shouldn't one include other field components for the transverse modes?

GLUCKSTERN: Yes. Although the only components which do not vanish in the x-z plane are the ones used, the relation between these components depend on the other components--in particular, on $\partial H_z / \partial y$. This has only been taken into account approximately in the present calculation.

LEISS: Isn't it true that both effects (resonant and nonresonant beam blow-up) are present together and are part of the same effect?

GLUCKSTERN: I do not believe the two effects are the same, but both effects should be taken together in any proper calculation.

LEISS: Aren't there important resonant effects in your calculation of nonresonant beam blow-up?

GLUCKSTERN: I don't believe that these modify the results by more than a factor 2.

REFERENCES

1. M. C. Crowley-Milling et al., Nature 191, 483 (1961).

2. P. B. Wilson, HEPL Report No. 297, Stanford.

3. J. E. Leiss and R. A. Schrack, "Transient and Beam-Loading Phenomena in Linear Electron Accelerators", NBS Internal Report, October 30, 1962.

4. See, for example, H. Hahn, Rev. Sci. Instr. 34, 1094 (1963).

DYNAMIC EFFECTS OF HIGHER RF HARMONICS

Frank J. Kriegler
Midwestern Universities Research Association

The acceleration process of a bunch of charged particles can be significantly altered when the passage of one bunch of particles through an accelerating gap of an rf cavity removes a significant fraction of the energy stored in the cavity. In a linear accelerator the ratio of energy removed by one bunch passing through one cell to the energy stored in one cell is of the order of 10^{-4}. However, in a circular accelerator this ratio may approach a value of 0.2.[1] The purpose of this paper is to investigate the particle dynamics for cases in which a high proportion of the energy is removed from the cavity by one bunch of particles. Clearly, this effect is extremely small in linear accelerators but the method of solution is of general interest.

In order to study the dynamics of beam-cavity interactions, we need a suitable representation of the beam induced voltage across the accelerating gap of the cavity. We may consider the cavity as a lumped RLC circuit upon which a sinusoidal voltage is impressed. The capacitor of this circuit may be thought of as representing the accelerating gap of an rf cavity. This representation is shown in Fig. 1a. Consider a charged particle repetitively passing through the capacitor thereby inducing a voltage change, $\Delta V = e/C$, on the capacitor, C. The distorted voltage waveform on the capacitor is shown in Fig. 1b. It must be noted that the particle may not pass through the capacitor at exactly the same phase in every period of the applied voltage, but rather at a slowly varying phase, which corresponds to the synchrotron oscillations of the particles. However, if the damping time for the circuit transients is less than the phase oscillation period of the particles, i.e., if

$$Q \ll \frac{f_{rev}}{f_{phase\ osc.}} , \qquad (1)$$

the transient amplitude behaves adiabatically.[2] Transients are not appreciably excited by the particles. We need, therefore, consider only steady-state response of the cavity to the particle current. This steady-state solution can be obtained by Fourier analysis of the beam current and the voltage waveform on the capacitor. A suitable expression for the voltage waveform shown in Fig. 1b is

$$V(t) = V_o (1 + k f_o t) \sin (2\pi f_o t + \theta_p) \quad \text{for } 0 \leq f_o t \leq 1 . \qquad (2)$$

By Fourier analyzing the voltage waveform of Eq. (2) the higher harmonics can be obtained. It may be shown that a convenient representation of the higher harmonics can be approximated by the following expression,

$$\frac{1}{2\pi} \sum_{n=2}^{\infty} V_n e^{j 2n\pi f_o t} \approx \Delta V \, (0.5 - f_o t) \cos (2\pi f_o t)$$
$$0 \leq f_o t \leq 1 . \qquad (3)$$

Thus, a particle (equivalently, a delta function pulse of current) passing through a narrow accelerating gap (a delta function gap) produces a distorted voltage waveform which may be Fourier analyzed. The usefulness of this for particle dynamics is now presented.

The beam current in a periodic accelerating structure may be Fourier analyzed:

$$I(\theta, t) = \sum_n a_n e^{in(\theta - \omega_o t)} = \sum_n a_n e^{in\theta'}, \quad \theta' = \theta - \omega_o t \qquad (4)$$

where ω_o is the circular frequency of the rf source, θ is the angular coordinate relative to the synchronous particle, and the coefficients a_n are slowly varying. Each Fourier component of the beam excites fields in the cavity. The longitudinal electric field may be written as

$$E_z(\theta, t) = \sum_n \sum_{\ell} b_{n\ell} a_n e^{i(\ell\theta - n\omega_o t)} . \qquad (5)$$

The terms for which $n \neq \ell$ are traveling waves which slip by the particles, causing the fields to vary rapidly at any particle position. We, therefore, neglect them as is customary in studying rf acceleration problems. The terms for which $n = \ell$ give a synchronous induced field

$$E_s(\theta, t) = \sum_n b_{nn} a_n e^{in(\theta - \omega_o t)} \qquad (6)$$

or in the rotating coordinate system

$$E_s(\theta') = \sum_n b_{nn} a_n e^{in\theta'} . \qquad (7)$$

In Eqs. (4) and (7) the a_n are given by

$$a_n = \frac{1}{2\pi} \int_0^{2\pi} I(\theta') e^{-in\theta'} d\theta' . \tag{8}$$

Substituting Eq. (8) into (7) and rearranging terms gives

$$E_s(\theta) = \int_o^{2\pi} I(\theta'') K(\theta' - \theta'') d\theta'' \tag{9}$$

where

$$K(\theta) = \frac{1}{2\pi} \sum_n b_{nn} e^{in\theta} . \tag{10}$$

Equation (9) has the same form as a space-charge field, except that the kernel, Eq. (10), has a different spatial dependence determined by the cavity geometry. It is possible to calculate a kernel for specific cavity geometries. A MURA computer program[3] exists that calculates a kernel for axially symmetric cavities of the types shown in Fig. 2. However, to see the meaning of the kernel more clearly and to illustrate the principles involved, the cavity is taken as the lumped RLC circuit considered previously. The capacitance represents a narrow gap located at $\theta = 0$, so that

$$E(\theta, t) = \frac{\delta(\theta) V(t)}{R} \tag{11}$$

where $V(t)$ is the gap voltage and R is the orbit radius. This delta function representation allows us to write immediately the $b_{n\ell}$ of Eq. (5) as

$$b_{n\ell} = \frac{V_n}{2\pi R} \tag{12}$$

where V_n is the voltage induced by a unit current at each harmonic frequency $n\omega_o$. The kernel can then be written as

$$K(\theta) = \frac{1}{2\pi} \sum_n \frac{V_n}{2\pi R} e^{in\theta} . \tag{13}$$

Thus the voltage waveform expression derived for the lumped RLC circuit may now be used in the subsequent calculations. Substituting Eq. (3) into Eq. (13) yields

$$K(\theta) = \frac{V}{2\pi R}\left(0.5 - \frac{\theta}{2\pi}\right)\cos\theta \,. \tag{14}$$

Figure 3 shows a plot of this kernel and a plot of a kernel obtained for a typical ferrite-loaded accelerator cavity having a narrow gap. The fundamental frequency component induced by the beam is not included in Eq. (14). The magnitude of the fundamental would depend upon a number of considerations such as Q of the cavity, internal impedance of the rf source and feedback loops. However, in this paper the results presented are based on the assumption that the fundamental is kept constant by some mechanism.

As was pointed out above, the kernel function generated by a particle passing an accelerating gap is similar to a space-charge force. Previous investigations[4, 5] have been made concerning the effects of space-charge forces on the rf acceleration process. Thus, the same techniques may be used to investigate effects of higher harmonics.

One result of these space-charge investigations is a MURA computer program[5] which integrates the equations of motion for a particle under the influence of a combined rf and space-charge field. A particle whose energy is sufficiently different from transition energy is governed by the following equations,

$$\dot{\theta} = f\frac{df}{dE}W \tag{15}$$

$$\dot{W} = -\dot{W}_S + e V_o \sin\theta + 2\pi e R\,\xi(\theta, t)\,, \tag{16}$$

where θ measures angles in a coordinate system rotating with the beam, $\dot{W}_S$ is related to the energy gain per turn of the synchronous particle, $\dot{W}$ is the energy gain of a particle relative to the synchronous particle, and V_o is the accelerating voltage on the gap. The electric field $\xi(\theta, t)$ is the beam-cavity interaction field. The term containing the frequency change with energy, $f\frac{df}{dE}$, can be taken as a constant (for example, + 1 for particles below transition and - 1 for cases above transition). The basic approach to the problem is to specify as many as 10,000 pairs of initial conditions (particles), θ, $\dot{W}$. The field $\xi(\theta, t)$ is computed by convolution (Eq. (9)) of the kernel function with the particle density at the beginning of each time-step. The integration is then performed by a linear integration of Eqs. (15) and (16). For example, Eq. (15) is written as

$$\theta (t + \Delta t) = \theta (t) \pm W (t) \Delta t , \qquad (17)$$

and similarly for Eq. (16). It must be emphasized that since 10,000 or less particles are carried in the computation, the charge of these particles is greater than the electronic charge, e. The magnitude of charge on these "macroparticles" is determined by scaling the constant, $V = \Delta Q/C$, in the kernel function (Eq. (14)).

The numerical results obtained using this computer program are presented by Figs. 4 to 9. Figure 4 shows a phase plot in which no higher harmonic beam-cavity interaction takes place. This figure is shown merely to provide a reference figure for the form of the computer results as the rf capture process takes place. The initial conditions are a band of 1935 macroparticles spread uniformly in energy and phase, as shown in the top diagrams. The middle diagrams are an intermediate result of the computation. The bottom diagrams are the final buckets. The three diagrams on the right are for particles below transition, while the diagrams on the left are for particles above transition. The number of particles captured is 503 from the initial 1935. Figure 5 shows the effect of higher harmonic beam interaction. The magnitude of the kernel is based on an equivalent circuit in which the capacitance is 8 pf, the rf accelerating voltage is 2×10^4 volts, and a bucket contains 10^{13} particles. Thus, if all the particles passed through the capacitor at the same instant, the voltage change would be 2×10^5 volts. The constant, ΔV, in the kernel function (Eq. (14)) is $\Delta V = 2 \times 10^5/1935 = 103$. For this case, the initial conditions were the same as the unperturbed case shown in Fig. 4. In Fig. 5 the bucket boundary for the unperturbed case is outlined for comparison. Below transition the higher harmonic beam interaction reduces the number of particles captured from 510 to 205, while above transition the number of particles captured increases to 670. Figure 6 shows the distorted voltage waveform on the accelerating gap for the above case for particles below transition; Fig. 7 is the voltage waveform above transition. Figure 8 displays a severe case above transition for which the parameters are the same except that the bucket contains 6×10^{13} protons (the kernel is six times larger). The voltage waveform of this case is shown in Fig. 9.

The computer time required to run one case was from one to one and one-half hours on an IBM 704 computer. The running time varies approximately linearly with the number of macroparticles used.

ACKNOWLEDGEMENTS

I would like to express appreciation to Professor K. R. Symon and E. M. Rowe for helpful suggestions and comments. I would like to thank Dr. R. A. Dory for valuable help in providing his computer program.

SWENSON: Does Fig. 8 correspond to above or below transition?

KRIEGLER: This case is above transition.

SWENSON: In this terminology are all linacs essentially below transition?

KRIEGLER: Yes, and above transition the particles get a larger energy "kick" and take longer to come back again. This analysis would not hold too well with respect to linear accelerators. I assume that the particle comes back again and sees its effect, although I suppose if you stretch your imagination you could say that if one particle goes through, it starts to excite these higher harmonics and the next one will feel essentially the same effect, although it is a different particle. I have assumed up to now that the fundamental stays constant; there is a feedback mechanism which increases power into the cavity as the beam requires and keeps the fundamental constant. We could put in some kind of transfer function associated with a feedback loop. This would be done for a particular structure; here I have just tried to present general results.

J. H. MARTIN: You spoke of a feedback loop involving amplitude. Do you have any consideration for that involving phase?

KRIEGLER: I guess we were talking about including this. There is another consideration, the magnitude and phase of the fundamental would vary considerably if you're off resonance. Results could be obtained for all these considerations; however, it seems desirable to perform computer experiments of that type only for a specific accelerating system.

REFERENCES

1. E. M. Rowe, MURA Technical Note TN-471 (unpublished, 1964).

2. K. R. Symon, private communication.

3. F. J. Kriegler, F. E. Mills, and J. Van Bladel, Jour. Appl. Phys., Vol. 35, No. 6, pp. 1721-1726, June 1964.

4. C. E. Nielsen and A. M. Sessler, MURA Report No. 480 (unpublished, 1959).

5. R. A. Dory, MURA Report No. 654 (unpublished, 1962).

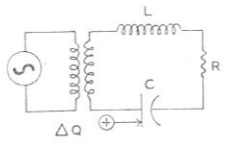

(a) EQUIVALENT CIRCUIT FOR ACCELERATOR CAVITY

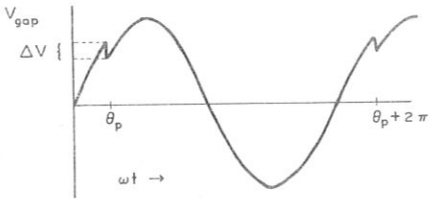

(b) VOLTAGE WAVEFORM ON ACCELERATING GAP (CAPACITOR)

FIG. 1

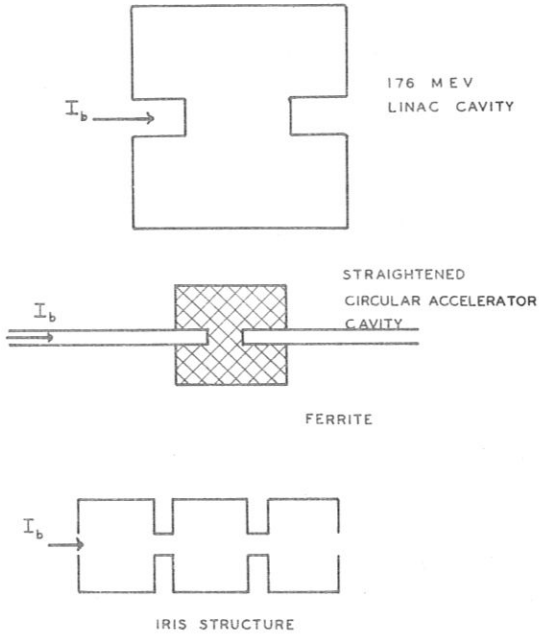

FIG. 2 AXIALLY SYMMETRIC ACCELERATOR CAVITIES

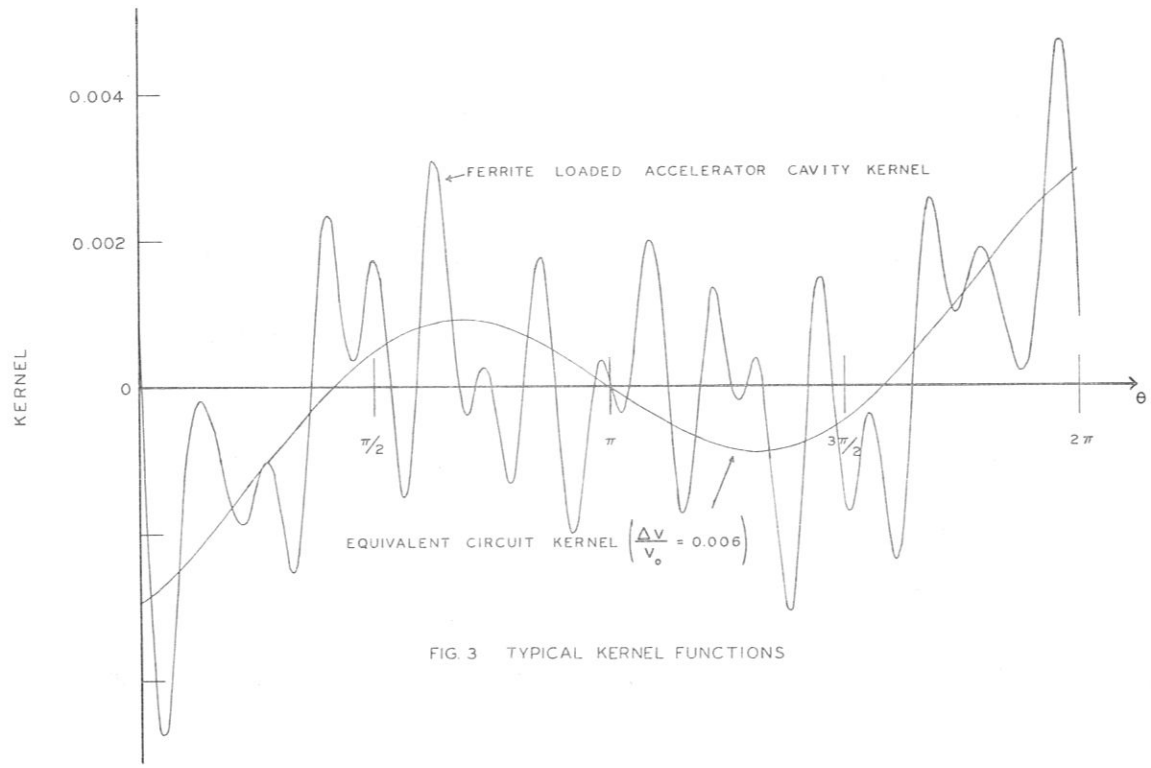

FIG. 3 TYPICAL KERNEL FUNCTIONS

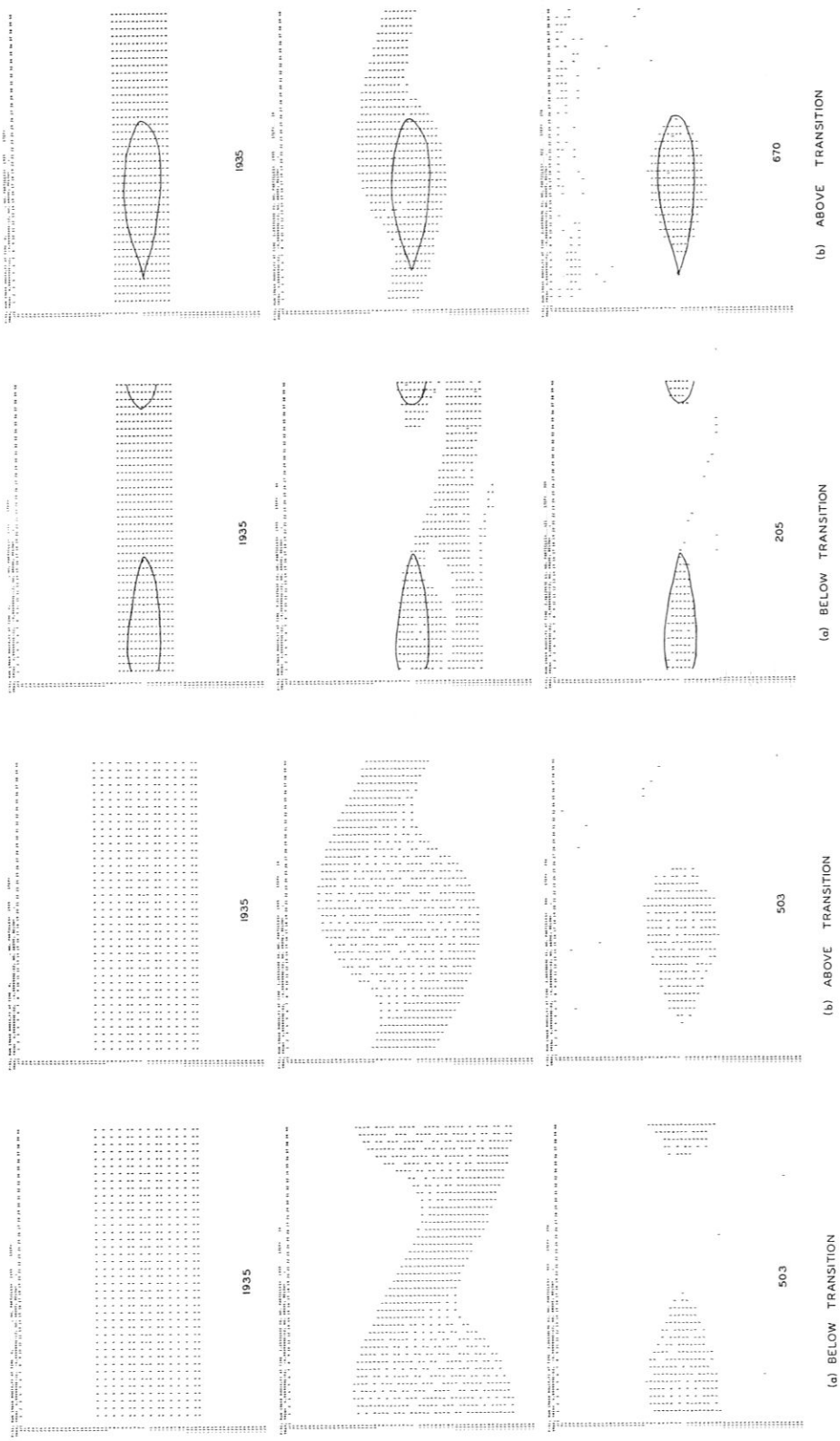

FIG. 4 PHASE PLOT FOR NO BEAM CAVITY INTERACTIONS

FIG. 5 PHASE PLOT FOR HIGHER HARMONIC BEAM CAVITY INTERACTIONS ($N = 10^{13}$ PARTICLES)

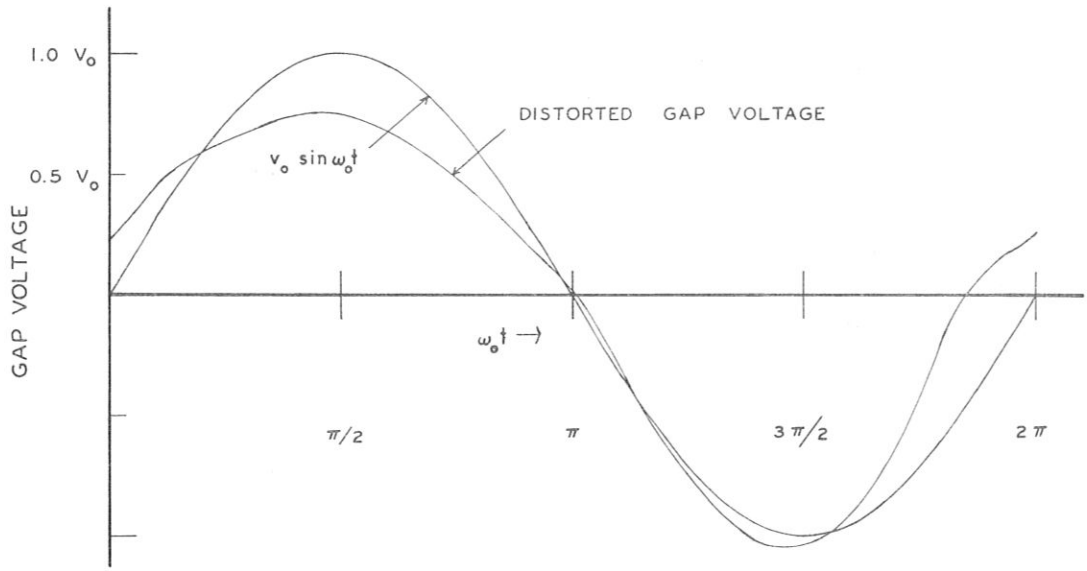

FIG. 6 VOLTAGE WAVEFORM ON ACCELERATOR GAP BELOW TRANSITION FOR 10^{13} PROTONS AND C_{gap} = 8 PF

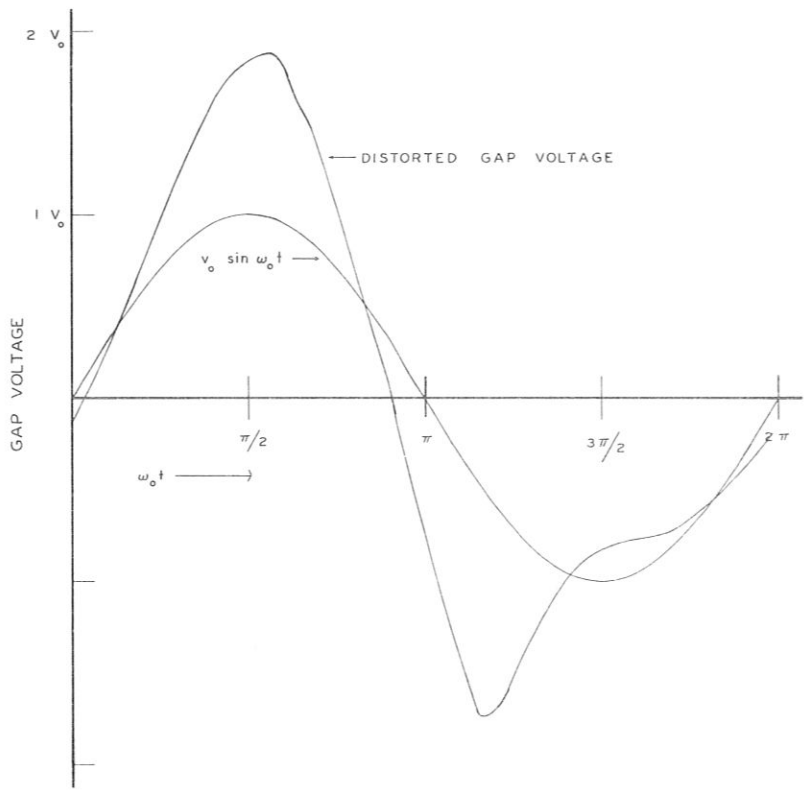

FIG. 7 VOLTAGE WAVEFORM ON ACCELERATOR GAP ABOVE TRANSITION FOR 10^{13} PROTONS AND C_{gap} = 8 PF

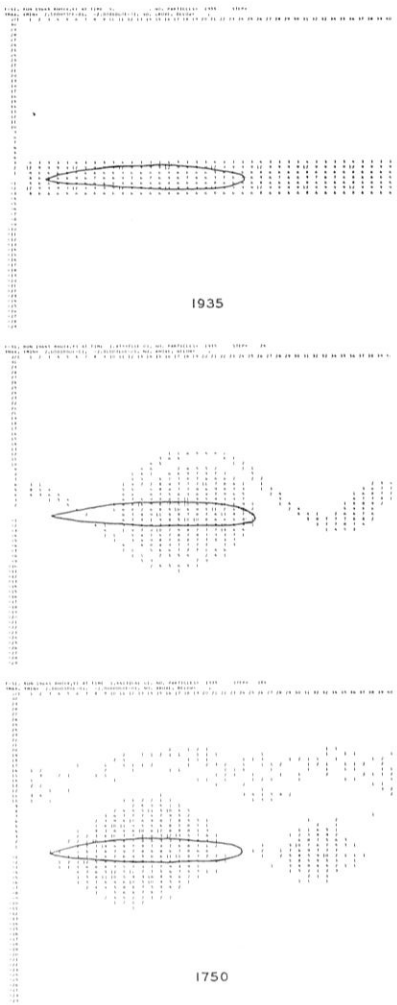

FIG. 8 PHASE PLOT FOR HIGHER HARMONIC BEAM CAVITY INTERACTION ($N=6\times10^{13}$ PARTICLES)

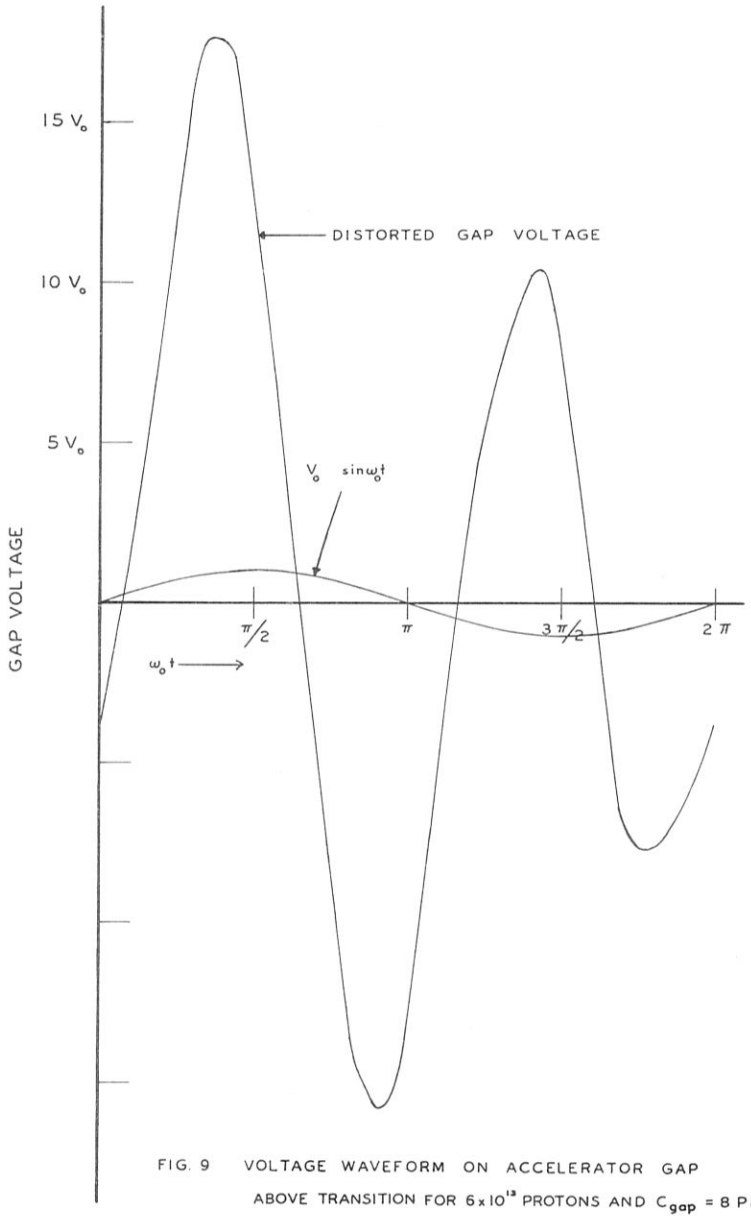

FIG. 9 VOLTAGE WAVEFORM ON ACCELERATOR GAP ABOVE TRANSITION FOR 6×10^{13} PROTONS AND C_{gap} = 8 PF

AN APPROACH TO THE STUDY OF BEAM LOADING FOR THE LINEAR ACCELERATOR

T. Nishikawa*
Brookhaven National Laboratory

1. Introduction

Most studies on the effects of beam loading in linear accelerators have been made using the power relations or the equivalent circuit analogies. On the other hand, the field equation for cavities and the equation of motion for the charged particles will give a more complete picture of this effect, especially when the accelerator is a standing wave type. This study was made for the iris-loaded structure being considered by the Brookhaven-Yale proton linac project.[1] The method is similar to the theories developed for microwave electronic devices, particularly traveling wave tubes, and the purpose is to give a brief physical picture but not exact numerical calculations.

2. Principle and Assumptions

According to Slater's well known theory for resonant cavities,[2] the solution of Maxwell's equations is expanded in terms of a summation over certain normal modes, which possess orthogonality properties. Any vector field can be broken into new fields, one of which is solenoidal and the other is irrotational and, so far as the wave propagation is considered, the space-charge effect can be separated for the first approximation. The effect of the beam current on the cavity field which is operated near the n^{th} mode is quite generally expressed by**

$$-\frac{1}{\epsilon \omega_{no}} \frac{\int \vec{J}\vec{F}_n^{\,*} dv}{\int \vec{E}\vec{F}_n^{\,*} dv} = j\left(\frac{\omega}{\omega_n} - \frac{\omega_n}{\omega}\right) + \frac{1}{Q_n} \quad . \tag{1}$$

$\vec{J}$ is the current density, $\vec{E}$ the field, and $\vec{F}_n$ is the solenoidal normal mode field. $\vec{F}_n$ is obtained by solving Maxwell's equations when there is no current in the cavity and the walls are either short-circuited or open-circuited. ω_{no} is the resonant angular frequency of the n^{th} mode and ω_n is that of the case when the effect of wall losses is taken into account. Rigorously $\omega_{no} \neq \omega_n$, but one can safely use ω_n instead of ω_{no} if the unloaded

---

* On leave from the Department of Physics, University of Tokyo.

** This equation is slightly modified from Slater's and immediately derived from the wave equation for the vector potential, and is quite general for the relativistic case. See Ref. 9 and its reference.

Q, Q_{on}, is sufficiently high. The total Q value of the cavity without beam, Q_n, is expressed by

$$\frac{1}{Q_n} = \frac{1}{Q_{on}} + \sum_i \frac{g_i}{Q_{ext,\ n,\ i}} \quad , \tag{2}$$

where $Q_{ext,\ n,\ i}$ is the external Q to the i^{th} output and g_i is the real part of the reduced admittance of the i^{th} guide. If we study a standing wave type accelerator such as those operating in the π-mode, one section having N cells can be considered as a closed cavity of $Q_n = Q_{on}$. For simplicity throughout this paper a uniform cell structure in each cavity will be assumed, while an actual π-mode cavity would have nonuniform structure as discussed in the Appendix. The actual field, $\vec{E}$, is also assumed to vary as $e^{j\omega t}$ with the operating frequency ω, and the integration is performed over the cavity volume.

The effect of beam loading in a linac can be estimated from the left-hand side of (1); its imaginary part gives the shift of the resonant frequency or the detuning effect and the real part gives the further power loss or the beam Q-value.

3. Effect of Tightly Bunched Beam (Light-loading)

The assumption throughout this paper is that a tightly bunched beam interacts with the field propagating along the cavity axis. The beam is also assumed to be confined to a region having a small diameter about this axis (z axis).

In the first step, we neglect the field induced by the beam and the reaction of the field on the beam. This approximation will be valid when the loading is sufficiently small or in a transient stage when the induced field has not yet built up.

In terms of the field equation the stored energy for the n^{th} mode may be written as

$$W_n = \frac{1}{2} \epsilon \int \vec{E}\vec{F}_n^{\,*} dv \int \vec{E}^{*}\vec{F}_n dv \ . \tag{3}$$

This equation may also be written in terms of circuit parameters as

$$\omega_n W_n = Q_{on} R \quad L = \frac{Q_{on} E_{no}{}^2 L}{r_{sn}} \quad , \tag{4}$$

where R is the wall loss per unit length, L the cavity length, E_{no} the axial-field amplitude (peak value of the field strength) of the n^{th} harmonic field, and $r_{sn} = E_{no}{}^2/R$ the shunt impedance for the n^{th} mode field. Substituting (3) and (4) into (1), we obtain

$$-\int \vec{J}\vec{F}_n{}^* dv \int \vec{E}^* \vec{F}_n dv = \frac{2Q_{on}}{r_{sn}} E_{no}{}^2 L \left[j\left(\frac{\omega}{\omega_n} - \frac{\omega_n}{\omega} \right) + \frac{1}{Q_n} \right] \tag{5}$$

Now the beam is assumed to be bunched in a wave having the propagation exponent $j(\omega' t - k' z)$ with a bunch width $\delta\phi$ at a center phase ϕ_o. The current density of such beam is analyzed in a Fourier series as

$$J = J_o + \mathrm{Re} \sum_{\nu=1}^{\infty} 4J_o \frac{\sin \frac{\nu \delta\phi}{2}}{\nu \delta\phi} e^{j\nu(\omega' t - k' z + \phi_o)} \tag{6}$$

where J_o is the mean density during one pulse of the linac operation. When $\nu \delta\phi << 1$, the ν component is

$$J_\nu \doteq 2J_o \mathrm{Re}\, e^{j\nu(\omega' t - k' z + \phi_o)} \tag{6'}$$

So far as a steady state solution is considered, only the term of $\omega_b = \nu\omega' \approx \omega_n$* should be important in the estimation of integral $\int \vec{J}\vec{F}_n{}^* dv$. Taking $k_b = \nu k'$ and $\phi_b = \nu \phi_o$, it becomes

---

* ν is four for the proton linac planned by Brookhaven.

$$\int \vec{J}\vec{F}_n^{\,*} dv = -2jI_o F_{no} e^{j\phi_b} \left\{ \frac{1}{k_n + k_b} \left[1 - e^{-j(k_n+k_b)L} \right] \right. \tag{7}$$

$$\left. + \frac{1}{k_n - k_b} \left[1 - e^{-j(k_n - k_b)L} \right] \right\},$$

where I_o is the mean current, F_{no} is the axial-field amplitude of the n^{th} normal mode field which is given by $2F_{no} \cos k_n z$ in the standing wave case. For a π -mode, $k_n L = \pi N$ with the total number of cells, N, so that $k_n L >> 1$. In such a case, one can easily see that the right hand side of (7) is dominant for $|k_n - k_b| \approx 0$, or for the synchronized wave which hereafter is designated by n. It also should be pointed out that from here on only the synchronized primary mode will be considered, and the effects of all other modes have been neglected. Taking $|k_n - k_b| L << 1$, we get from (7),

$$\int \vec{J}\vec{F}_n^{\,*} dv \approx 2I_o F_{no} L e^{j\phi_b} . \tag{8}$$

Combining (5) and (8),

$$I_o e^{j\phi_{bn}} = - \frac{Q_{on}}{r_{sn}} E_{no} \left[j \left(\frac{\omega}{\omega_n} - \frac{\omega_n}{\omega} \right) + \frac{1}{Q_n} \right], \tag{9}$$

where we used a relation, $\vec{E} = \sum \vec{F}_n \int \vec{E}\vec{F}_n^{\,*} dv = \sum \vec{E}_n$ for the n^{th} harmonic field $\vec{E}_n$; and ϕ_{bn} is the relative phase of the beam bunch to the n^{th} harmonic field. Then we have the frequency shift, $\Delta\omega_n = \omega - \omega_n$, and the beam Q-value, Q_{bn}, as

$$\frac{2\,\Delta\omega_n}{\omega_n} = -\frac{r_{sn}}{Q_{on}}\,\frac{I_o}{E_{no}}\,\sin\phi_{bn} \tag{10a}$$

$$\frac{1}{Q_{bn}} = \frac{r_{sn}\,I_o}{Q_{on}\,E_{no}}\,\cos\phi_{bn}\,, \tag{10b}$$

where the total Q-value is expressed by $\frac{1}{Q_{tn}} = \frac{1}{Q_n} + \frac{1}{Q_{bn}}$.

4. Effect of Induced Field due to Beam Loading

If the beam loading increases, the field induced by the beam increases and becomes an appreciable part of the field, so that it should not be neglected. The actual field in a cavity can be divided into two parts; one is excited by the external source, $\vec{E}_e$, and the other is induced by the beam, $\vec{E}_b$. The total field is given by

$$\vec{E}_t = \vec{E}_e + \vec{E}_b \tag{11}$$

The induced field is also given by the use of (1), which is the so-called circuit equation in the present paper. The n^{th} harmonic field of E_b is

$$\vec{E}_{bn} = \vec{F}_n \int \vec{E}_b\,\vec{F}_n^{\,*}\,dv \tag{12}$$

and its axial component will be given by

$$\dot{E}_{bno} = F_{no} \int \vec{E}_b\,\vec{F}_n^{\,*}\,dv \tag{12'}$$

where $\dot{E}_{bno}$ is the complex amplitude including the phase. The axial-field amplitude of the n^{th} normal mode, F_{no}, which is, of course, a real number, is obtained from (3) and (4), where $\vec{E}$ is taken by $\vec{F}_n$. Since $W_n = \frac{\epsilon}{2}$ for the normal mode,

$$F_{no} = \sqrt{\frac{\epsilon}{2} \frac{r_{sn}\ \omega_n}{Q_{on}\ L}} \quad . \tag{13}$$

The value of integral in (12') is given as

$$\int \vec{E}_b\ \vec{F}_n{}^* dv = - \frac{\int \vec{J}\vec{F}_n{}^* dv}{\epsilon\, \omega_n \left[j \left(\frac{\omega_b}{\omega_n} - \frac{\omega_n}{\omega_b} \right) + \frac{1}{Q_n} \right]}$$

$$= - \sqrt{\frac{r_{sn} L}{2 Q_{on} \epsilon\, \omega_n}} \frac{2 I_o\, e^{j\phi_b}}{\left[j \left(\frac{\omega_n}{\omega_n} - \frac{\omega_n}{\omega_b} \right) + \frac{1}{Q_n} \right]} \tag{14}$$

from (1) and (8). Substituting (13) and (14) into (12')

$$\dot{E}_{bno} = - \frac{r_{sn}}{Q_{on}} \frac{I_o\, e^{j\phi_b}}{\left[j \left(\frac{\omega_b}{\omega_n} - \frac{\omega_n}{\omega_b} \right) + \frac{1}{Q_n} \right]} \quad , \tag{15}$$

just corresponding to (9).

In order to discuss the effect of induced field, we must consider the relation between ω_b and ω_n. The normal mode frequency, ω_n, is the proper frequency of the free oscillation of the cavity and is just the operating resonant frequency, ω_o, when beam is not present. If the beam comes in, the dynamic resonant frequency will move due to the reactive component of the load and differ from ω_n, the amount of this shift being given by (10a) in the first approximation. We can make a readjustment of the tuning of the cavity to resonate at the frequency ω_o, in order to keep the synchronous condition for the beam and the wave

velocities. In such a case, the normal mode frequency is moved in turn by the tuning process and is no longer equal to ω_o. Because of the phase oscillation in the preceding part of the accelerator, the beam will be bunched to the wave of ω_o rather than that of ω_n, or $\omega_b \approx \omega_o \neq \omega_n$. Howevever, as we can see from (10a) and (10b), if $|\phi_b| << 1$ or $Q_b >> Q_{on}$, we may put $|\omega_b - \omega_n| << \omega_n/Q_n$, and we have the expression

$$\dot{E}_{bno} = -\frac{Q_n}{Q_{on}} r_{sn} I_o e^{j\phi_b} \equiv -E_{bno} e^{j\phi_b}, \qquad (15')$$

where E_{bno} is the real amplitude or the peak strength of the induced field. The induced field is out of phase with that of the beam bunch and proportional to the shunt impedance.[3] In the present-designed accelerator, $\phi_b = \frac{\pi}{6}$ and $Q_b \gtrsim 2\,Q_{on}$, so that the approximation of (15') would be correct.

Superposing the induced field to the external field and repeating the process in paragraph 3, we have the following results as,

$$\frac{2\Delta W_n}{\omega_n} = -\frac{r_{sn}}{Q_{on}} \frac{I_o E_{eno} \sin\phi_{bn}}{E_{eno}^2 + E_{bno}^2 - 2E_{eno} E_{bno} \cos\phi_{bn}}$$

$$= -\frac{1}{Q_n} \frac{B_n \sin\phi_{bn}}{1 + B_n^2 - 2B_n \cos\phi_{bn}} \qquad (16a)$$

$$\frac{1}{Q_b} = \frac{r_{sn}}{Q_{on}} \frac{I_o (E_{eno} \cos\phi_{bn} - E_{bno})}{E_{eno}^2 + E_{bno}^2 - 2E_{eno} E_{bno} \cos\phi_{bn}}$$

$$= \frac{1}{Q_n} \frac{B_n \cos\phi_{bn} - B_n^2}{1 + B_n^2 - 2B_n \cos\phi_{bn}} \qquad (16b)$$

instead of (10a) and (10b), with the beam loading parameter,

$$B_n = \frac{E_{bno}}{E_{eno}} = \frac{Q_n}{Q_{on}} \frac{r_{sn} I_o}{E_{eno}} , \tag{17}$$

E_{eno} being the n^{th} harmonic amplitude of external field. If we take r_{sn} as 20 MΩ/m, I_o as 0.1 A (the maximum design value), E_{eno} as 4 MeV/m and $Q_n = Q_{on}$, we find $B_n = 0.5$, leading to $\Delta\omega_n / \omega_n = 1.5 \times 10^{-5}$ ($\sim$ 10 kc for an 800 Mc accelerator) and $Q_{bn} = 4 \times 10^4$ for $Q_{on} = 2 \times 10^4$ and $\phi_{bn} = \pi/6$.

5. Self-Consistent Field

Up to the preceding section, the reaction of the field on the charged particles is neglected. In order to find the complete picture, we must solve the self-consistent field taking into account the induced current. The self-consistent field is the solution of the combination of the circuit equation and the equation of motion (electronic equation), this method has been extensively developed in studies of traveling wave tubes.[4] In contrast to the usual TWT theory, the following points should be considered:

a. The injected beam is already tightly bunched and the induced field is important. Also some of the nonlinear behavior should be considered.

b. The motion of the charged particle is relativistic.

c. The circuit is used for standing waves and not for traveling waves.

For the tightly bunched beam, the so-called small-signal theory should not be valid. In a small-signal theory, the velocity, v, and the linear charge density, ρ, of particles are expressed as

$$v = v_o + v_1 e^{j(\omega_b t - k_b z)}$$

$$|v_1| << v_o$$

$$\rho = \rho_o + \rho_1 e^{j(\omega_b t - k_b z)}$$

$$\rho_1 << \rho_o$$

The condition for v will still be valid in the present case, but the condition for ρ is violated since $\rho_1 \sim \rho_o$. Such a case is called a moderately large signal case,[5] and since the beam impedance is still high compared with the circuit impedance, the coupling between the wave and the beam should not be so strong. This is seen through estimation of the dimensionless coupling parameter, C, defined by Pierce,[4] the cube root of the ratio of circuit impedance to the beam impedance. As will soon be shown, C is of the order of 10^{-2} for the present case or of the same order as in the usual TWT. The weak coupling nonlinear theories for the TWT have been presented by Nordsiek and others,[6] and some numerical results are also available. Unfortunately, because of the different working conditions, these numerical results cannot be used for the present case.

On the other hand, by comparison of these numerical results with the results from the simple small-signal theory, Pierce pointed out that, if the beam is overbunched, the effect of nonlinearity can be estimated, at least qualitatively and almost quantitatively, from the results of the small-signal linear theory by setting the amplitude of the varying current equal to $2I_o$.[7] In order to obtain the physical picture, we examine the self-consistent field in this manner.

The circuit equation is again equation (1), and we make some modifications in order to express it in terms of the propagation constants. Then, corresponding to (9),

$$\dot{E}_{no} = - \frac{\omega_n r_{sn}}{2Q_{on} v_{ge}} \frac{\Gamma_n}{\left[(\Gamma_n^2 - \Gamma^2) + \alpha \Gamma_n\right]} \dot{I}_1 \qquad (18)$$

where $\dot{E}_{no}$ and $\dot{I}$ are the complex amplitudes of field and current, having time and z-dependence as $\exp(j\omega t - \Gamma z)$. Taking the phase velocities, v_{pn} and v_p, for the case without and with the beam respectively, $\Gamma_n = j\,\omega/v_{pn}$ and $\Gamma = j\,\omega/v_p \left(\approx j\,\omega_n/v_{pn}\right)$. The effective group velocity, v_{ge}, is defined as

$$- j\, v_{ge} \equiv \frac{\omega - \omega_n}{\Gamma_n - \Gamma}, \qquad (19)$$

and the attenuation constant α is

$$\alpha \equiv \frac{\omega_n}{v_{ge} Q_{on}} \quad . \tag{20}$$

Equation (18) has the same form as given by Pierce for TWT theory and the solutions for both forward and backward waves.

The equation of motion for the changed particle is expressed by

$$\dot{I}_1 = \frac{e}{m_\ell} \frac{I_o}{v_o^2} \frac{\Gamma_b}{(\Gamma_b - \Gamma)^2} \dot{E}_{no} \tag{21}$$

where $\Gamma_b = jk_b = j\omega/v_o$. This is also derived in the similar manner as in TWT theory, [2, 4] provided the relativistic effect is taken into the longitudinal phase motion by taking the longitudinal mass $m_\ell = m_o (1 - v_o^2/c^2)^{-3/2}$. To derive this equation the standing wave is divided into forward and backward waves, and is assumed to interact with the beam only through the forward wave due to the phase synchronism condition.*

Combining (18) and (21), the self-consistent field is obtained. Taking $\Gamma_b = \Gamma_n$ (or $v_o = v_{pn}$), the solution for the forward wave is given by

$$\delta^2 (\delta + \tfrac{\alpha}{2}) = C^3 k_b^3 , \tag{22}$$

where $\delta = \Gamma_b - \Gamma$ and the coupling parameter C is given by

$$C^3 = \left(\frac{e}{4m_\ell} \frac{r_{sn} I_o}{v_{ge} \omega Q_{on}} \right) . \tag{23}$$

---

* The particular situation of the π-mode, which is pointed out by Leiss, can be taken into the calculation of shunt impedance, which will be twice that which was calculated for the forward wave only (J. E. Leiss, Minutes of the Conference on Proton Linear Accelerators at Yale University, October 21-25, 1963, p. 74).

The following values of parameters: $\omega = 2\pi \times 800$ Mc/sec, $r_{sn} = 20\ M\Omega/m$, $Q_{on} = 2 \times 10^4$, $v_{ge} = 4 \times 10^5$ m/sec, $I_o = 0.1$ A, and the proton kinetic energy = 200 MeV, are taken leading to $C = 1.1 \times 10^{-2}$. The estimate of v_{ge} is difficult especially for a π-mode cavity. As is discussed in the Appendix, the group velocity will vary along the guide to keep the field distribution uniform in an actual cavity. However, assuming the uniform cell structure as is in the present approximation, we may use its average value $\langle v_g \rangle = \omega L/2 Q_{on}$. This is about 3.7×10^5 m/sec for L = 3 m.

Now the two limiting cases will be considered; one is $\alpha << Ck_b$ and the other is $\alpha >> Ck_b$. As is shown later, the present case is the latter, while such effects as beam blow-up would occur in the former.

(1) Case 1, $\alpha << Ck_b$

As in the TWT theory, we have three roots of (22) for the forward wave. They are

$$\delta_1 = \frac{1}{2} (\sqrt{3} - j) Ck_b \tag{24a}$$

$$\delta_2 = \frac{1}{2} (-\sqrt{3} - j) Ck_b \tag{24b}$$

$$\delta_3 = j Ck_b \tag{24c}$$

which correspond to the increasing, decreasing, and unattenuated waves, respectively. We have also another solution for the backward wave which is given by

$$\Gamma_4 = -\Gamma_b - \delta_4 \tag{24d}$$

and

$$\delta_4 \doteq \frac{\alpha}{2} - j\frac{C^3 k_b}{4} \quad , \tag{24d'}$$

Since $C \ll 1$, we must take into account α for the δ_4 and may neglect the second term on the right-hand side.

These four waves should be superposed with the proper boundary condition. A finite beam current $I_1(0)$ at the input ($z = 0$) is considered and the standing wave conditions at the input and the output are taken as follows, at $z = 0$ assuming $|\delta_i| \ll k_b$,

$$\dot{E}_1(0) + \dot{E}_2(0) + \dot{E}_3(0) = \dot{E}_4(0) + \dot{E}_e(0) \tag{25a}$$

$$\frac{\dot{E}_1(0)}{\delta_1^2} + \frac{\dot{E}_2(0)}{\delta_2^2} + \frac{\dot{E}_3(0)}{\delta_3^2} = -jK\dot{I}_1(0) \tag{25b}$$

$$\frac{\dot{E}_1(0)}{\delta_1} + \frac{\dot{E}_2(0)}{\delta_2} + \frac{\dot{E}_3(0)}{\delta_3} = 0 \quad , \tag{25c}$$

and at $z = L$

$$\dot{E}_1(0)e^{\delta_1 L} + \dot{E}_2(0)e^{\delta_2 L} + \dot{E}_3(0)e^{\delta_3 L} = \dot{E}_4(0)e^{(2jk_b + \delta_4)L} \tag{25d}$$

where suffixes n and o for E are omitted for simplicity. The suffix i (= 1, 2, 3 and 4) of $\dot{E}_i$ corresponds to the above four solutions of δ_i and zero in parenthesis means $z = 0$. The constant K is given by

$$K = \frac{m_\ell v_o^2}{e k_b I_o} \tag{26}$$

from (21), and the third condition (25c) comes from the assumption of $v_1(0) = 0$. The solutions for $\dot{E}_i$ are given by

$$\dot{E}_i(0) = (-1)^{i+1} \frac{\dot{E}e(0)\,\Delta_{i1} + jK\dot{I}_1(0)\,\Delta_{i2}}{\Delta} , \tag{27}$$

where

$$\Delta = \begin{vmatrix} 1 & 1 & 1 & -1 \\ \frac{1}{\delta_1^2} & \frac{1}{\delta_2^2} & \frac{1}{\delta_3^2} & 0 \\ \frac{1}{\delta_1} & \frac{1}{\delta_2} & \frac{1}{\delta_3} & 0 \\ e^{\delta_1 L} & e^{\delta_2 L} & e^{\delta_3 L} & -e^{(2jk_b+\delta_4)L} \end{vmatrix} \tag{28}$$

and $\Delta_{i,j}$ is the subdeterminant of the i^{th} column and the j^{th} row. Taking δ_4 as $\alpha/2$,

$$\dot{E}_1(0) = \frac{\dot{E}_e(0) - jK\dot{I}_1(0)\ \delta_1^2 \left[1 - e^{-(2jk_b+\frac{\alpha}{2})L}\ \frac{\delta_2 e^{\delta_2 L} - \delta_3 e^{\delta_3 L}}{\delta_2 - \delta_3}\right]}{3 - e^{-(2jk_b+\frac{\alpha}{2})L}\left(e^{\delta_1 L} + e^{\delta_2 L} + e^{\delta_3 L}\right)} \tag{29a}$$

The components $\dot{E}_2(0)$ and $\dot{E}_3(0)$ are found by interchanging subscripts and the component $\dot{E}_4(0)$ is

$$\dot{E}_4(0) = \frac{e^{-(2jk_b + \frac{\alpha}{2})L}\left(\dot{E}_1^0 e^{\delta_1 L} + \dot{E}_2^0 e^{\delta_2 L} + \dot{E}_3^0 e^{\delta_3 L}\right)}{3 - e^{-(2jk_b + \frac{\alpha}{2})L}\left(e^{\delta_1 L} + e^{\delta_2 L} + e^{\delta_3 L}\right)} , \qquad (29b)$$

where

$$\dot{E}_i^0 = \dot{E}_e(0) - jK\dot{I}_1(0)\delta_i^2 . \qquad (30)$$

Terms having the form proportional to $jK\dot{I}_1(0)\delta_i^2$ give the induced field.

(2) Case 2, $\alpha >> Ck_b$

In this case the corresponding four roots of δ are

$$\delta_1 = \frac{1}{\sqrt{2}} (1 - j) Dk_b \qquad (31a)$$

$$\delta_2 \doteq - \frac{\alpha}{2} \qquad (31b)$$

$$\delta_3 \doteq - \frac{1}{\sqrt{2}} (1 - j) Dk_b \qquad (31c)$$

$$\delta_4 \doteq \frac{\alpha}{2} \qquad (31d)$$

assuming $\alpha << k_b$. The modified coupling parameter D is

$$D = \sqrt{\frac{2\,Ck_b}{\alpha}}\,C. \tag{32}$$

General solutions are also obtained from (27) and (28), while, in the first approximation, they are

$$\dot{E}_1(0) \doteq \frac{\frac{\delta_1}{\alpha}\,e^{\frac{\alpha}{2}L}}{2\sinh\frac{\alpha}{2}L}\,\dot{E}_e(0) - \frac{jK\delta_1^{\,2}}{2}\,\dot{I}_1(0) \tag{33a}$$

$$\dot{E}_2(0) \doteq \frac{e^{\frac{\alpha}{2}L}}{2\sinh\frac{\alpha}{2}L}\,\dot{E}_e(0) + \left(\frac{e^{\frac{\alpha}{2}L} - \cosh\delta_1 L}{\sinh\frac{\alpha L}{2}}\right)\frac{jK\,\delta_1^{\,2}}{2}\,\dot{I}_1(0) \tag{33b}$$

$$\dot{E}_3(0) \doteq -\frac{\frac{\delta_1}{\alpha}\,e^{\frac{\alpha}{2}L}}{2\sinh\frac{\alpha}{2}L}\,\dot{E}_e(0) - \frac{jK\delta_1^{\,2}}{2}\,\dot{I}_1(0) \tag{33c}$$

$$\dot{E}_4(0) \doteq \frac{e^{-\frac{\alpha}{2}L}}{2\sinh\frac{\alpha}{2}L}\,\dot{E}_e(0) + \left(\frac{e^{-\frac{\alpha}{2}L} - \cosh\delta_1 L}{\sinh\frac{\alpha L}{2}}\right)\frac{jK\,\delta_1^{\,2}}{2}\,\dot{I}_1(0)\,, \tag{33d}$$

where we have assumed the resonance condition $2k_bL = 2\pi \times$ integer. When the phase shift due to the beam is sufficiently small as is expected in the present design, this assumption will not change the results. In the actual accelerator, α will also vary as z increases, for v_g varies. As

we have used the average value of $<v_g>$ $(= \omega_n L/2\, Q_{on})$ for the uniform-cell assumption, one may use the corresponding $\alpha = \omega_n / <v_g> Q_{on} = 2/L$. This value of α is about ten times larger than the parameter Ck_b for L = 3 m so that we can easily see, from numerical checks, that the above expressions (33a) ~ (33d) should be sufficiently close to exact calculated values. Using (20), (23), (26), (31a) and (32), the induced field given by the summation of the second terms in E_i's is found to be expressed as

$$\dot{E}_b = - f(z)\, r_{sn}\, \mathring{I}_1(0) \quad , \tag{34}$$

where f(z) is a function of z taking almost real-positive values. Using the above stated values for α, C and other parameters, f(z) is estimated to be about 0.27 at z = o and 0.73 at z = L. It is interesting to compare these values with that given by (15'), taking $I_1(0) = 2I_o$. Since the coupling effect between the beam and the field was neglected, f(z) was constant and equal to 0.5 in the preceding section. Taking into account the coupling interaction in a lossy guide, the induced field increases as z increases. This is because the assumed interaction is one-directional or the beam interacts only with the forward wave.

6. Discussion of the Beam Blow-up Effect

In a linear accelerator, which is heavily loaded by the coupling interaction between the beam and the wave, the so-called beam blow-up effect would occur as in electron linacs and traveling wave tubes. The beam blow-up effect in electron linacs is caused by the excitation of a deflecting mode HEM having a backward group velocity. Theoretical studies have been done by a method similar to the theory of backward wave tube oscillators leading to good agreement with experiments.[8, 9] Of course, a similar mechanism is possible in high energy proton linacs; however, if we use the π-mode structure, the excitation of the deflecting mode is only possible at its space-harmonics having a forward group velocity. Therefore, the wave excitation of a backward wave tube type cannot occur in this case. The regenerative wave excitation will only occur through the standing wave type interaction, or the feedback due to the backward phase velocity wave, when the loss at the walls has been compensated by the wave amplification due to the beam. Furthermore, the effective shunt impedance to excite such a space-harmonic wave should be much smaller than that for the fundamental wave, therefore one can expect that the starting current for the beam blow-up due to this mode should be relatively high in the present case. This problem has been

treated by Gluckstern who obtained a starting current as high as 40 A for the Brookhaven linac.[10]

On the other hand, in a standing wave linac, the regenerative interaction due to feedback through the backward phase velocity wave would also occur at the other modes having high shunt impedances, for example, at fundamental harmonics of TM modes. Similar phenomena have often been observed as an internal feedback oscillation in TWT's with low loss structures and may be referred to as longitudinal beam blow-up.

Since the beam blow-up effect could start even from a small signal such as the noise field, the small-signal theory would be applicable except for nonlinear effects as a coherent interaction due to the tightly bunched beam. The starting current will be sufficiently high to compensate losses, so that the Case 1 of $k_n C \gg \alpha$ (still $C < 1$) is probable rather than Case 2. After a numerical calculation in TWT theory including losses,[4] even when $k_n C/\alpha \sim 1$, the solution for δ_i, given by the Case 1 approximation, are still close to the exact calculations.

Then, the starting current for a longitudinal beam blow-up is examined as follows:

First, because of the relatively large value of Ck_bL, simultaneous tuning for the three forward waves cannot be made; i.e. wave 3 will be completely detuned when waves 1 and 2 have been adjusted to resonate the cavity so as to make the wave-beam interaction. Second, the $\delta_2 L$ decreasing wave 2 will have high attenuation so that terms of $e^{\delta_2 L}$ can be neglected. Thus, the beam blow-up effect will occur when the denominators in (29a) and (29b) become zero if we consider only the amplification due to wave 1, or

$$3 - e^{\frac{\alpha}{2} L} e^{\mathrm{Re}(\delta_1 L)} = 0 \tag{35}$$

Taking $\alpha = \frac{2}{L}$, we have $\sqrt{3}/2\ Ck_bL = 2.10$, and the starting current is given by using (23) as